Politecnico di Torino

Philosophiæ Doctor in Applied Mathematics

Advanced numerical techniques for the simulation of flows in fractured media

Candidate:
Andrea Borio

Tutor:
Stefano Berrone

Abstract

The thesis deals with theoretical and applicative aspects of some innovative numerical techniques for the simulation of the flow in Discrete Fracture Networks (DFN). In particular, the recently developed Virtual Element Method (VEM) is considered. A VEM-SUPG stabilized formulation for advection-diffusion problems is defined and studied theoretically and numerically, as well as a residual a posteriori error estimate which does not include any term depending on the VEM stabilization form. Regarding DFN flow simulations, an approach based on Virtual Elements and standard domain decomposition techniques such as Mortar methods is introduced and studied, also in combination with the use of orthogonal polynomials to avoid numerical instabilities that arise when computing polynomial projections on very badly shaped elements.

Finally, we consider a constrained optimization formulation of the problem of computing the flow in DFNs and we develop a residual based a posteriori error estimate that contains non standard terms related to the geometrical non-conformity of the mesh on each fracture to the intersections between them.

Contents

Chapter 1

Introduction

The scientific interest in the study of fractured media has grown recently, driven by applications in strategical sectors, including radioactive nuclear storage, hot dry rock plants, gas shales, carbon dioxide deep geological storage, oil/gas reservoirs and groundwater management. From the computational point of view, many difficulties have to be tackled, originating both from the nature of the equations to solve and the geometrical complexity of the domain. This thesis focuses on a particular class of models for fractured media, called Discrete Fracture Networks, which describe a medium as a set of planar polyogns mutually intersecting in space. These models are valid under the hypothesis that the permeability of the surrounding rock matrix is negligible. Un such domains, the first interest in applications is the computation of the stationary distribution of the hydraulic head, which can be modeled locally on each fracture by the Darcy law, yielding a system of local diffusion equations coupled by the continuity of the solution and the balance of fluxes at intersections. Standard approaches of domain decomposition are not applicable in realistic Discrete Fracture Networks because the meshing process is computationally too heavy. To relax the mesh conformity requirements needed by standard methods, many strategies have been devised. Here, the main focus is on some particular aspects of the recently developed methodologies based on the Virtual Element Method and its flexibility in handling a very large class of polygons [1–4]. In the appendix, instead, we deal with another kind of method, based on a PDE-constrained optimization formulation of the problem, that allows complete non-conformity of the local meshes to intersection [5–8].

Chapter 3 introduces a SUPG-like formulation for advection-diffusion problems for Virtual Element Methods (VEM) on general domains, which avoids the numerical instabilities due to high mesh Péclet numbers. This stabilized formulation of the problem is suitable for the simulation of non-stationary transport of a passive scalar, such as the density of a pollutant in the underground. Chapter 4 deals with the issue of a posteriori error estimation, with the particular aim of avoiding to estimate the VEM stabilization terms. This estimate can be used as a base for adaptive meshing strategies in the DFN context. In Chapter 5 a general framework for DFN simulations using VEM is developed, establishing a link between the two approaches developed so far in this context. In Chapter 6 we give details about one of the two cited methods, namely the coupling between the Virtual Element Method and the Mortar method, which is applied here to Discrete Fracture Networks, but can be of general use for domain decomposition. In Chapter 7 we make some considerations about the use of orthogonal polynomials as basis to compute polynomial projections in the VEM context, in order to prevent the numerical instabilities that can arise on badly shaped polygons such

as the one that are generated by the meshing process described in the previous chapters. In Chapter 8, we summarize the results obtained about VEM and point out some possible developments and future works. Finally, in Appendix A we turn our attention to another approach to DFN flow simulations, namely a PDE constrained optimization formulation of the problem that allows completely non-conforming meshes on each of the fractures. In this context we develop an a posteriori error estimate that takes into account both the error due to the discretization of the model and the error due to the non conformity of the mesh.

1.1 General notation

Throughout the paper, Ω indicates the domain of interest, a bounded open set. This may be, depending on the context, either a subset of $\mathbb{R}^2$ or a Discrete Fracture Network (defined in Chapter 5). The notation throughout the thesis is as follows: $(\cdot,\cdot)_\omega$ and $\|\cdot\|_\omega$ denote the $\mathrm{L}^2(\omega)$ scalar products and norms, for any $\omega \subseteq \Omega$; $\|\cdot\|_{\alpha,\omega}$ and $|\cdot|_{\alpha,\omega}$ denote the $\mathrm{H}^\alpha(\omega)$ norm and semi-norm; whereas $\|\cdot\|_{\mathrm{W}^q_p(\omega)}$ and $|\cdot|_{\mathrm{W}^q_p(\omega)}$ denote the $\mathrm{W}^q_p(\omega)$ norm and semi-norm, where p is the Lebesgue regularity and q is the order of the Sobolev space; finally, we denote by $\langle\cdot,\cdot\rangle_{\pm\alpha,\omega}$ the duality product ${}_{\mathrm{H}^{-\alpha}(\omega)}\langle\cdot,\cdot\rangle_{\mathrm{H}^\alpha(\omega)}$. In general, we omit ω if it coincides with the whole domain (for example, $\|\cdot\|$ is the $\mathrm{L}^2(\Omega)$ norm).

Regarding inequalities, we make use of the symbols $\lesssim$ and $\gtrsim$ to intend inequalities up to a multiplicative constant which does not depend either on the mesh parameter or the problem data (but may depend on the mesh regularity), while the symbols $\precsim$ and $\succsim$ when constants depend also on the physical data (but still not on the mesh parameter). Finally, $\sim$ will denote an equivalence up to multiplicative constants not dependent on the mesh parameter or the problem data.

References for Chapter 1

[1] M. Benedetto, S. Berrone, A. Borio, S. Pieraccini, and S. Scialò. "A Hybrid Mortar Virtual Element Method For Discrete Fracture Network Simulations". In: *J. Comput. Phys.* 306 (2016), pp. 148–166. DOI: 10.1016/j.jcp.2015.11.034.

[2] M. Benedetto, S. Berrone, A. Borio, S. Pieraccini, and S. Scialò. "Order preserving SUPG stabilization for the virtual element formulation of advection-diffusion problems". In: *Computer Methods in Applied Mechanics and Engineering* 311 (2016), pp. 18–40. ISSN: 0045-7825. DOI: 10.1016/j.cma.2016.07.043.

[3] M. Benedetto, S. Berrone, S. Pieraccini, and S. Scialò. "The virtual element method for discrete fracture network simulations". In: *Comput. Methods Appl. Mech. Engrg.* 280.0 (2014), pp. 135–156. ISSN: 0045-7825. DOI: 10.1016/j.cma.2014.07.016.

[4] M. Benedetto, S. Berrone, and S. Scialò. "A Globally Conforming Method For Solving Flow in Discrete Fracture Networks Using the Virtual Element Method". In: *Finite Elem. Anal. Des.* 109 (2016), pp. 23–36. DOI: 10.1016/j.finel.2015.10.003.

[5] S. Berrone, A. Borio, and S. Scialò. "A posteriori error estimate for a PDE-constrained optimization formulation for the flow in DFNs". In: *SIAM J. Numer. Anal.* 54.1 (2016), pp. 242–261. DOI: 10.1137/15M1014760.

[6] S. Berrone, S. Pieraccini, and S. Scialò. "A PDE-constrained optimization formulation for discrete fracture network flows". In: *SIAM J. Sci. Comput.* 35.2 (2013), B487–B510. ISSN: 1064-8275. DOI: 10.1137/120865884.

[7] S. Berrone, S. Pieraccini, and S. Scialò. "An optimization approach for large scale simulations of discrete fracture network flows". In: *J. Comput. Phys.* 256 (2014), pp. 838–853. ISSN: 0021-9991. DOI: 10.1016/j.jcp.2013.09.028.

[8] S. Berrone, S. Pieraccini, and S. Scialò. "On simulations of discrete fracture network flows with an optimization-based extended finite element method". In: *SIAM J. Sci. Comput.* 35.2 (2013), A908–A935. ISSN: 1064-8275. DOI: 10.1137/120882883.

Chapter 2

The Virtual Element Method for elliptic problems

In this chapter we briefly recall the Virtual Element Method (VEM) applied to an elliptic model problem. The general framework of the method is described, highlighting the hypotheses needed to obtained the well posedness of the problem and optimal convergence rates. The VEM notation defined here will be used also in the following chapters. The text of this chapter is partially borrowed from [13].

2.1 Introduction

In the recent years a large interest on polythopal methods for PDEs has rapidly grown. In many fields of computational engineering and scientific computing the geometrical complexity is often as relevant as the model complexity. In all these situations the introduction of polyhedral or polygonal methods can introduce a large and useful flexibility that can play a relevant role in simulations.

The Virtual Element Method (VEM) is a recently developed Galerkin-type approach to the discretization of partial differential equations, that generalizes Mimetic Finite Differences [8, 16, 21]. The main target is to overcome traditional simplicial discretizations in 2D and in 3D and allow the use of an arbitrary polytopal mesh, allowing, for examples, also polygons with different number of edges in 2D. VEM discretizations require only some basic regularity assumptions on the mesh elements, at the price of enlarging the standard polynomial spaces to include some additional basis functions, whose expression is never to be explicitly evaluated. Stability, consistency and polynomial approximation properties are provided by a suitable choice of the degrees of freedom and by suitable stabilization terms of the discrete bilinear form. First established in [1, 3, 5, 6] for general second order elliptic problems, the VEM is currently under continuous development, in order to deal with a larger and larger number of models, including primal [2, 4, 9–11, 13, 18–20, 22] and mixed [7, 17] formulations. Furthermore, the flexibility of the VEM in handling star-shaped polygons with any number of edges and hanging nodes has been exploited in the context of Discrete Fracture Network flow simulations to circumvent mesh generation problems [12, 14, 15].

This chapter is organized as follows: in Section 2.2 we state the model problem that is used here to present the method, in Sections 2.3 and 2.4 we describe the VEM mesh and functional spaces, in Section 2.5 we show the virtual element formulation of our model problem, and

finally in Section 2.6 we propose a review of the results about a priori error estimation in the VEM context that can be found in the literature. The proofs of these results are not reported here, but can be obtained from the ones in the following chapter and in the cited papers.

2.2 The elliptic model problem

Let $\Omega \subset \mathbb{R}^2$ be a bounded open set and let us consider the following convection-diffusion-reaction problem:

$$\begin{cases} -\nabla \cdot (\mathsf{K}\nabla u) + \beta \cdot \nabla u + \gamma u = f & \text{in } \Omega\,, \\ u = 0 & \text{on } \partial\Omega\,. \end{cases} \tag{2.1}$$

We assume that $\mathsf{K} \in \mathrm{L}^\infty(\Omega)$ is a positive function satisfying $\mathsf{K}(x) \geq \mathsf{K}_0 \ \forall x \in \Omega$ for a given $\mathsf{K}_0 > 0$, $\beta \in [\mathrm{L}^\infty(\Omega)]^2$, $\nabla \cdot \beta \in \mathrm{L}^2(\Omega)$ and $\gamma \in \mathrm{L}^\infty(\Omega)$. For simplicity, we additionally assume $\nabla \cdot \beta = 0$. More general boundary conditions can be assumed as well, and K can be taken as a symmetric positive definite tensor, with minor changes in the definitions of the norms, which, in any case, are always computed componentwise.

For future reference, we recall the classical weak formulation of the problem. Defining $\mathscr{B}\colon \mathrm{H}^1_0(\Omega) \times \mathrm{H}^1_0(\Omega) \to \mathbb{R}$ and $F\colon \mathrm{H}^1_0(\Omega) \to \mathbb{R}$ such that

$$\mathscr{B}(w, v) := (\mathsf{K}\nabla w, \nabla v) + (\beta \cdot \nabla w, v) + (\gamma u, v) \quad \forall w, v \in \mathrm{H}^1_0(\Omega)\,, \tag{2.2}$$

and

$$F(v) := (f, v) \quad \forall v \in \mathrm{H}^1_0(\Omega)\,, \tag{2.3}$$

the variational form of (2.1) is

$$\mathscr{B}(u, v) = F(v) \quad \forall v \in \mathrm{H}^1_0(\Omega)\,. \tag{2.4}$$

2.3 Mesh

Let δ be a mesh parameter, and let $\mathcal{T}_\delta$ be a discretization of Ω with open star-shaped polygons with any number of sides (even different from one polygon to another). We even allow angles of 180° at vertices, i.e. an edge in the geometric sense may be subdivided in adiacent segments that we consider as separate edges. Let $\mathcal{E}_\delta$ be the set of this generalised edges, $\mathcal{V}_\delta$ the set of the extrema of such edges, which will be the vertices of our mesh. As a regularity assumption, we ask that there exists a constant $\gamma > 0$ such that, for all $E \in \mathcal{T}_\delta$, E is star-shaped with respect to a ball of radius greater or equal than γh_E, being h_E the diameter of E. We set $h := \max_{E \in \mathcal{T}_\delta} h_E$.

2.4 Functional space

To define the Virtual Element space of order $k > 0$, for some $k \in \mathbb{N}$, we denote by $\mathbb{P}_k(\mathcal{T}_\delta)$ the space of possibly discontinuous functions which are polynomials of degree less than or equal to k on each polygon and we introduce the piecewise polynomial oblique projection $\Pi^\nabla_k\colon \mathrm{H}^1(\Omega) \to \mathbb{P}_k(\mathcal{T}_\delta)$ such that, $\forall E \in \mathcal{T}_\delta$,

$$\begin{cases} \left(\nabla\left(\Pi^\nabla_k v\right), \nabla p\right)_E = (\nabla v, \nabla p) & \forall p \in \mathbb{P}_k(E)\,, \\ \left(\Pi^\nabla_k v, 1\right)_{\partial E} = (v, 1)_{\partial E} & \text{if } k = 1\,, \\ \left(\Pi^\nabla_k v, 1\right)_E = (v, 1)_E & \text{if } k \geq 1\,, \end{cases}$$

The local virtual space of order k is defined as follows: $\forall E \in \mathcal{T}_\delta$,

$$V_\delta^E := \big\{ v_h \in \mathrm{H}^1(E) : \Delta v_h \in \mathbb{P}_k(E),\, v_h \in \mathbb{P}_k(e)\ \forall e \subset \partial E,\, \gamma_{\partial E}(v_h) \in \mathrm{C}^0(\partial E), \\ (v_h, p)_E = \big(\Pi_k^\nabla v_h, p\big)_E\ \forall p \in \mathbb{P}_k(E)/\mathbb{P}_{k-2}(E) \big\}, \quad (2.5)$$

where $\mathbb{P}_k(E)/\mathbb{P}_{k-2}(E)$ denotes the subspace of $\mathbb{P}_k(E)$ containing polynomials that are $\mathrm{L}^2(E)$-orthogonal to $\mathbb{P}_{k-2}(E)$ (see [6]; other options are possible, see, for example, [1]). The global VEM space $V_\delta \subset \mathrm{H}_0^1(\Omega)$ is obtained asking for global continuity:

$$V_\delta := \big\{ v_h \in \mathrm{C}^0(\Omega) : v_h \in V_\delta^E \quad \forall E \in \mathcal{T}_\delta \big\}. \quad (2.6)$$

A function belonging to such space is uniquely identified by its polynomial expression on each edge of the discretization and by its moments against polynomials of degree $\leq k-2$ (see [3]).

Definition 2.1. We choose the following set of degrees of freedom:

1. the values at the vertices of each polygon;
2. if $k \geq 2$, for each edge $e \subset \partial E$, the values at $k-1$ internal points of e. For practical purposes, we may choose these points to be the internal Gauss-Lobatto quadrature nodes;
3. if $k \geq 2$, for each $v_h \in V_\delta$ the scaled moments $\frac{1}{|E|}(v_h, m_{\boldsymbol{\alpha}})_E$, for each $E \in \mathcal{T}_\delta$ and all the monomials $m_{\boldsymbol{\alpha}} \in \mathcal{M}_{k-2}(E)$, defined as

$$m_{\boldsymbol{\alpha}}(x,y) := \frac{(x-x_E)^{\alpha_1}(y-y_E)^{\alpha_2}}{h_E^{\alpha_1+\alpha_2}} \quad \forall (x,y) \in E,$$

with $\boldsymbol{\alpha} = (\alpha_1, \alpha_2)$, $|\boldsymbol{\alpha}| = \alpha_1 + \alpha_2 \leq k-2$, and being (x_E, y_E) the center of the ball with respect to which E is star-shaped.

The above degrees of freedom are enough to compute, for any $v_h \in V_\delta$, the projection $\Pi_k^\nabla v_h$, and, once it is known, to compute the L^2-projection of v_h on $\mathbb{P}_k(\mathcal{T}_\delta)$, which will be indicated by $\Pi_k^0 v_h$ in the following, as well as the L^2-projection of ∇v_h on $\mathbb{P}_{k-1}(\mathcal{T}_\delta) \times \mathbb{P}_{k-1}(\mathcal{T}_\delta)$, which will be indicated by $\Pi_{k-1}^0 \nabla v_h$. This can be done by means of the Green formula (see [5]).

2.5 Discrete formulation of the problem

The VEM discretization of problem (2.1) is done without ever building an explicit basis for the space V_δ. Instead, we identify a discrete bilinear form that is computable using only the polynomial projections of the basis functions of V_δ, whose analytical expression is not known.

For any $E \in \mathcal{T}_\delta$, and $\forall v_\delta, w_\delta \in V_\delta$, let

$$\begin{aligned} a_\delta^E(w_h, v_h) &:= \big(\Pi_{k-1}^0 \nabla w_\delta, \Pi_{k-1}^0 \nabla v_\delta\big)_E + S^E\big(w_\delta - \Pi_k^\nabla w_\delta, v_\delta - \Pi_k^\nabla v_\delta\big), \quad (2.7) \\ b_\delta^E(w_h, v_h) &:= \big(\beta \cdot \Pi_{k-1}^0 \nabla w_\delta, \Pi_{k-1}^0 v_\delta\big)_E, \\ c_\delta^E(w_h, v_h) &:= \big(\gamma \Pi_{k-1}^0 w_\delta, \Pi_{k-1}^0 v_\delta\big)_E, \end{aligned}$$

where S^E: $V_\delta \times V_\delta \to \mathbb{R}$ in (2.7) must satisfy the following property:

$$S^E(v_\delta, v_\delta) \sim \|\nabla v_\delta\|_E^2 \quad \forall v_\delta \in \ker \Pi_k^\nabla. \quad (2.8)$$

Remark 2.1. A possible choice for S^E is

$$S^E(w_\delta, v_\delta) = \sum_{i=1}^{N_E} \chi_i(v_\delta)\chi_i(w_\delta), \tag{2.9}$$

where N_E is the number of degrees of freedom on the element E and χ_i is the operator that selects the i-th degree of freedom.

We define the discrete bilinear form $\mathscr{B}_\delta\colon V_\delta \times V_\delta \to \mathbb{R}$ such that

$$\mathscr{B}_\delta(w_\delta, v_\delta) := \sum_{E\in\mathcal{T}_\delta} a_\delta^E(w_\delta, v_\delta) + b_\delta^E(w_\delta, v_\delta) + c_\delta^E(w_\delta, v_\delta) \quad \forall w_\delta, v_\delta \in V_\delta\,, \tag{2.10}$$

and the discrete forcing term

$$F_\delta(v_\delta) = \big(f, \Pi^0_{k-1} v_\delta\big) \quad \forall v_\delta \in V_\delta\,. \tag{2.11}$$

The discrete VEM problem is to find $u_\delta \in V_\delta$ such that

$$\mathscr{B}_\delta(u_\delta, v_\delta) = F_\delta(v_\delta) \quad \forall v_\delta \in V_\delta\,. \tag{2.12}$$

2.6 A priori error analysis

The well posedness of problem (2.12) follows from the approximation properties of the projection operators Π^0_{k-1} and Π^∇_k and (2.8) and it can be proved that the approximation error decays with optimal rates of convergence. In this section we show the most fundamental a priori error analysis results for future reference. Their proofs can be found in [6] or can be obtained easily from the proofs in Chapter 3.

First of all, we have the following approximation results.

Proposition 2.1. *Let $E \in \mathcal{T}_\delta$, $\varphi \in \mathrm{H}^s(E)$, for some $0 \le s \le k+1$. Then,*

$$\left\|\varphi - \Pi^0_k\varphi\right\|_{m,E} \lesssim h_E^{s-m} |\varphi|_{s,E} \quad \forall m\colon m \le s\,, \tag{2.13}$$

and, if $s \ge 1$,

$$\left\|\nabla\varphi - \Pi^0_{k-1}\nabla\varphi\right\|_{m,E} \lesssim h_E^{s-m} |\varphi|_{s,E} \quad \forall m\colon m \le s-1\,, \tag{2.14}$$

$$\left\|\varphi - \Pi^\nabla_k\varphi\right\|_{m,E} \lesssim h_E^{s-m} |\varphi|_{s,E} \quad \forall m\colon m \le s-1\,. \tag{2.15}$$

Moreover, there exists an operator $I_\delta\colon \mathrm{H}^s(\Omega) \to V_\delta$ such that

$$\|\varphi - I_\delta\varphi\|_{m,E} \lesssim h_E^{s-m} |\varphi|_{s,E} \quad \text{if } s \ge 1\,. \tag{2.16}$$

Remark 2.2. While for $s > 1$ I_δ can be built easily using pointwise interpolation, a proof of (2.16) for $s = 1$ can be found [18] under the additional hypothesis that for any edge $e \subset \partial E$, $h_e \ge \gamma h_E$.

Using (2.14) and (2.15) we obtain approximation rates between the continuous and discrete bilinear forms (see the analogous Lemmas 3.1 to 3.3), by which we prove the following stability estimate, from which the well-posedness of problem (2.12) follows.

Theorem 2.1. *Let $v_\delta \in V_\delta$ and suppose $\mathsf{K} \in \mathrm{L}^\infty(\Omega)$ and $\beta \in \left[\mathrm{W}^1_\infty(\Omega)\right]^2$. Then, for h sufficiently small there holds*

$$\sup_{w_\delta \in V_\delta} \frac{\mathscr{B}_\delta(v_\delta, w_\delta)}{|w_\delta|_{1,\Omega}} \gtrsim |v_\delta|_{1,\Omega} \, . \tag{2.17}$$

Concerning a priori error analysis, we have the following optimality result in the energy norm.

Theorem 2.2. *Suppose $u \in \mathrm{H}^{s+1}(\Omega)$, $f \in \mathrm{H}^s(\Omega)$, $\mathsf{K} \in \mathrm{W}^s_\infty(\Omega)$, $\beta \in \left[\mathrm{W}^{s+1}_\infty(\Omega)\right]^2$, $\gamma \in \mathrm{W}^s_\infty(\Omega)$ for some $s \in \{1, \ldots, k\}$. Then, for h sufficiently small,*

$$\|u - u_\delta\|_1 \precsim h^s \left(\|u\|_{s+1} + \|f\|_s \right) \, .$$

Finally, thanks to standard duality arguments, we can also prove optimal rates of convergence in the $\mathrm{L}^2(\Omega)$ norm.

Theorem 2.3. *Suppose $u \in \mathrm{H}^{s+1}(\Omega)$, $f \in \mathrm{H}^s(\Omega)$, $\mathsf{K} \in \mathrm{W}^s_\infty(\Omega)$, $\beta \in \left[\mathrm{W}^{s+1}_\infty(\Omega)\right]^2$, $\gamma \in \mathrm{W}^s_\infty(\Omega)$ for some $s \in \{1, \ldots, k\}$. Then, for h sufficiently small,*

$$\|u - u_\delta\| \precsim h^{s+1} \left(\|u\|_{s+1} + \|f\|_s \right) \, .$$

We remark again that the proofs for all the stated results can be easily obtained from the ones in the next chapter.

References for Chapter 2

[1] B. Ahmad, A. Alsaedi, F. Brezzi, L. D. Marini, and A. Russo. "Equivalent projectors for virtual element methods". In: *Computers & Mathematics with Applications* 66 (3 Sept. 2013), pp. 376–391.

[2] P. F. Antonietti, L. Beirão da Veiga, D. Mora, and M. Verani. "A Stream Virtual Element Formulation of the Stokes Problem on Polygonal Meshes". In: *SIAM Journal on Numerical Analysis* 52.1 (2014), pp. 386–404. DOI: 10.1137/13091141X.

[3] L. Beirão da Veiga, F. Brezzi, A. Cangiani, G. Manzini, L. D. Marini, and A. Russo. "Basic principles of virtual element methods". In: *Mathematical Models and Methods in Applied Sciences* 23.01 (2013), pp. 199–214.

[4] L. Beirão da Veiga, F. Brezzi, and L. D. Marini. "Virtual Elements for Linear Elasticity Problems". In: *SIAM Journal on Numerical Analysis* 51.2 (2013), pp. 794–812. DOI: 10.1137/120874746.

[5] L. Beirão Da Veiga, F. Brezzi, L. D. Marini, and A. Russo. "The hitchhiker's guide to the Virtual Element method". In: *Math. Models Methods Appl. Sci* 24.8 (2014), pp. 1541–1573.

[6] L. Beirão da Veiga, F. Brezzi, L. D. Marini, and A. Russo. "Virtual Element Methods for General Second Order Elliptic Problems on Polygonal Meshes". In: *Mathematical Models and Methods in Applied Sciences* 26.04 (2015), pp. 729–750. DOI: 10.1142/S0218202516500160.

[7] L. Beirão da Veiga, F. Brezzi, L. Marini, and A. Russo. *Mixed Virtual Element Methods for general second order elliptic problems on polygonal meshes*. 2015. arXiv: 1506.07328.

[8] L. Beirão da Veiga, K. Lipnikov, and G. Manzini. *The Mimetic Finite Difference Method for Elliptic Problems*. Vol. 11. Modeling, Simulation & Applications. Springer, 2014.

[9] L. Beirão da Veiga, C. Lovadina, and D. Mora. "A Virtual Element Method for elastic and inelastic problems on polytope meshes". In: *Computer Methods in Applied Mechanics and Engineering* 295 (2015), pp. 327–346. ISSN: 0045-7825. DOI: 10.1016/j.cma.2015.07.013.

[10] L. Beirão da Veiga and G. Manzini. "A virtual element method with arbitrary regularity". In: *IMA Journal of Numerical Analysis* 34.2 (2014), pp. 759–781. DOI: 10.1093/imanum/drt018.

[11] L. Beirão da Veiga, C. Lovadina, and A. Russo. *Stability Analysis for the Virtual Element Method*. 2016. arXiv: 1607.05988.

[12] M. Benedetto, S. Berrone, A. Borio, S. Pieraccini, and S. Scialò. "A Hybrid Mortar Virtual Element Method For Discrete Fracture Network Simulations". In: *J. Comput. Phys.* 306 (2016), pp. 148–166. DOI: 10.1016/j.jcp.2015.11.034.

[13] M. Benedetto, S. Berrone, A. Borio, S. Pieraccini, and S. Scialò. "Order preserving SUPG stabilization for the virtual element formulation of advection-diffusion problems". In: *Computer Methods in Applied Mechanics and Engineering* 311 (2016), pp. 18–40. ISSN: 0045-7825. DOI: 10.1016/j.cma.2016.07.043.

[14] M. Benedetto, S. Berrone, S. Pieraccini, and S. Scialò. "The virtual element method for discrete fracture network simulations". In: *Comput. Methods Appl. Mech. Engrg.* 280.0 (2014), pp. 135–156. ISSN: 0045-7825. DOI: 10.1016/j.cma.2014.07.016.

[15] M. Benedetto, S. Berrone, and S. Scialò. "A Globally Conforming Method For Solving Flow in Discrete Fracture Networks Using the Virtual Element Method". In: *Finite Elem. Anal. Des.* 109 (2016), pp. 23–36. DOI: 10.1016/j.finel.2015.10.003.

[16] F. Brezzi, A. Buffa, and K. Lipnikov. "Mimetic finite differences for elliptic problems". In: *ESAIM: Mathematical Modelling and Numerical Analysis* 43 (2 2009), pp. 277–295.

[17] F. Brezzi, R. S. Falk, and L. D. Marini. "Basic principles of mixed virtual element methods". In: *ESAIM: Mathematical Modelling and Numerical Analysis* 48.04 (2014), pp. 1227–1240.

[18] A. Cangiani, E. H. Georgoulis, T. Pryer, and O. J. Sutton. *A posteriori error estimates for the virtual element method*. 2016. arXiv: 1603.05855.

[19] A. Cangiani, G. Manzini, and O. J. Sutton. "Conforming and nonconforming virtual element methods for elliptic problems". In: *IMA Journal of Numerical Analysis* (2016). DOI: 10.1093/imanum/drw036.

[20] B. A. de Dios, K. Lipnikov, and G. Manzini. "The nonconforming virtual element method". In: *ESAIM: Mathematical Modelling and Numerical Analysis* 50.3 (2016), pp. 879–904.

[21] K. Lipnikov, G. Manzini, and M. Shashkov. "Mimetic finite difference method". In: *Journal of Computational Physics* 257 (2014), pp. 1163–1227.

[22] S. S. P. F. Antonietti L. Beirão da Veiga and M. Verani. *A C^1 virtual element method for the Cahn-Hilliard equation with polygonal meshes*. 2015. arXiv: 1502.03259.

Chapter 3

SUPG stabilization for the Virtual Element formulation of advection-diffusion problems

This chapter is devoted to the introduction of a Streamwise Upwind Petrov-Galerkin stabilization (SUPG) formulation for Virtual Element Methods, with a priori estimations of the error and numerical tests validating the method. These results were published in [4].

3.1 Introduction

Recently, the VEM has been used in the treatment of fluid dynamics models involving underground flow simulations [3, 5, 6]: in that context, the application of the VEM was driven by the need of circumventing mesh generation problems. In these applications, the primal problem is solved to compute the Darcy velocity field, that can be used afterwards to simulate the transport of a dispersed, passive pollutant in a geological basin. The flow regimes in underground transport phenomena are usually transport-dominated, due to the very low diffusivity of the pollutant into the bulk fluid, thus calling for a stabilization of the VEM.

Many strategies have been devised to obtain a stable solution for standard Finite Element discretizations, involving, for example, local projections [19] or suitably built bubble functions [11, 18]. The Streamline Upwind Petrov-Galerkin (SUPG) stabilization method [12–14, 17, 20, 22, 23] has also been widely studied in very general settings. A first approach to the VEM-SUPG stabilization is discussed in [16], in a non-consistent formulation. Another issue related to advection-diffusion problems is the derivation of robust a posteriori error estimates. In such context, the term *robustness* refers to the property of obtaining a relation between the error and the error estimator with constants which are independent of the Péclet number [7–10, 25, 26]. An a posteriori analysis for the reaction-convection-diffusion problem with the VEM is provided in [15], not addressing robustness aspects and the SUPG-like stabilization issues.

The aim of this chapter is to devise a consistent SUPG formulation compatible with the VEM. A key aspect of the VEM is that the basis functions of the discrete functional space are not known explicitly, but only through their degrees of freedom. As a consequence, computability of discrete operators requires special care and, in particular, the consistent

VEM-SUPG formulation devised in the present work requires the introduction of a second-order term in the weak formulation of the problem, computed by resorting to polynomial projections of the virtual element basis functions. An *a priori* error estimate for the stabilized VEM discrete solution is also proven, showing that the order of convergence is not affected by the stabilizing perturbation added to the problem. The numerical tests proposed confirm the theoretical results on triangular and polygonal meshes in both the convection-dominated regime and the diffusion-dominated regime.

The chapter is organised as follows. In Section 3.2 we state the model problem, define some useful notations and make some standard hypothesis on the model parameters. In Section 3.3 we recall the standard SUPG formulation and adapt it to the VEM context. In particular, the VEM-SUPG formulation of the problem is presented in (3.12)–(3.17). In Section 3.4 the *a priori* error estimate for the stabilized VEM discrete solution is derived, the main result being stated in Theorem 3.2. Finally, in Section 3.5 we propose some numerical tests aimed at confirming the theoretical results.

3.2 The model problem

Let $\Omega \subset \mathbb{R}^2$ be a bounded open set and let us consider this reduced form of problem (2.1):

$$\begin{cases} -\nabla \cdot (\mathsf{K}\nabla u) + \beta \cdot \nabla u = f & \text{in } \Omega\,, \\ u = 0 & \text{on } \partial\Omega\,. \end{cases} \tag{3.1}$$

As for (2.1), we assume that $\mathsf{K} \in \mathrm{L}^\infty(\Omega)$ is a positive function satisfying $\mathsf{K}(x) \geq \mathsf{K}_0 \ \forall x \in \Omega$ for a given $\mathsf{K}_0 > 0$, and $\beta \in [\mathrm{L}^\infty(\Omega)]^2$, with $\nabla \cdot \beta = 0$. The variational form (2.4) is still valid: if we define $\mathscr{B}$ and F as in (2.2) (with $\gamma = 0$) and (2.3), we have

$$\mathscr{B}(u, v) = F(v) \quad \forall v \in \mathrm{H}^1_0(\Omega)\ .$$

3.3 VEM-SUPG formulation

It is well known that discretizing the variational formulation (2.4) leads to instabilities when the convective term $(\beta \cdot \nabla w, v)$ is dominant with respect to the diffusive term $(\mathsf{K}\nabla w, \nabla v)$. In such situations a stabilized form of the problem is required in order to prevent spurious oscillations that can completely alter the numerical solution. In the following we recast the classical *Streamline Upwind Petrov Galerkin* (SUPG) approach [17] in the framework of the VEM, showing that the optimal order of convergence can be preserved. For this purpose, in the following we assume $\mathsf{K} \in \mathrm{W}^1_\infty(\Omega)$.

We define the space $V = \left\{ v \in \mathrm{H}^1_0(\Omega) : v \in \mathrm{H}^2(E)\,, \forall E \in \mathcal{T}_\delta \right\}$ and the bilinear form

$$\mathscr{B}_{\text{supg}} \colon V \to \mathbb{R} \quad \text{such that} \quad \mathscr{B}_{\text{supg}}(w, v) := a(w, v) + b(w, v) + d(w, v)\ , \tag{3.2}$$

being

$$a(w, v) := (\mathsf{K}\nabla w, \nabla v) + \sum_{E \in \mathcal{T}_\delta} \tau_E \left(\beta \cdot \nabla w, \beta \cdot \nabla v\right)\ , \tag{3.3}$$

$$b(w, v) := (\beta \cdot \nabla w, v)\ , \tag{3.4}$$

$$d(w, v) := -\sum_{E \in \mathcal{T}_\delta} \tau_E \left(\nabla \cdot (\mathsf{K}\nabla w), \beta \cdot \nabla v\right)_E\ . \tag{3.5}$$

The stability parameter τ_E is defined as usual [17], $\forall E \in \mathcal{T}_\delta$, by

$$\tau_E := \frac{h_E}{2\beta_E} \min\left\{\mathrm{Pe}_E, 1\right\} , \tag{3.6}$$

where Pe_E is the *mesh Péclet number* of E, given by

$$\mathrm{Pe}_E := m_k^E \frac{\beta_E h_E}{2\mathsf{K}_E} , \tag{3.7}$$

and

$$m_k^E := \begin{cases} \frac{1}{3} & \text{if } \nabla\cdot(\mathsf{K}\nabla v_\delta) = 0 \ \forall v_\delta \in V_\delta^E, \\ 2\tilde{C}_k^E & \text{otherwise,} \end{cases}$$

having set $\tilde{C}_k^E$ to be the largest constant satisfying the following inverse inequality:

$$\tilde{C}_k^E h_E^2 \left\|\nabla\cdot(\mathsf{K}\nabla v_\delta)\right\|_E^2 \le \left\|\mathsf{K}\nabla v_\delta\right\|_E^2 \quad \forall v_\delta \in V_\delta^E . \tag{3.8}$$

A proof of an inverse inequality in the VEM space is provided in [15, Lemma 10] in the case of constant K under the current mesh-regularity assumptions. Using standard manipulations, result (3.8) can then be obtained, with a constant $\tilde{C}_k^E$ depending on the variations of K on the element.

Remark 3.1. We point out that if $u \in \mathrm{H}^2(\Omega) \cap \mathrm{H}_0^1(\Omega)$, we have that, $\forall \mathcal{T}_\delta$,

$$\mathscr{B}_{\mathrm{supg}}(u,v) = F_{\mathrm{supg}}(v) := (f,v) + \sum_{E\in\mathcal{T}_\delta} \tau_E \left(f, \beta\cdot\nabla v\right) \quad \forall v \in \mathrm{H}_0^1(\Omega) . \tag{3.9}$$

Remark 3.2. From the definition of τ_E we have the following two estimates, that will be used in the following:

$$\tau_E \le \frac{\tilde{C}_k^E h_E^2}{2\mathsf{K}_E} \quad \text{if } \nabla\cdot(\mathsf{K}\nabla v_\delta) \neq 0 \text{ for some } v_\delta \in V_\delta^E , \tag{3.10}$$

$$\tau_E \le \frac{h_E}{2\beta_E} . \tag{3.11}$$

The Finite Element discretization of the bilinear form (3.2) has been widely studied, for example in [12, 17], in which optimal orders of convergence were proved. In order to write a *computable* VEM discretization of problem (3.9), we consider the framework defined in Chapter 2 and define the discrete bilinear form $\mathscr{B}_{\mathrm{supg},\delta}$: $V_\delta \times V_\delta \to \mathbb{R}$, being V_δ the functional space defined by (2.5) and (2.6), such that

$$\mathscr{B}_{\mathrm{supg},\delta}(w_\delta, v_\delta) := a_\delta(w_\delta, v_\delta) + b_\delta(w_\delta, v_\delta) + d_\delta(w_\delta, v_\delta) \quad \forall w_\delta, v_\delta \in V_\delta , \tag{3.12}$$

where

$$\begin{aligned} a_\delta(w_\delta, v_\delta) := {} & \left(\mathsf{K}\Pi_{k-1}^0\nabla w_\delta, \Pi_{k-1}^0\nabla v_\delta\right) + \sum_{E\in\mathcal{T}_\delta} \tau_E \left(\beta\cdot\Pi_{k-1}^0\nabla w_\delta, \beta\cdot\Pi_{k-1}^0\nabla v_\delta\right)_E \\ & + \left(\mathsf{K}_E + \tau_E\beta_E^2\right) S^E\left(\left(I-\Pi_k^\nabla\right) w_\delta, \left(I-\Pi_k^\nabla\right) v_\delta\right) , \end{aligned} \tag{3.13}$$

$$b_\delta(w_\delta, v_\delta) := \left(\beta\cdot\Pi_{k-1}^0\nabla w_\delta, \Pi_{k-1}^0 v\right) , \tag{3.14}$$

$$d_\delta(w_\delta, v_\delta) := -\sum_{E\in\mathcal{T}_\delta} \tau_E \left(\nabla\cdot\left(\mathsf{K}\Pi_{k-1}^0\nabla w_\delta\right), \beta\cdot\Pi_{k-1}^0\nabla v_\delta\right) , \tag{3.15}$$

where Π^0_r is the element-wise orthogonal L^2 projection on the space of polynomials of degree less than or equal to r, as used in [2]. The computation of Π^0_{k-1} is performed as in [1], using only the VEM degrees of freedom. As in Chapter 2, the stabilization form S^E: $V_\delta \times V_\delta \to \mathbb{R}$ in (3.13) must satisfy the following property:

$$S^E(v_\delta, v_\delta) \sim \|\nabla v_\delta\|^2_E \quad \forall v_\delta \in \ker \Pi^\nabla_k \, .$$

Using the above definitions we can state a SUPG-stabilized discrete formulation of (2.4) as: find $u_\delta \in V_\delta$ such that

$$\mathscr{B}_{\mathrm{supg},\delta}(u_\delta, v_\delta) = F_{\mathrm{supg},\delta}(v_\delta) \quad \forall v_\delta \in V_\delta \, , \tag{3.16}$$

having defined the discrete right-hand side as

$$F_{\mathrm{supg},\delta}(v_\delta) = \left(f, \Pi^0_{k-1} v_\delta\right) + \sum_{E \in \mathcal{T}_\delta} \tau_E \left(f, \beta \cdot \Pi^0_{k-1} \nabla v_\delta\right)_E \, . \tag{3.17}$$

Finally, in order to provide an estimation of the constant $\tilde{C}^E_k$ for each polygon, we can make use of classical theoretical results on triangles [21] thanks to the following proposition.

Proposition 3.1. *Given a regular polygon $E \in \mathcal{T}_\delta$, let $\mathcal{T}_{\delta,E}$ be a triangulation of E composed by triangular elements with an edge on the boundary of E and one vertex in the centre of the ball with respect to which E is star-shaped. Let $\tilde{C}^E_k$ be the constant of inequality* (3.8)*. Then,*

$$\tilde{C}^E_k \geq \frac{\min_{t \in \mathcal{T}_{\delta,E}} \tilde{C}^t_k h^2_t}{h^2_E} \, ,$$

where $\tilde{C}^t_k$ is such that, $\forall v_\delta \in V^E_\delta$,

$$\tilde{C}^t_k h^2_t \left\|\nabla \cdot (\mathsf{K} \nabla v_\delta)\right\|^2_t \leq \|\mathsf{K} \nabla v_\delta\|^2_t \quad \forall t \in \mathcal{T}_{\delta,E} \, .$$

Proof. Summing up the inequalities on internal triangles we have

$$\sum_{t \in \mathcal{T}_{\delta,E}} \tilde{C}^t_k h^2_t \left\|\nabla \cdot (\mathsf{K} \nabla v_\delta)\right\|^2_t \leq \sum_{t \in \mathcal{T}_{\delta,E}} \|\mathsf{K} \nabla v_\delta\|^2_t \, ,$$

from which it follows

$$\min_{t \in \mathcal{T}_{\delta,E}} \tilde{C}^t_k h^2_t \left\|\nabla \cdot (\mathsf{K} \nabla v_\delta)\right\|^2_E \leq \|\mathsf{K} \nabla v_\delta\|^2_E \, ,$$

and therefore

$$\frac{\min_{t \in \mathcal{T}_{\delta,E}} \tilde{C}^t_k h^2_t}{h^2_E} h^2_E \left\|\nabla \cdot (\mathsf{K} \nabla v_\delta)\right\|^2_E \leq \|\mathsf{K} \nabla v_\delta\|^2_E \, ,$$

which proves the thesis. □

3.4 Error Analysis

Let $h := \max_{E \in \mathcal{T}_\delta} h_E$ and define the following norm:

$$|\!|\!| v |\!|\!| := \left\{ \left\| \sqrt{\mathsf{K}} \nabla v \right\|^2 + \sum_{E \in \mathcal{T}_\delta} \tau_E \|\beta \cdot \nabla v\|^2_E \right\}^{\frac{1}{2}} \quad \forall v \in \mathrm{H}^1_0(\Omega) \, .$$

3.4.1 Discretization errors.

The following Lemmas are devoted to estimate the error of approximation of the bilinear forms defined by (3.3), (3.4) and (3.5) with the discrete ones defined by (3.13), (3.14) and (3.15), respectively. The results are based on the approximation results for polynomial projections in Proposition 2.1.

Lemma 3.1. *For any* $w \in \mathrm{H}^1(\Omega)$ *and* $\forall v_\delta \in V_\delta$,

$$b_\delta(w, v_\delta) \lesssim \max_{E \in \mathcal{T}_\delta} \frac{\beta_E}{\sqrt{\mathsf{K}_E^\vee}} \left\| \sqrt{\mathsf{K}} \nabla w \right\| \|v_\delta\| \ . \tag{3.18}$$

Moreover, if $w \in \mathrm{H}^{s+1}(\Omega)$ *and* $\beta \in [\mathrm{W}^s_\infty(\Omega)]^2$ *for some* $s \in \{0, \dots, k\}$, *then*

$$|b(w, v_\delta) - b_\delta(w, v_\delta)| \lesssim \max_{E \in \mathcal{T}_\delta} \|\beta\|_{\mathrm{W}^s_\infty(E)} \, h^{s+1} \, \|w\|_{s+1} \, \|v_\delta\|_1 \ . \tag{3.19}$$

Proof. Regarding (3.18), by the Cauchy-Schwarz inequality and the continuity of Π^0_{k-1} and Π^0_k we have, $\forall E \in \mathcal{T}_\delta$,

$$\left(\beta \cdot \Pi^0_{k-1} \nabla w, \Pi^0_{k-1} v_\delta\right)_E \le \beta_E \left\|\Pi^0_{k-1} \nabla w\right\|_E \left\|\Pi^0_{k-1} v_\delta\right\|_E \lesssim \frac{\beta_E}{\sqrt{\mathsf{K}_E^\vee}} \left\| \sqrt{\mathsf{K}} \nabla w \right\|_E \|v_\delta\|_E \ ,$$

from which (3.18) readily follows.

Concerning (3.19), let $E \in \mathcal{T}_\delta$ be fixed. By adding and subtracting $\left(\beta \cdot \Pi^0_{k-1} \nabla w, v_\delta\right)_E$ in the left-hand side and using the triangle inequality,

$$\begin{aligned} &\left|(\beta \cdot \nabla w, v_\delta)_E - \left(\beta \cdot \Pi^0_{k-1} \nabla w, \Pi^0_{k-1} v_\delta\right)_E\right| = \\ &\qquad = \left|\left(\beta \cdot \left(\nabla w - \Pi^0_{k-1} \nabla w\right), v_\delta\right)_E + \left(\beta \cdot \Pi^0_{k-1} \nabla w, v_\delta - \Pi^0_{k-1} v_\delta\right)_E\right| \le \\ &\qquad\qquad \le \left|\left(\beta \cdot \left(\nabla w - \Pi^0_{k-1} \nabla w\right), v_\delta\right)_E\right| + \left|\left(\beta \cdot \Pi^0_{k-1} \nabla w, v_\delta - \Pi^0_{k-1} v_\delta\right)_E\right| \ . \end{aligned}$$

We consider the two terms in the sum separately. The first one can be written as

$$\left(\beta \cdot \left(\nabla w - \Pi^0_{k-1} \nabla w\right), v_\delta\right)_E = \sum_{i=1}^{2} \left(\frac{\partial w}{\partial x_i} - \Pi^0_{k-1} \frac{\partial w}{\partial x_i}, \beta_i v_\delta \right)_E \ .$$

Estimating each term in the right-hand side we have, $\forall i \in \{1, 2\}$,

$$\begin{aligned} \left(\frac{\partial w}{\partial x_i} - \Pi^0_{k-1} \frac{\partial w}{\partial x_i}, \beta_i v_\delta \right)_E &= \left(\frac{\partial w}{\partial x_i} - \Pi^0_{k-1} \frac{\partial w}{\partial x_i}, \beta_i v_\delta - \Pi^0_{k-1}(\beta_i v_\delta) \right)_E \le \\ &\le \left\| \frac{\partial w}{\partial x_i} - \Pi^0_{k-1} \frac{\partial w}{\partial x_i} \right\|_E \left\| \beta_i v_\delta - \Pi^0_{k-1}(\beta_i v_\delta) \right\|_E \lesssim h_E^s \, |w|_{s+1,E} \cdot h_E \, |\beta_i v_\delta|_{1,E} \le \\ &\qquad \le h_E^{s+1} \, \|\beta_i\|_{\mathrm{W}^1_\infty(E)} \, |w|_{s+1,E} \, \|v_\delta\|_{1,E} \ . \end{aligned}$$

Concerning the second term, we have that

$$\left(\beta \cdot \Pi^0_{k-1} \nabla w, v_\delta - \Pi^0_{k-1} v_\delta\right)_E = \sum_{i=1}^{2} \left(\beta_i \Pi^0_{k-1} \frac{\partial w}{\partial x_i}, v_\delta - \Pi^0_{k-1} v_\delta \right)_E \ .$$

Thus, using the properties of projectors to add polynomials of degree less or equal than $k-1$,

we have

$$\left(\beta_i\Pi^0_{k-1}\frac{\partial w}{\partial x_i}, v_\delta - \Pi^0_{k-1}v_\delta\right)_E = \left(\beta_i\Pi^0_{k-1}\frac{\partial w}{\partial x_i} - \Pi^0_{k-1}\left(\beta_i\Pi^0_{k-1}\frac{\partial w}{\partial x_i}\right), v_\delta - \Pi^0_{k-1}v_\delta\right)_E \leq$$
$$\leq \left\|\beta_i\Pi^0_{k-1}\frac{\partial w}{\partial x_i} - \Pi^0_{k-1}\left(\beta_i\Pi^0_{k-1}\frac{\partial w}{\partial x_i}\right)\right\|_E \left\|v_\delta - \Pi^0_{k-1}v_\delta\right\|_E \leq$$
$$\leq h_E \left\|\beta_i\Pi^0_{k-1}\frac{\partial w}{\partial x_i} - \Pi^0_{k-1}\left(\beta_i\Pi^0_{k-1}\frac{\partial w}{\partial x_i}\right)\right\|_E \|\nabla v_\delta\|_E ,$$

and the proof ends using the best approximation property of the projection, the triangle inequality, (2.13) and (2.14):

$$\left\|\beta_i\Pi^0_{k-1}\frac{\partial w}{\partial x_i} - \Pi^0_{k-1}\left(\beta_i\Pi^0_{k-1}\frac{\partial w}{\partial x_i}\right)\right\|_E \leq \left\|\beta_i\Pi^0_{k-1}\frac{\partial w}{\partial x_i} - \Pi^0_{k-1}\left(\beta_i\frac{\partial w}{\partial x_i}\right)\right\|_E \leq$$
$$\leq \left\|\beta_i\Pi^0_{k-1}\frac{\partial w}{\partial x_i} - \beta_i\frac{\partial w}{\partial x_i}\right\|_E + \left\|\beta_i\frac{\partial w}{\partial x_i} - \Pi^0_{k-1}\left(\beta_i\frac{\partial w}{\partial x_i}\right)\right\|_E \leq h_E^s\beta_E |w|_{s+1,E} + h_E^s \left|\beta_i\frac{\partial w}{\partial x_i}\right|_{s,E} \leq$$
$$\leq h_E^s \left(\beta_E |w|_{s+1,E} + \|\beta_i\|_{\mathrm{W}^s_\infty(E)} \|w\|_{s+1,E}\right) .$$

□

Lemma 3.2. *For any $w \in \mathrm{H}^1(\Omega)$ and $\forall v_\delta \in V_\delta$,*

$$d_\delta(w, v_\delta) \lesssim \max_{E\in\mathcal{T}_\delta} \frac{\mathsf{K}_E}{\mathsf{K}^\vee_E} \left\|\sqrt{\mathsf{K}}\nabla w\right\| \left\|\sqrt{\mathsf{K}}\nabla v_\delta\right\| . \tag{3.20}$$

Moreover, if $w \in \mathrm{H}^{s+1}(\Omega)$, $\mathsf{K} \in \mathrm{W}^s_\infty(\Omega)$ and $\beta \in \left[\mathrm{W}^{s+1}_\infty(\Omega)\right]^2$ for some $s \in \{0, \dots, k\}$, then

$$|d(w, v_\delta) - d_\delta(w, v_\delta)| \lesssim \max_{E\in\mathcal{T}_\delta} \frac{\|\beta\|_{\mathrm{W}^{s+1}_\infty(E)} \|\mathsf{K}\|_{\mathrm{W}^s_\infty(E)} (\mathsf{K}_E + \beta_E)}{\mathsf{K}_E\beta_E\sqrt{\mathsf{K}^\vee_E}} \times$$
$$\times h^{s+1} \|w\|_{s+1} \left\|\sqrt{\mathsf{K}}\nabla v_\delta\right\| . \tag{3.21}$$

Proof. To prove (3.20), we assume $\nabla\cdot(\mathsf{K}\nabla w) \neq 0$, since otherwise the inequality is obviously true. We use (3.11), the Cauchy-Schwarz inequality, the continuity of Π^0_{k-1} and (3.8): $\forall E \in \mathcal{T}_\delta$,

$$\tau_E \left(\nabla\cdot\left(\mathsf{K}\Pi^0_{k-1}\nabla w\right), \beta\cdot\Pi^0_{k-1}\nabla v_\delta\right)_E \leq \beta_E \frac{h_E}{2\beta_E} \left\|\nabla\cdot\left(\mathsf{K}\Pi^0_{k-1}\nabla w\right)\right\|_E \left\|\Pi^0_{k-1}\nabla v_\delta\right\|_E \lesssim$$
$$\lesssim \frac{1}{2\sqrt{\tilde{C}_E}} \left\|\mathsf{K}\Pi^0_{k-1}\nabla w\right\|_E \|\nabla v_\delta\|_E \lesssim \frac{\mathsf{K}_E}{2\sqrt{\tilde{C}_E}} \left\|\Pi^0_{k-1}\nabla w\right\|_E \|\nabla v_\delta\|_E \lesssim$$
$$\lesssim \frac{\mathsf{K}_E}{2\mathsf{K}^\vee_E\sqrt{\tilde{C}_E}} \left\|\sqrt{\mathsf{K}}\nabla w\right\|_E \left\|\sqrt{\mathsf{K}}\nabla v_\delta\right\|_E .$$

Regarding (3.21), by applying the triangle inequality we have:

$$\left|\sum_{E\in\mathcal{T}_\delta} \tau_E (\nabla\cdot(\mathsf{K}\nabla w), \beta\cdot\nabla v_\delta)_E - \tau_E \left(\nabla\cdot\left(\mathsf{K}\Pi^0_{k-1}\nabla w\right), \beta\cdot\Pi^0_{k-1}\nabla v_\delta\right)_E\right| \leq$$
$$\leq \sum_{E\in\mathcal{T}_\delta} \tau_E \left|\left(\nabla\cdot(\mathsf{K}\nabla w - \mathsf{K}\Pi^0_{k-1}\nabla w), \beta\cdot\nabla v_\delta\right)_E\right|$$
$$+ \tau_E \left|\left(\nabla\cdot\left(\mathsf{K}\Pi^0_{k-1}\nabla w\right), \beta\cdot\left(\nabla v_\delta - \Pi^0_{k-1}\nabla v_\delta\right)\right)_E\right| . \tag{3.22}$$

To estimate the first term of the right-hand-side of (3.22), we suppose

$$\nabla \cdot (\mathsf{K}\nabla w - \mathsf{K}\Pi^0_{k-1}\nabla w) \neq 0\,,$$

and we use the Cauchy-Schwarz inequality, (3.10), (3.8) and (2.14):

$$\begin{aligned}
\tau_E \left|\left(\nabla \cdot (\mathsf{K}\nabla w - \mathsf{K}\Pi^0_{k-1}\nabla w), \beta \cdot \nabla v_\delta\right)_E\right| &\leq \frac{\tilde{C}_E h_E^2 \beta_E}{2\mathsf{K}_E} \left\|\nabla \cdot \left(\mathsf{K}\nabla w - \mathsf{K}\Pi^0_{k-1}\nabla w\right)\right\|_E \times \\
&\times \left\|\nabla v_\delta\right\|_E \leq \frac{\sqrt{\tilde{C}_E} h_E \beta_E}{2\mathsf{K}_E} \left\|\mathsf{K}\nabla w - \mathsf{K}\Pi^0_{k-1}\nabla w\right\|_E \left\|\nabla v_\delta\right\|_E \leq \\
\leq \frac{\sqrt{\tilde{C}_E}\beta_E}{2\sqrt{\mathsf{K}^\vee_E}} h_E \left\|\nabla w - \Pi^0_{k-1}\nabla w\right\|_E \left\|\sqrt{\mathsf{K}}\nabla v_\delta\right\|_E &\lesssim \frac{\sqrt{\tilde{C}_E}\beta_E}{2\sqrt{\mathsf{K}^\vee_E}} h_E^{s+1} \left|w\right|_{s+1,E} \left\|\sqrt{\mathsf{K}}\nabla v_\delta\right\|_E\,.
\end{aligned}$$

Concerning the second term of (3.22), we have

$$\begin{aligned}
\tau_E \left(\nabla \cdot \left(\mathsf{K}\Pi^0_{k-1}\nabla w\right), \beta \cdot \left(\nabla v_\delta - \Pi^0_{k-1}\nabla v_\delta\right)\right)_E &= \\
&= \tau_E \sum_{i=1}^{2} \left(\beta_i \nabla \cdot \left(\mathsf{K}\Pi^0_{k-1}\nabla w\right), \frac{\partial v_\delta}{\partial x_i} - \Pi^0_{k-1}\left(\frac{\partial v_\delta}{\partial x_i}\right)\right)_E\,,
\end{aligned}$$

and we can bound each term of the sum by using the properties of the projection, the Cauchy-Schwarz inequality and the triangle inequality:

$$\begin{aligned}
\tau_E \left(\beta_i \nabla \cdot \left(\mathsf{K}\Pi^0_{k-1}\nabla w\right), \frac{\partial v_\delta}{\partial x_i} - \Pi^0_{k-1}\frac{\partial v_\delta}{\partial x_i}\right)_E &= \\
\tau_E \left(\nabla \cdot \left(\beta_i \mathsf{K}\Pi^0_{k-1}\nabla w\right), \frac{\partial v_\delta}{\partial x_i} - \Pi^0_{k-1}\frac{\partial v_\delta}{\partial x_i}\right)_E &\\
+ \tau_E \left(-\nabla\beta_i \cdot \left(\mathsf{K}\Pi^0_{k-1}\nabla w\right), \frac{\partial v_\delta}{\partial x_i} - \Pi^0_{k-1}\frac{\partial v_\delta}{\partial x_i}\right)_E &= \\
= \tau_E \left(\nabla \cdot \left(\beta_i \mathsf{K}\Pi^0_{k-1}\nabla w\right) - \nabla \cdot \left(\Pi^0_{k-1}\left(\beta_i \mathsf{K}\Pi^0_{k-1}\nabla w\right)\right), \frac{\partial v_\delta}{\partial x_i} - \Pi^0_{k-1}\frac{\partial v_\delta}{\partial x_i}\right)_E &\\
+ \tau_E \left(\Pi^0_{k-1}\left(\nabla\beta_i \cdot \left(\mathsf{K}\Pi^0_{k-1}\nabla w\right)\right) - \nabla\beta_i \cdot \left(\mathsf{K}\Pi^0_{k-1}\nabla w\right), \frac{\partial v_\delta}{\partial x_i} - \Pi^0_{k-1}\frac{\partial v_\delta}{\partial x_i}\right)_E &\lesssim \\
\lesssim \frac{\tau_E}{\sqrt{\mathsf{K}^\vee_E}} \left(\left\|\nabla \cdot \left(\beta_i \mathsf{K}\Pi^0_{k-1}(\nabla w) - \Pi^0_{k-1}\left(\beta_i \mathsf{K}\Pi^0_{k-1}\nabla w\right)\right)\right\|_E\right. &\\
\left. + \left\|\Pi^0_{k-1}\left(\nabla\beta_i \cdot \left(\mathsf{K}\Pi^0_{k-1}\nabla w\right)\right) - \nabla\beta_i \cdot \left(\mathsf{K}\Pi^0_{k-1}\nabla w\right)\right\|_E\right) \left\|\sqrt{\mathsf{K}}\nabla v_\delta\right\|_E\,.
\end{aligned}$$

We consider the two terms inside the parentheses separately. To estimate the first one, we first use the fact that Π^0_{k-1} is the best $\mathrm{L}^2(E)$ approximation in $\mathbb{P}_{k-1}(E)$, then inequalities

(3.10) and (3.8), and finally (2.13) and (2.14):

$$\begin{aligned}
\tau_E \left\|\nabla\cdot\left(\beta_i \mathsf{K}\Pi^0_{k-1}\nabla w - \Pi^0_{k-1}\left(\beta_i\mathsf{K}\Pi^0_{k-1}\nabla w\right)\right)\right\|_E \leq \\
\leq \frac{\tilde{C}_E h_E^2}{2\mathsf{K}_E}\left\|\nabla\cdot\left(\beta_i \mathsf{K}\Pi^0_{k-1}\nabla w - \Pi^0_{k-1}\left(\beta_i\mathsf{K}\Pi^0_{k-1}\nabla w\right)\right)\right\|_E \leq \\
\leq \frac{\sqrt{\tilde{C}_E}h_E}{2\mathsf{K}_E}\left\|\beta_i \mathsf{K}\Pi^0_{k-1}\nabla w - \Pi^0_{k-1}\left(\beta_i\mathsf{K}\Pi^0_{k-1}\nabla w\right)\right\|_E \leq \\
\leq \frac{\sqrt{\tilde{C}_E}h_E}{2\mathsf{K}_E}\left\|\beta_i \mathsf{K}\Pi^0_{k-1}\nabla w - \Pi^0_{k-1}(\beta_i\mathsf{K}\nabla w)\right\|_E \leq \frac{\sqrt{\tilde{C}_E}h_E}{2\mathsf{K}_E}\left(\left\|\beta_i\mathsf{K}\left(\Pi^0_{k-1}\nabla w - \nabla w\right)\right\|_E\right. \\
\left. + \left\|\beta_i\mathsf{K}\nabla w - \Pi^0_{k-1}(\beta_i\mathsf{K}\nabla w)\right\|_E\right) \lesssim \frac{\sqrt{\tilde{C}_E}h_E}{2\mathsf{K}_E}\left(h_E^s\beta_E\mathsf{K}_E\left|w\right|_{s+1,E} + h_E^s\left|\beta_i\mathsf{K}\nabla w\right|_{s,E}\right) \lesssim \\
\lesssim \frac{\sqrt{\tilde{C}_E}h_E^{s+1}}{2\mathsf{K}_E}\left(\beta_E\mathsf{K}_E\left|w\right|_{s+1,E} + \left\|\beta\right\|_{\mathrm{W}^s_\infty(E)}\left\|\mathsf{K}\right\|_{\mathrm{W}^s_\infty(E)}\left\|w\right\|_{s+1,E}\right).
\end{aligned}$$

To estimate the second term we use the fact that Π^0_{k-1} is the best approximation in $\mathbb{P}_{k-1}(E)$, the triangle inequality, inequality (3.11) and the estimates (2.13) and (2.14):

$$\begin{aligned}
\tau_E \left\|\Pi^0_{k-1}\left(\nabla\beta_i\cdot\left(\mathsf{K}\Pi^0_{k-1}\nabla w\right)\right) - \nabla\beta_i\cdot\left(\mathsf{K}\Pi^0_{k-1}\nabla w\right)\right\|_E \leq \\
\leq \tau_E\left\|\Pi^0_{k-1}(\nabla\beta_i\cdot\mathsf{K}\nabla w) - \nabla\beta_i\cdot\mathsf{K}\Pi^0_{k-1}\nabla w\right\|_E \leq \\
\leq \frac{h_E}{2\beta_E}\left(\left\|\Pi^0_{k-1}(\nabla\beta_i\cdot\mathsf{K}\nabla w) - \nabla\beta_i\cdot\mathsf{K}\nabla w\right\|_E + \left\|\nabla\beta_i\cdot\mathsf{K}\left(\nabla w - \Pi^0_{k-1}\nabla w\right)\right\|_E\right) \lesssim \\
\lesssim \frac{h_E}{2\beta_E}\left(h_E^s\left|\nabla\beta_i\cdot\mathsf{K}\nabla w\right|_{s,E} + h_E^s\mathsf{K}_E\left\|\beta\right\|_{\mathrm{W}^1_\infty(E)}\left|w\right|_{s+1,E}\right) \lesssim \\
\lesssim \frac{h_E^{s+1}}{2\beta_E}\left(\left\|\mathsf{K}\right\|_{\mathrm{W}^s_\infty(E)}\left\|\beta\right\|_{\mathrm{W}^{s+1}_\infty(E)}\left\|w\right\|_{s+1,E} + \mathsf{K}_E\left\|\beta\right\|_{\mathrm{W}^1_\infty(E)}\left|w\right|_{s+1,E}\right).
\end{aligned}$$

□

Lemma 3.3. *For any $w \in \mathrm{H}^1(\Omega)$ and $\forall v_\delta \in V_\delta$,*

$$a_\delta(w, v_\delta) \lesssim \max_{E\in\mathcal{T}_\delta}\frac{\mathsf{K}_E + \tau_E\beta_E^2}{\mathsf{K}_E^\vee}\left\|\sqrt{\mathsf{K}}\nabla w\right\|\left\|\sqrt{\mathsf{K}}\nabla v_\delta\right\|. \tag{3.23}$$

Moreover, if $w \in \mathrm{H}^{s+1}(\Omega)$, $\mathsf{K} \in \mathrm{W}^s_\infty(\Omega)$ and $\beta \in [\mathrm{W}^s_\infty(\Omega)]$ for some $s \in \{0,\dots,k\}$, then

$$\left|a(w, v_\delta) - a_\delta(w, v_\delta)\right| \lesssim \left(\max_{E\in\mathcal{T}_\delta}\frac{\left\|\mathsf{K}\right\|_{\mathrm{W}^s_\infty(E)} + \frac{\left\|\beta\right\|^2_{\mathrm{W}^s_\infty(E)}}{\beta_E}}{\sqrt{\mathsf{K}_E^\vee}}\right)h^s\left\|w\right\|_{s+1}\left\|\sqrt{\mathsf{K}}\nabla v_\delta\right\|. \tag{3.24}$$

Proof. Let $v_\delta \in V_\delta$, $w \in \mathrm{H}^1(\Omega)$. We first prove (3.23) considering $E \in \mathcal{T}_\delta$. Regarding the terms involving the VEM stabilization, we first point out that, as a consequence of (2.8), we have

$$S^E\left(\left(I - \Pi^\nabla_k\right)w, \left(I - \Pi^\nabla_k\right)v_\delta\right) \lesssim \left\|\nabla\left(w - \Pi^\nabla_k w\right)\right\|_E\left\|\nabla\left(v_\delta - \Pi^\nabla_k v_\delta\right)\right\|_E. \tag{3.25}$$

Applying the Cauchy-Schwarz inequality, (3.25) and the continuity of projectors,

$$a_\delta^E(w,v_\delta) = \left(\mathsf{K}\Pi_{k-1}^0\nabla w, \Pi_{k-1}^0\nabla v_\delta\right)_E + \tau_E\left(\beta\cdot\Pi_{k-1}^0\nabla w, \beta\cdot\Pi_{k-1}^0\nabla v_\delta\right)_E\left(\mathsf{K}_E+\tau_E\beta_E^2\right)\times$$
$$\times S^E\left(\left(I-\Pi_k^\nabla\right)w, \left(I-\Pi_k^\nabla\right)v_\delta\right) \lesssim \left(\mathsf{K}_E+\tau_E\beta_E^2\right)\left(\left\|\Pi_{k-1}^0\nabla w\right\|_E\left\|\Pi_{k-1}^0\nabla v_\delta\right\|_E\right.$$
$$\left.+\left\|\left(I-\Pi_k^\nabla\right)w\right\|_E\left\|\left(I-\Pi_k^\nabla\right)v_\delta\right\|_E\right) \lesssim \frac{\mathsf{K}_E+\tau_E\beta_E^2}{\mathsf{K}_E^\vee}\left\|\sqrt{\mathsf{K}}\nabla w\right\|_E\left\|\sqrt{\mathsf{K}}\nabla v_\delta\right\|_E.$$

Concerning (3.24), by adding and subtracting

$$\left(\mathsf{K}\nabla w, \Pi_{k-1}^0\nabla v_\delta\right)_E = \left(\Pi_{k-1}^0(\mathsf{K}\nabla w), \nabla v_\delta\right)_E$$

and

$$\left(\beta\beta^\intercal\nabla w, \Pi_{k-1}^0\nabla v_\delta\right)_E = \left(\Pi_{k-1}^0(\beta\beta^\intercal\nabla w), \nabla v_\delta\right)_E$$

and exploiting the triangle inequality we have, $\forall E\in\mathcal{T}_\delta$,

$$\left|a^E(w,v_\delta)-a_\delta^E(w,v_\delta)\right| \le \left|\left(\mathsf{K}\nabla w-\mathsf{K}\Pi_{k-1}^0\nabla w, \Pi_{k-1}^0\nabla v_\delta\right)_E\right|$$
$$+\left|\left(\mathsf{K}\nabla w-\Pi_{k-1}^0(\mathsf{K}\nabla w), \nabla v_\delta\right)_E\right| + \left(\mathsf{K}_E+\tau_E\beta_E^2\right)\left|S^E\left(\left(I-\Pi_k^\nabla\right)w, \left(I-\Pi_k^\nabla\right)v_\delta\right)\right|$$
$$+\tau_E\left|\left(\beta\beta^\intercal\nabla w-\beta\beta^\intercal\Pi_{k-1}^0\nabla w, \Pi_{k-1}^0\nabla v_\delta\right)_E\right| + \tau_E\left|\left(\beta\beta^\intercal\nabla w-\Pi_{k-1}^0(\beta\beta^\intercal\nabla w), \nabla v_\delta\right)_E\right|.$$

The first term is bounded as follows, exploiting the definition of projection, its continuity and (2.14):

$$\left(\mathsf{K}\left(\nabla w-\Pi_{k-1}^0\nabla w\right), \Pi_{k-1}^0\nabla v_\delta\right)_E \lesssim \sqrt{\mathsf{K}_E}\left\|\nabla w-\Pi_{k-1}^0\nabla w\right\|_E\left\|\sqrt{\mathsf{K}}\nabla v_\delta\right\|_E \lesssim$$
$$\lesssim \sqrt{\mathsf{K}_E}h_E^s\left|w\right|_{s+1,E}\left\|\sqrt{\mathsf{K}}\nabla v_\delta\right\|_E. \quad (3.26)$$

The second term is bounded by the Cauchy-Schwarz inequality and (2.13):

$$\left(\mathsf{K}\nabla w-\Pi_{k-1}^0(\mathsf{K}\nabla w), \nabla v_\delta\right)_E \le \left\|\mathsf{K}\nabla w-\Pi_{k-1}^0(\mathsf{K}\nabla w)\right\|_E\left\|\nabla v_\delta\right\|_E \lesssim$$
$$\lesssim h_E^s\left|\mathsf{K}\nabla w\right|_{s,E}\left\|\nabla v_\delta\right\|_E \le h_E^s\frac{\left\|\mathsf{K}\right\|_{\mathrm{W}_\infty^s(E)}}{\sqrt{\mathsf{K}_E^\vee}}\left\|w\right\|_{s+1,E}\left\|\sqrt{\mathsf{K}}\nabla v_\delta\right\|. \quad (3.27)$$

The third term is estimated using (3.11), the Cauchy-Schwarz inequality, the continuity of Π_{k-1}^0 and (2.14):

$$\tau_E\left(\beta\beta^\intercal\left(\nabla w-\Pi_{k-1}^0\nabla w\right), \Pi_{k-1}^0\nabla v_\delta\right)_E \lesssim \frac{\beta_E}{2}h_E\left\|\nabla w-\Pi_{k-1}^0\nabla w\right\|_E\left\|\nabla v_\delta\right\|_E \lesssim$$
$$\lesssim \frac{\beta_E}{2\sqrt{\mathsf{K}_E^\vee}}h_E^{s+1}\left|w\right|_{s+1,E}\left\|\sqrt{\mathsf{K}}\nabla v_\delta\right\|_E \lesssim \frac{\left\|\beta\right\|_{\mathrm{W}_\infty^s(E)}^2}{\beta_E\sqrt{\mathsf{K}_E^\vee}}h_E^{s+1}\left|w\right|_{s+1,E}\left\|\sqrt{\mathsf{K}}\nabla v_\delta\right\|_E.$$

The fourth term can be estimated similarly:

$$\tau_E\left(\beta\beta^\intercal\nabla w-\Pi_{k-1}^0(\beta\beta^\intercal\nabla w), \nabla v_\delta\right)_E \lesssim \tau_E\left\|\beta\beta^\intercal\nabla w-\Pi_{k-1}^0(\beta\beta^\intercal\nabla w)\right\|_E\left\|\nabla v_\delta\right\| \lesssim$$
$$\lesssim \tau_E\frac{h_E^s}{\sqrt{\mathsf{K}_E^\vee}}\left|\beta\beta^\intercal\nabla w\right|_{s,E}\left\|\sqrt{\mathsf{K}}\nabla v_\delta\right\|_E \lesssim \frac{\left\|\beta\right\|_{\mathrm{W}_\infty^s(E)}^2}{\beta_E\sqrt{\mathsf{K}_E^\vee}}h_E^{s+1}\left\|w\right\|_{s+1,E}\left\|\sqrt{\mathsf{K}}\nabla v_\delta\right\|.$$

Finally, we consider the terms involving the VEM stabilization and, applying again (3.25), we are left to estimate projection errors. Proceeding as above, exploiting the continuity of Π_k^∇, (2.15) and the estimate on τ_E in (3.11) we obtain

$$\mathsf{K}_E \left\|\nabla\left(w-\Pi_k^\nabla w\right)\right\|_E \left\|\nabla\left(v_\delta-\Pi_k^\nabla v_\delta\right)\right\|_E \leq \frac{\mathsf{K}_E}{\sqrt{\mathsf{K}_E^\vee}} h_E^s \left|w\right|_{s+1,E} \left\|\sqrt{\mathsf{K}}\nabla v_\delta\right\|_E , \tag{3.28}$$

$$\tau_E\beta_E^2 \left\|\nabla\left(w-\Pi_k^\nabla w\right)\right\|_E \left\|\nabla\left(v_\delta-\Pi_k^\nabla v_\delta\right)\right\|_E \leq \frac{\beta_E}{2\sqrt{\mathsf{K}_E^\vee}} h_E^{s+1} \left|w\right|_{s+1,E} \left\|\sqrt{\mathsf{K}}\nabla v_\delta\right\|_E .$$

□

3.4.2 Well-posedness of the discrete problem.

In this subsection we prove, in Theorem 3.1, an inf-sup condition for the discrete bilinear form defined by (3.12), which ensures the well-posedness of problem (3.16).

Lemma 3.4. *There exist a constant $\alpha > 0$ such that*

$$a_\delta(v_\delta, v_\delta) \geq \alpha \left\|\!\left| v_\delta \right|\!\right\|^2 \quad \forall v_\delta \in V_\delta . \tag{3.29}$$

Proof. Let $v_\delta \in V_\delta$ and fix $E \in \mathcal{T}_\delta$. From the definition of a_δ in (3.13) we have

$$\begin{aligned} a_\delta^E(v_\delta, v_\delta) := & \left\|\sqrt{\mathsf{K}}\Pi_{k-1}^0\nabla v_\delta\right\|_E^2 + \tau_E \left\|\beta\cdot\Pi_{k-1}^0\nabla v_\delta\right\|_E^2 \\ & + \left(\mathsf{K}_E + \tau_E\beta_E^2\right) S^E\left(\left(I-\Pi_k^\nabla\right)v_\delta, \left(I-\Pi_k^\nabla\right)v_\delta\right) . \end{aligned}$$

From (2.8) and the properties of the orthogonal projection, we have that there exists $c^* > 0$ such that, $\forall E \in \mathcal{T}_\delta$,

$$S^E\left(\left(I-\Pi_k^\nabla\right)v_\delta, \left(I-\Pi_k^\nabla\right)v_\delta\right) \geq c^* \left\|\nabla\left(v_\delta-\Pi_k^\nabla v_\delta\right)\right\|_E^2 \geq c^* \left\|\nabla v_\delta - \Pi_{k-1}^0\nabla v_\delta\right\|_E^2 ,$$

and then

$$\begin{aligned} \left(\mathsf{K}_E + \tau_E\beta_E^2\right) S^E\left(\left(I-\Pi_k^\nabla\right)v_\delta, \left(I-\Pi_k^\nabla\right)v_\delta\right) & \geq c^* \left(\mathsf{K}_E + \tau_E\beta_E^2\right) \left\|\nabla v_\delta - \Pi_{k-1}^0\nabla v_\delta\right\|_E^2 \geq \\ & \geq c^* \left(\left\|\sqrt{\mathsf{K}}\left(\nabla v_\delta - \Pi_{k-1}^0\nabla v_\delta\right)\right\|_E^2 + \tau_E \left\|\beta\cdot\left(\nabla v_\delta - \Pi_{k-1}^0\nabla v_\delta\right)\right\|_E^2\right) . \end{aligned}$$

The thesis is thus proven choosing $\alpha = \min\{c^*, 1\}$:

$$\begin{aligned} a_\delta^E(v_\delta, v_\delta) \geq & \left\|\sqrt{\mathsf{K}}\Pi_{k-1}^0\nabla v_\delta\right\|_E^2 + \sum_{E\in\mathcal{T}_\delta} \tau_E \left\|\beta\cdot\Pi_{k-1}^0\nabla v_\delta\right\|_E^2 + c^* \left(\left\|\sqrt{\mathsf{K}}\left(\nabla v_\delta - \Pi_{k-1}^0\nabla v_\delta\right)\right\|_E^2\right. \\ & \left. + \tau_E \left\|\beta\cdot\left(\nabla v_\delta - \Pi_{k-1}^0\nabla v_\delta\right)\right\|_E^2\right) \geq \min\{c^*, 1\} \left(\left\|\sqrt{\mathsf{K}}\Pi_{k-1}^0\nabla v_\delta\right\|^2\right. \\ & \left. + \left\|\sqrt{\mathsf{K}}\left(\nabla v_\delta - \Pi_{k-1}^0\nabla v_\delta\right)\right\|^2 + \tau_E \left\|\beta\cdot\Pi_{k-1}^0\nabla v_\delta\right\|_E^2 + \tau_E \left\|\beta\cdot\left(\nabla v_\delta - \Pi_{k-1}^0\nabla v_\delta\right)\right\|_E^2\right) \geq \\ & \geq \{c^*, 1\} \left(\left\|\sqrt{\mathsf{K}}\nabla v_\delta\right\|^2 + \tau_E \left\|\beta\cdot\nabla v_\delta\right\|_E^2\right) . \end{aligned}$$

□

Lemma 3.5. *Let $q \in \mathrm{H}_0^1(\Omega)$. Then there exists $q^* \in V_\delta$ such that*

$$a_\delta(q^*, v_\delta) = a(q, v_\delta) \quad \forall v_\delta \in V_\delta \,.$$

Moreover,

$$|||q^*||| \leq \frac{1}{\alpha} |||q||| \,, \tag{3.30}$$

$$\|q - q^*\| \precsim h \, |||q||| \,, \tag{3.31}$$

being α the coercivity constant in (3.29).

Proof. The proof is formally the same as the one in [2, Lemma 5.6]. The well-posedness of Lemma 3.5 follows from the coercivity of a_δ on V_δ (see Lemma 3.4). By (3.29) and Lax-Milgram Lemma, we also have the estimate (3.30):

$$|||q_\delta^*|||^2 \leq \frac{1}{\alpha} a_\delta(q_\delta^*, q_\delta^*) = \frac{1}{\alpha} a(q^*, q_\delta) \leq \frac{1}{\alpha} |||q^*||| \, |||q_\delta^*||| \,.$$

To prove (3.31), we define $\psi \in \mathrm{H}^2(\Omega) \cap \mathrm{H}_0^1(\Omega)$ as the solution of

$$-\Delta\psi = q^* - q_\delta^* \quad \text{in } \mathrm{L}^2(\Omega) \,. \tag{3.32}$$

As solution of the above problem, ψ statisfies the following estimate:

$$\|\Delta\psi\| \leq \|q^* - q_\delta^*\| \,. \tag{3.33}$$

Let $\psi_I \in V_\delta$ be the VEM interpolant of ψ. We know from a simple application of [2, Lemma 5.1] and since the interpolation is a continuous operator that

$$\|\nabla(\psi - \psi_I)\| \lesssim h \, |\psi|_2 \,, \tag{3.34}$$

$$|\psi_I|_2 \lesssim |\psi|_2 \,. \tag{3.35}$$

From Lemma 3.5, (3.32), (3.24), (3.35), (3.33) and (3.34) we have, since $q^* - q_\delta^* \in \mathrm{H}_0^1(\Omega)$,

$$\begin{aligned} \|q^* - q_\delta^*\|^2 = (q^* - q_\delta^*, q^* - q_\delta^*) = a(\psi, q^* - q_\delta^*) = a(\psi - \psi_I, q^* - q_\delta^*) + a(\psi_I, q^* - q_\delta^*) = \\ = a(\psi - \psi_I, q^* - q_\delta^*) + a_\delta(\psi_I, q_\delta^*) - a(\psi_I, q_\delta^*) \leq a(\psi - \psi_I, q^* - q_\delta^*) + |a_\delta(\psi_I, q_\delta^*) - a(\psi_I, q_\delta^*)| \lesssim \\ \lesssim |||\psi - \psi_I||| \, |||q^* - q_\delta^*||| + h \, |\psi_I|_2 \left\| \sqrt{\mathsf{K}} \nabla q_\delta^* \right\| \lesssim h \, |\psi|_2 \, |||q^*||| \leq h \, |\psi|_2 \, |||q^*||| \,, \end{aligned}$$

and the proof is concluded because

$$|\psi|_2 \lesssim \|\Delta\psi\| \leq \|q^* - q_\delta^*\| \,.$$

□

Lemma 3.6. *For any $v_\delta \in V_\delta$,*

$$\mathscr{B}_{\mathrm{supg}}(v_\delta, v_\delta) \geq \frac{1}{2} |||v_\delta|||^2 \,. \tag{3.36}$$

Proof. Let $v_\delta \in V_\delta$. Since we have homogeneous Dirichlet boundary conditions and $\nabla \cdot \beta = 0$, it holds

$$(\beta \cdot \nabla v_\delta, v_\delta) = -\frac{1}{2} \left(\nabla \cdot \beta, v_\delta^2 \right) = 0 \,.$$

We have, using the definition of $\mathscr{B}_{\text{supg}}$, and the Cauchy-Schwarz and Young inequalities and the estimate (3.8),

$$\begin{aligned}\mathscr{B}_{\text{supg}}(v_\delta, v_\delta) &= \left\|\sqrt{\mathsf{K}}\nabla v_\delta\right\|^2 + \sum_{E\in\mathcal{T}_\delta} \tau_E \left\|\beta\cdot\nabla v_\delta\right\|_E^2 - \tau_E \left(\nabla\cdot\left(\sqrt{\mathsf{K}}\nabla v_\delta\right), \beta\cdot\nabla v_\delta\right)_E \geq \\ &\geq \left\|\sqrt{\mathsf{K}}\nabla v_\delta\right\|^2 + \sum_{E\in\mathcal{T}_\delta} \tau_E \left\|\beta\cdot\nabla v_\delta\right\|_E^2 - \tau_E \left\|\nabla\cdot\left(\sqrt{\mathsf{K}}\nabla v_\delta\right)\right\|_E \left\|\beta\cdot\nabla v_\delta\right\|_E \geq \\ &\geq \left\|\sqrt{\mathsf{K}}\nabla v_\delta\right\|_E^2 + \sum_{E\in\mathcal{T}_\delta} \frac{1}{2}\tau_E \left\|\beta\cdot\nabla v_\delta\right\|_E^2 - \frac{1}{2}\tau_E \left\|\nabla\cdot(\mathsf{K}\nabla v_\delta)\right\|_E^2 \geq \left\|\sqrt{\mathsf{K}}\nabla v_\delta\right\|^2 \\ -\sum_{E\in\mathcal{T}_\delta}\frac{1}{4}\left\|\sqrt{\mathsf{K}}\nabla v_\delta\right\|_E^2 &+ \frac{1}{2}\tau_E \left\|\beta\cdot\nabla v_\delta\right\|_E^2 \geq \frac{3}{4}\left\|\sqrt{\mathsf{K}}\nabla v_\delta\right\|^2 + \sum_{E\in\mathcal{T}_\delta}\frac{1}{2}\tau_E\left\|\beta\cdot\nabla v_\delta\right\|_E^2 \geq \frac{1}{2}\left|\!\left|\!\left|v_\delta\right|\!\right|\!\right|^2 .\end{aligned}$$

□

Theorem 3.1. *Suppose* $\mathsf{K}\in \mathrm{L}^\infty(\Omega)$ *and* $\beta\in\left[\mathrm{W}^1_\infty(\Omega)\right]^2$. *Then,* $\forall v_\delta\in V_\delta$ *and for* h *sufficiently small,*

$$\sup_{w_\delta\in V_\delta}\frac{\mathscr{B}_{\text{supg},\delta}(v_\delta, w_\delta)}{\left|\!\left|\!\left|w_\delta\right|\!\right|\!\right|} \gtrsim \left|\!\left|\!\left|v_\delta\right|\!\right|\!\right| . \tag{3.37}$$

Proof. Let $v_\delta\in V_\delta$ be fixed and let $v_\delta^*\in V_\delta$ be the function, whose existence is guaranteed by Lemma 3.5, such that $a_\delta(v_\delta^*, w_\delta) = a(v_\delta, w_\delta)$, $\forall w_\delta\in V_\delta$. By definitions (3.2) and (3.12), since a_δ is symmetric, we have, by (3.36),

$$\begin{aligned}\mathscr{B}_{\text{supg},\delta}(v_\delta, v_\delta^*) &= a_\delta(v_\delta, v_\delta^*) + b_\delta(v_\delta, v_\delta^*) + d_\delta(v_\delta, v_\delta^*) = a(v_\delta, v_\delta) + b_\delta(v_\delta, v_\delta^*) + d_\delta(v_\delta, v_\delta^*) = \\ &= \mathscr{B}_{\text{supg}}(v_\delta, v_\delta) + r\left(v_\delta, v_\delta^*\right) \geq \frac{1}{2}\left|\!\left|\!\left|v_\delta\right|\!\right|\!\right|^2 + r\left(v_\delta, v_\delta^*\right) ,\end{aligned}$$

where

$$r\left(v_\delta, v_\delta^*\right) = b_\delta(v_\delta, v_\delta^*) - b(v_\delta, v_\delta^*) + b(v_\delta, v_\delta^* - v_\delta) + d_\delta(v_\delta, v_\delta^*) - d(v_\delta, v_\delta^*) + d(v_\delta, v_\delta^* - v_\delta) .$$

By Lemmas 3.1 and 3.2, the continuity of b and d, that can be proven as for (3.18) and (3.20), and by (3.30) and (3.31), there exists a constant $C_r > 0$ depending on $\|\mathsf{K}\|_{\mathrm{L}^\infty(\mathsf{K})}$, $\|\beta\|_{\mathrm{W}^1_\infty(\Omega)}$ and on the approximation constants in (2.13), (2.14) and (2.15), such that

$$\left|r\left(v_\delta, v_\delta^*\right)\right| \leq C_r h \left\|\sqrt{\mathsf{K}}\nabla v_\delta\right\| \left\|\sqrt{\mathsf{K}}\nabla v_\delta^*\right\| \leq C_r h \left|\!\left|\!\left|v_\delta\right|\!\right|\!\right| \left|\!\left|\!\left|v_\delta^*\right|\!\right|\!\right| \leq C_r h \left|\!\left|\!\left|v_\delta\right|\!\right|\!\right|^2 . \tag{3.38}$$

Then, by (3.30) and (3.38) the following lower bound holds:

$$\mathscr{B}_{\text{supg},\delta}(v_\delta, v_\delta) \geq \frac{1}{2}\left|\!\left|\!\left|v_\delta\right|\!\right|\!\right|^2 + r\left(v_\delta, v_\delta^*\right) \geq \left(\frac{\alpha}{2} - C_r h\right)\left|\!\left|\!\left|v_\delta\right|\!\right|\!\right| \left|\!\left|\!\left|v_\delta^*\right|\!\right|\!\right| ,$$

which yields the thesis for

$$h < \frac{\alpha}{2C_r} .$$

□

3.4.3 A priori error estimate.

To derive an a priori estimate that shows optimality of the rate of convergence of this SUPG approach, we use the estimate (2.16) on the VEM interpolator with $s \geq 2$.

We are now ready to prove the following result.

Theorem 3.2. *Suppose $u \in \mathrm{H}^{s+1}(\Omega)$, $f \in \mathrm{H}^{s}(\Omega)$, $\mathsf{K} \in \mathrm{W}^{s}_{\infty}(\Omega)$, $\beta \in \left[\mathrm{W}^{s+1}_{\infty}(\Omega)\right]^2$ for some $s \in \{1, \ldots, k\}$. Then, for h sufficiently small,*

$$\left|\!\left|\!\left| u - u_\delta \right|\!\right|\!\right| \precsim h^s \left(\|u\|_{s+1} + \|f\|_s \right) . \tag{3.39}$$

Proof. First, by the triangle inequality we have

$$\left|\!\left|\!\left| u - u_\delta \right|\!\right|\!\right|^2 \leq \left|\!\left|\!\left| u - u_I \right|\!\right|\!\right|^2 + \left|\!\left|\!\left| u_\delta - u_I \right|\!\right|\!\right|^2 ,$$

and, by (2.16),

$$\begin{aligned}\left|\!\left|\!\left| u - u_I \right|\!\right|\!\right|^2 &= \sum_{E\in\mathcal{T}_\delta} \left\| \sqrt{\mathsf{K}} \nabla \left(u - u_I\right) \right\|^2_E + \left\| \beta \cdot \nabla \left(u - u_I\right) \right\|^2_E \leq \\ &\leq \sum_{E\in\mathcal{T}_\delta} \left(\mathsf{K}_E + \beta_E^2 \right) \left\| \nabla \left(u - u_I\right) \right\|^2_E \lesssim \sum_{E\in\mathcal{T}_\delta} \left(\mathsf{K}_E + \beta_E^2 \right) h_E^{2s} \left|u\right|^2_{s+1,E} .\end{aligned}$$

We are left to estimate the norm of $e_\delta := u_\delta - u_I$. Since $e_\delta \in V_\delta$, by (3.37) there exists $w_\delta \in V_\delta$ such that

$$\mathscr{B}_{\mathrm{supg},\delta}(e_\delta, w_\delta) \gtrsim \left|\!\left|\!\left| e_\delta \right|\!\right|\!\right| \left|\!\left|\!\left| w_\delta \right|\!\right|\!\right| .$$

Using the exact and discrete problems (3.9) and (3.16),

$$\begin{aligned}\left|\!\left|\!\left| e_\delta \right|\!\right|\!\right| \left|\!\left|\!\left| w_\delta \right|\!\right|\!\right| &\precsim \mathscr{B}_{\mathrm{supg},\delta}(u_\delta - u_I, w_\delta) = F_{\mathrm{supg},\delta}(w_\delta) - \mathscr{B}_{\mathrm{supg},\delta}(u_I, w_\delta) = \\ &= F_{\mathrm{supg},\delta}(w_\delta) - F_{\mathrm{supg}}(w_\delta) + \mathscr{B}_{\mathrm{supg}}(u, w_\delta) - \mathscr{B}_{\mathrm{supg},\delta}(u_I, w_\delta) = F_{\mathrm{supg},\delta}(w_\delta) \\ &\quad - F_{\mathrm{supg}}(w_\delta) + \mathscr{B}_{\mathrm{supg},\delta}(u - u_I, w_\delta) + \mathscr{B}_{\mathrm{supg}}(u, w_\delta) - \mathscr{B}_{\mathrm{supg},\delta}(u, w_\delta) .\end{aligned} \tag{3.40}$$

Note that for our choice of the degrees of freedom and stabilization (defined in (2.9)), it makes sense to compute $\mathscr{B}_{\mathrm{supg},\delta}(u, w_\delta)$ as in (3.12)–(3.15), because $u \in \mathrm{H}^2(\Omega) \subset \mathrm{C}^0(\Omega)$ for $\Omega \subset \mathbb{R}^2$. If the solution u does not have the regularity for pointwise evaluation, definition (2.9) for the VEM-stabilization function has to be properly modified.

The first difference in (3.40) can be written as:

$$F_{\mathrm{supg},\delta}(w_\delta) - F_{\mathrm{supg}}(w_\delta) = \sum_{E\in\mathcal{T}_\delta} \left(f, \left(\Pi^0_{k-1} - I\right) w_\delta + \beta \cdot \left(\Pi^0_{k-1} - I\right) \nabla w_\delta \right)_E . \tag{3.41}$$

The first term of the sum in (3.41) is bounded as follows:

$$\begin{aligned}\left(f, \left(\Pi^0_{k-1} - I\right) w_\delta \right) &= \left(\left(I - \Pi^0_{k-1}\right) f, \left(\Pi^0_{k-1} - I\right) w_\delta \right) \leq \left\| f - \Pi^0_{k-1} f \right\|_E \times \\ &\times \left\| w_\delta - \Pi^0_{k-1} w_\delta \right\|_E \lesssim h_E^{s-1} \left|f\right|_{s-1,E} h_E \left\|\nabla w_\delta\right\| \leq \frac{h_E^s}{\sqrt{\mathsf{K}^\vee_E}} \left|f\right|_{s-1,E} \left\| \sqrt{\mathsf{K}} \nabla w_\delta \right\|_E \leq \\ &\leq \frac{h_E^s}{\sqrt{\mathsf{K}^\vee_E}} \left|f\right|_{s-1,E} \left\| w_\delta \right\|_E .\end{aligned} \tag{3.42}$$

The second term of the sum in (3.41) can be treated as follows:

$$\begin{aligned}\left(f, \beta\cdot\left(\Pi^0_{k-1}-I\right)\nabla w_\delta\right)_E &= \sum_{i=1}^{2}\left(\left(\Pi^0_{k-1}-I\right)(\beta_i f), \frac{\partial w_\delta}{\partial x_i}\right)_E \leq \\ &\leq \sum_{i=1}^{2}\left\|\left(I-\Pi^0_{k-1}\right)(\beta_i f)\right\|_E \left\|\frac{\partial w_\delta}{\partial x_i}\right\|_E \lesssim \frac{h^s}{\sqrt{\mathsf{K}^\vee_E}}\sum_{i=1}^{2}|\beta_i f|_{s,E}\left\|\sqrt{\mathsf{K}}\nabla w_\delta\right\|_E \leq \\ &\leq \frac{\|\beta\|_{\mathrm{W}^s_\infty(E)}}{\sqrt{\mathsf{K}^\vee_E}} h^s_E \|f\|_{s,E} |\!|\!| w_\delta |\!|\!|_E \ . \end{aligned} \tag{3.43}$$

Going back to (3.40), we estimate the continuity of $\mathscr{B}_{\mathrm{supg},\delta}$, given by (3.18), (3.20) and (3.23), and the estimate on the VEM interpolator in (2.16):

$$\begin{aligned}\mathscr{B}_{\mathrm{supg}}(u-u_I, w_\delta) &= \left(\mathsf{K}\nabla(u-u_I), \nabla w_\delta\right) + \left(\beta\cdot\nabla(u-u_I), w_\delta\right) + \sum_{E\in\mathcal{T}_\delta}\tau_E \times \\ &\times\left(\beta\cdot\nabla(u-u_I) - \nabla\cdot\left(\mathsf{K}\nabla(u-u_I)\right), \beta\cdot\nabla w_\delta\right)_E = \left(\mathsf{K}\nabla(u-u_I), \nabla w_\delta\right) \\ &- \left(u-u_I, \beta\cdot\nabla w_\delta\right) + \sum_{E\in\mathcal{T}_\delta}\tau_E\left(\beta\cdot\nabla(u-u_I) - \nabla\cdot\left(\mathsf{K}\nabla(u-u_I)\right), \beta\cdot\nabla w_\delta\right)_E \leq \\ &\leq \left\|\sqrt{\mathsf{K}}\nabla(u-u_I)\right\|\left\|\sqrt{\mathsf{K}}\nabla w_\delta\right\| + \|u-u_I\|\,\|\beta\cdot\nabla w_\delta\| + \sum_{E\in\mathcal{T}_\delta}\left(\tau_E\|\beta\cdot\nabla(u-u_I)\|_E\right. \\ &\left.+\tau_E\|\nabla\cdot\left(\mathsf{K}\nabla(u-u_I)\right)\|_E\right)\|\beta\cdot\nabla w_\delta\|_E \leq \left(\left\|\sqrt{\mathsf{K}}\nabla(u-u_I)\right\|^2 + \sum_{E\in\mathcal{T}_\delta}\tau_E^{-1}\|u-u_I\|^2_E\right. \\ &\left.+\tau_E\|\beta\cdot\nabla(u-u_I)\|^2_E + \tau_E\|\nabla\cdot\left(\mathsf{K}\nabla(u-u_I)\right)\|^2_E\right)^{\frac{1}{2}} |\!|\!| w_\delta |\!|\!| \lesssim \\ &\lesssim \left[\sum_{E\in\mathcal{T}_\delta} h^{2s}_E\left(\frac{\|\mathsf{K}\|^2_{\mathrm{W}^1_\infty(E)}}{\mathsf{K}^2_E}\beta_E h_E H\left(\mathrm{Pe}_E-1\right) + \|\mathsf{K}\|_{\mathrm{W}^1_\infty(E)} H\left(1-\mathrm{Pe}_E\right)\right)\right]^{\frac{1}{2}} \|u\|_{s+1} |\!|\!| w_\delta |\!|\!| \ . \end{aligned}$$

The estimate of the last difference in (3.40) is obtained by applying (3.19), (3.21) and (3.24):

$$\begin{aligned}\left|\mathscr{B}_{\mathrm{supg}}(u, w_\delta) - \mathscr{B}_{\mathrm{supg},\delta}(u, w_\delta)\right| &\leq |a(u, w_\delta) - a_\delta(u, w_\delta)| \\ &+ |b(u, w_\delta) - b_\delta(u, w_\delta)| + |d(u, w_\delta) - d_\delta(u, w_\delta)| \precsim h^s \|u\|_{s+1} \|w_\delta\|_1 \ . \end{aligned}$$

From all of the above results we obtain

$$|\!|\!| u_\delta - u_I |\!|\!| \precsim h^s\left(\|u\|_{s+1} + \|f\|_s\right) \ . \tag{3.44}$$

□

Finally, we end this section with an $\mathrm{L}^2(\Omega)$ a priori error estimate, resorting to classical duality arguments.

Theorem 3.3. *Suppose $u \in \mathrm{H}^{s+1}(\Omega)$, $f \in \mathrm{H}^s(\Omega)$, $\mathsf{K} \in \mathrm{W}^s_\infty(\Omega)$, $\beta \in \left[\mathrm{W}^{s+1}_\infty(\Omega)\right]^2$ for some $s \in \{1, \ldots, k\}$. Then, for h sufficiently small,*

$$\|u - u_\delta\| \precsim h^{s+1}\left(\|u\|_{s+1} + \|f\|_s\right) \ . \tag{3.45}$$

Proof. Let $\mathscr{B}^*\colon \mathrm{H}^1_0(\Omega)\times\mathrm{H}^1_0(\Omega)\to\mathbb{R}$ be the adjoint operator of $\mathscr{B}$, such that $\mathscr{B}^*(w,v) = (\mathsf{K}\nabla w,\nabla v) - (\beta\cdot\nabla w, v)$. Let $\psi\in\mathrm{H}^2(\Omega)\cap\mathrm{H}^1_0(\Omega)$ be the solution of

$$\mathscr{B}^*(\psi,v) = (u-u_\delta,v)\quad\forall v\in\mathrm{H}^1_0(\Omega)\,,$$

and let ψ_I be the VEM interpolant of ψ. From (2.16) and the definition of ψ we get

$$|\!|\!|\psi-\psi_I|\!|\!| \precsim h\,|\psi|_2 \precsim h\,\|u-u_\delta\|\,, \tag{3.46}$$

$$\|\nabla\psi\| \precsim \|u-u_\delta\|\,. \tag{3.47}$$

Then, setting $\forall E\in\mathcal{T}_\delta$

$$\mathcal{E}_{\mathrm{supg}}(u-u_\delta,\psi_I) := \sum_{E\in\mathcal{T}_\delta}\tau_E\left(\beta\cdot\nabla(u-u_\delta)+\nabla\cdot(\mathsf{K}\nabla(u-u_\delta)),\beta\cdot\nabla\psi_I\right)_E,$$

we have

$$\begin{aligned}\|u-u_\delta\|^2 &= \mathscr{B}^*(\psi,u-u_\delta) = \mathscr{B}(u-u_\delta,\psi) = \mathscr{B}(u-u_\delta,\psi-\psi_I)+\mathscr{B}(u-u_\delta,\psi_I) =\\ &= \mathscr{B}(u-u_\delta,\psi-\psi_I)+\mathscr{B}_{\mathrm{supg}}(u-u_\delta,\psi_I)-\mathcal{E}_{\mathrm{supg}}(u-u_\delta,\psi_I) =\\ &= \mathscr{B}(u-u_\delta,\psi-\psi_I)+F_{\mathrm{supg}}(\psi_I)-F_{\mathrm{supg},\delta}(\psi_I)\\ &\qquad+\mathscr{B}_{\mathrm{supg},\delta}(u_\delta,\psi_I)-\mathscr{B}_{\mathrm{supg}}(u_\delta,\psi_I)-\mathcal{E}_{\mathrm{supg}}(u-u_\delta,\psi_I)\,.\end{aligned}$$

We now focus on the terms of the right-hand side separately. First, making use of the Cauchy-Schwarz inequality, of the a priori estimate (3.39) and of (3.46), we get

$$\begin{aligned}\mathscr{B}(u-u_\delta,\psi-\psi_I) &\le \|u-u_\delta\|_1\,\|\psi-\psi_I\|_1 \precsim h^s\left(\|u\|_{s+1}+\|f\|_s\right)\|\psi-\psi_I\|_1 \precsim\\ &\precsim h^{s+1}\left(\|u\|_{s+1}+\|f\|_s\right)|\psi|_2 \precsim h^{s+1}\left(\|u\|_{s+1}+\|f\|_s\right)\|u-u_\delta\|\,.\end{aligned}$$

Concerning the term $F_{\mathrm{supg}}(\psi_I)-F_{\mathrm{supg},\delta}(\psi_I)$, considering that ψ_I is the interpolant of a $\mathrm{H}^2(\Omega)$ function, we may follow again the lines of the proof of Theorem 3.2 (see (3.41) and the following equations): the increased regularity allows us to improve relations (3.42) and (3.43), obtaining

$$|F_{\mathrm{supg}}(\psi_I)-F_{\mathrm{supg},\delta}(\psi_I)| \precsim h^{s+1}\|f\|_s\,|\psi|_2 \precsim h^{s+1}\|f\|_s\,\|u-u_\delta\|\,.$$

Next, the estimate

$$\left|\mathscr{B}_{\mathrm{supg},\delta}(u_\delta,\psi_I)-\mathscr{B}_{\mathrm{supg}}(u_\delta,\psi_I)\right| \precsim h^{s+1}\|u\|_{s+1}\left(\|\nabla\psi\|+|\psi|_2\right) \precsim h^{s+1}\|u\|_{s+1}\,\|u-u_\delta\|$$

can be obtained using (3.19), (3.21), and an improved version of (3.24) in which the increased regularity of ψ allows for an extra power of h in (3.26), (3.27) and (3.28). In particular, regarding (3.26),

$$\begin{aligned}&\left(\mathsf{K}\left(\nabla u_\delta-\Pi^0_{k-1}\nabla u_\delta\right),\Pi^0_{k-1}\nabla\psi_I\right)_E =\\ &\quad=\left(\nabla u_\delta-\Pi^0_{k-1}\nabla u_\delta,\mathsf{K}\Pi^0_{k-1}\nabla\psi_I-\Pi^0_{k-1}\left(\mathsf{K}\Pi^0_{k-1}\nabla\psi_I\right)\right)_E \le \left\|\nabla u_\delta-\Pi^0_{k-1}\nabla u_\delta\right\|_E\times\\ &\quad\times\left\|\mathsf{K}\Pi^0_{k-1}\nabla\psi_I-\Pi^0_{k-1}\left(\mathsf{K}\Pi^0_{k-1}\nabla\psi_I\right)\right\|_E \precsim \left(\|\nabla(u-u_\delta)\|_E+\left\|\nabla u-\Pi^0_{k-1}\nabla u\right\|_E+\right.\\ &\qquad\left.\left\|\Pi^0_{k-1}(\nabla(u-u_\delta))\right\|_E\right)\left\|\mathsf{K}\Pi^0_{k-1}\nabla\psi_I-\Pi^0_{k-1}(\mathsf{K}\nabla\psi_I)\right\|_E \precsim\\ &\quad\precsim h_E^s\,\|u\|_{s+1,E}\left(\left\|\mathsf{K}\Pi^0_{k-1}\psi_I-\mathsf{K}\nabla\psi_I\right\|_E+\left\|\mathsf{K}\nabla\psi_I-\Pi^0_{k-1}(\mathsf{K}\nabla\psi_I)\right\|_E\right) \precsim\\ &\qquad\precsim h_E^{s+1}\,\|u\|_{s+1,E}\left(\|\nabla\psi_I\|_E+|\psi_I|_{2,E}\right) \precsim h_E^{s+1}\,\|u\|_{s+1,E}\left(\|\nabla\psi\|_E+|\psi|_{2,E}\right),\end{aligned}$$

while regarding (3.27),

$$\begin{aligned}\left(\mathsf{K}\nabla u_\delta - \Pi^0_{k-1}(\mathsf{K}\nabla u_\delta)\,,\nabla\psi_I\right)_E &= \left(\mathsf{K}\nabla u_\delta - \Pi^0_{k-1}(\mathsf{K}\nabla u_\delta)\,,\nabla\psi_I - \Pi^0_{k-1}\nabla\psi_I\right)_E \leq \\ &\leq \left\|\mathsf{K}\nabla u_\delta - \Pi^0_{k-1}(\mathsf{K}\nabla u_\delta)\right\|_E \left\|\nabla\psi_I - \Pi^0_{k-1}\nabla\psi_I\right\|_E \leq (\|\mathsf{K}\nabla u_\delta - \mathsf{K}\nabla u\|_E + \\ &\left\|\mathsf{K}\nabla u - \Pi^0_{k-1}(\mathsf{K}\nabla u)\right\|_E + \left\|\Pi^0_{k-1}(\mathsf{K}\nabla u - \mathsf{K}\nabla u_\delta)\right\|_E)\left\|\nabla\psi_I - \Pi^0_{k-1}\nabla\psi_I\right\|_E \precsim \\ &\precsim h_E^{s+1}\|u\|_{s+1,E}\,|\psi_I|_{2,E} \precsim h_E^{s+1}\|u_\delta\|_{s+1,E}\,|\psi|_{2,E}\,.\end{aligned}$$

Finally, regarding the term $\mathcal{E}_{\text{supg}}(u-u_\delta,\psi_I)$, using inequalities (3.10) and (3.11) for τ_E, the estimate (2.16) for the VEM interpolant, the a priori estimate (3.39), (3.47) and the Hölder inequality, we get

$$\begin{aligned}&\left|\sum_{E\in\mathcal{T}_\delta}\tau_E\left(\beta\cdot\nabla(u_\delta-u)+\nabla\cdot(\mathsf{K}\nabla(u_\delta-u))\,,\beta\cdot\nabla\psi_I\right)_E\right| \leq \\ &\qquad\leq\left(\max_{E\in\mathcal{T}_\delta}\tau_E\right)\left|\sum_{E\in\mathcal{T}_\delta}\left(\beta\cdot\nabla(u_\delta-u)+\nabla\cdot(\mathsf{K}\nabla(u_\delta-u))\,,\beta\cdot\nabla\psi_I\right)_E\right| \precsim \\ &\precsim\left(\max_{E\in\mathcal{T}_\delta}\tau_E\right)\left(\|u-u_\delta\|_1\|\nabla\psi_I\|+\left(\sum_{E\in\mathcal{T}_\delta}\|\nabla\cdot(\mathsf{K}\nabla(u-u_\delta))\|_E^2\right)^{\frac{1}{2}}\|\nabla\psi_I\|\right)\precsim \\ &\precsim\left(h^{s+1}\|u\|_{s+1}+h^2\left(\sum_{E\in\mathcal{T}_\delta}\|u-u_I\|_{2,E}^2+\|\nabla\cdot(\mathsf{K}\nabla(u_I-u_\delta))\|_E^2\right)^{\frac{1}{2}}\right)\|\nabla\psi\|\precsim \\ &\qquad\precsim h_E^{s+1}\|u\|_{s+1}\|u-u_\delta\|\,,\end{aligned}$$

where the error $\sum_{E\in\mathcal{T}_\delta}\|\nabla\cdot(\mathsf{K}\nabla(u_I-u_\delta))\|_E^2$ is estimated using (3.8) and (3.44):

$$\sum_{E\in\mathcal{T}_\delta}\|\nabla\cdot(\mathsf{K}\nabla(u_I-u_\delta))\|_E^2 \precsim \sum_{E\in\mathcal{T}_\delta}h_E^{-2}\|u_I-u_\delta\|_{1,E}^2 \lesssim h^{2(s-1)}\|u\|_{s+1}^2\,.$$

□

3.5 Numerical Results

In this section we will consider three benchmark problems in the domain $\Omega=(0,1)\times(0,1)$ in order to numerically evaluate the rates of convergence of the discussed VEM-SUPG stabilization both in the convection-dominated regime and the diffusion-dominated regime. VEM orders from one to three are used.

3.5.1 Test 1. As a first test we consider problem (3.1) with constant K and β. In particular the transport velocity field is

$$\beta(x,y)=\left(\tfrac{1}{2},-\tfrac{1}{3}\right),$$

and we perform two sets of simulations corresponding to two different values of K: in a first set of simulations we use $\mathsf{K}=10^{-3}$, whereas $\mathsf{K}=10^{-9}$ is used for a second set of simulations. The meshsize range is chosen in such a way that for all values of the VEM order k, the mesh Péclet number is both greater and lower than one for $\mathsf{K}=10^{-3}$, while it is much greater than one for $\mathsf{K}=10^{-9}$.

The exact solution for this problem is given by

$$u(x,y) = \frac{65536}{729}x^3(1-x)y^3(1-y)\,.$$

In Figures 3.1a to 3.1f we show the convergence curves obtained with $\mathsf{K} = 10^{-3}$ (left) and $\mathsf{K} = 10^{-9}$ (right). The errors reported are based on the difference between the exact solution and the projection of the discrete solution on the space of polynomials of degree k, accordingly to the VEM order k varying from 1 to 3, and they are computed as follows:

$$err_{\mathrm{L}^2} = \sqrt{\sum_{E\in\mathcal{T}_\delta} \|u - \Pi_k^0 u_\delta\|_E^2}\,,$$
$$err_{\mathrm{H}_0^1} = \sqrt{\sum_{E\in\mathcal{T}_\delta} \|\nabla\left(u - \Pi_k^0 u_\delta\right)\|_E^2}\,.$$

The errors are plotted versus the number of degrees of freedom (Ndof). For each mesh we also report the values of the minimum and maximum mesh Péclet numbers. Note that the left y-axes scales refer to the mesh Péclet numbers, whereas the right ones refer to the error measure. The very good agreement between the numerical behaviour and the expected rates of convergence in (3.39) is evident.

3.5.2 Test 2.

For the second test, non-constant coefficients are used and the flow regime is transport dominated in all the simulations performed. We have set:

$$\mathsf{K}(x,y) = 10^{-7}\begin{pmatrix} 1+x^2 & xy \\ xy & 1+y^2 \end{pmatrix},$$
$$\beta(x,y) = \left(\tfrac{1}{3} + 10y(x+y^2)^4, -\tfrac{1}{2} - 5(x+y^2)^4\right),$$

and the exact solution in this case is:

$$u(x,y) = 600xy(1-x)(1-y)\left(x-\frac{1}{5}\right)\left(y-\frac{2}{5}\right)\left(y-\frac{3}{5}\right).$$

We compare the solution obtained with the VEM-SUPG method described in the present work on a family of polygonal Voronoi meshes generated by `PolyMesher` [24], made up of polygons with four to eight edges (see Figure 3.2a), with the solution obtained on standard triangular meshes. Figures 3.2c and 3.2d show a comparison between the unstabilized solution and the one obtained using the SUPG stabilization for second order VEM, showing a very good agreement with the exact solution (Figure 3.2b) for a given polygonal mesh.

Convergence curves were obtained for VEM formulations of order from 1 to 3 and are reported in Figure 3.3. The error was obtained by comparing the exact solution to the polynomial projections of the discrete solutions. On each plot we also report the maximum and minimum mesh Péclet number for each considered meshsize. Also in this case, the left y-axes refer to the mesh Péclet numbers, whereas the right ones refer to the error measure. Note that for all orders and meshes, this problem is always convection-dominant ($\min_{E\in\mathcal{T}_\delta} \mathrm{Pe}_E \gg 1$ for all meshes). Once again, the plots show a very good agreement between the experimental orders of convergence and the ones provided by Theorem 3.2, independently of the used mesh.

3.5.3 Test 3.

As a final test, we revisit a classic problem studied in [17] in the context of standard Finite Elements. The geometry of the problem is depicted in Figure 3.4. Dirichlet

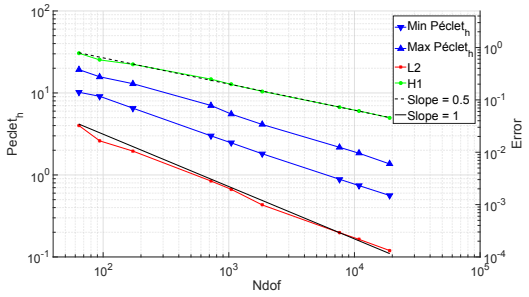

(a) Order 1, $\mathsf{K} = 10^{-3}$

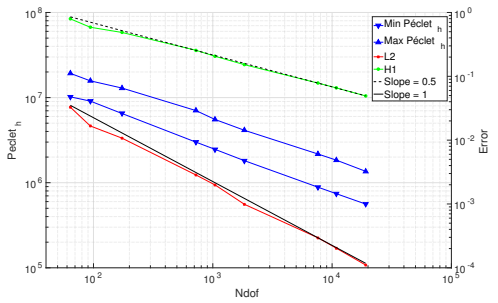

(b) Order 1, $\mathsf{K} = 10^{-9}$

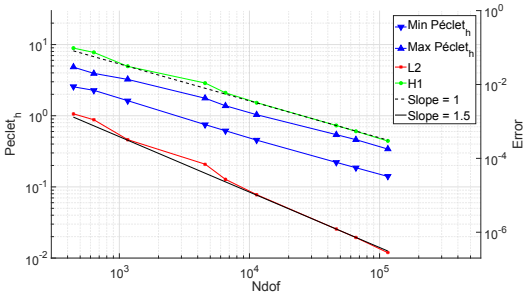

(c) Order 2, $\mathsf{K} = 10^{-3}$

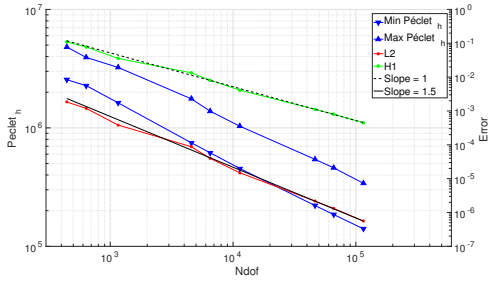

(d) Order 2, $\mathsf{K} = 10^{-9}$

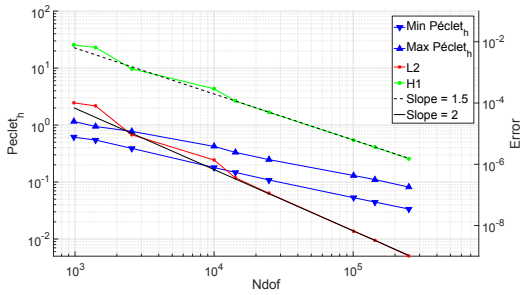

(e) Order 3, $\mathsf{K} = 10^{-3}$

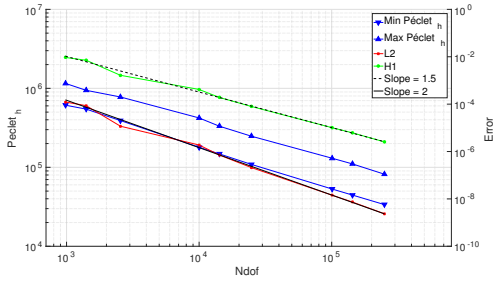

(f) Order 3, $\mathsf{K} = 10^{-9}$

Figure 3.1: **Test 1** Convergence curves

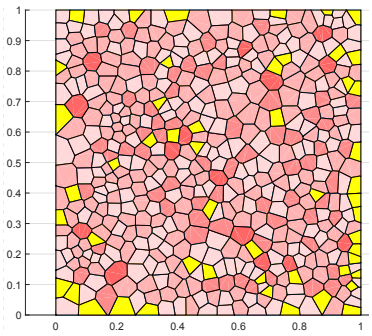

(a) Sample random polygonal mesh

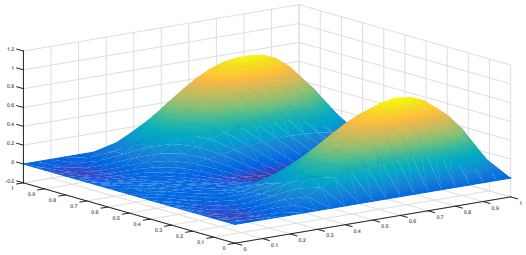

(b) Exact solution

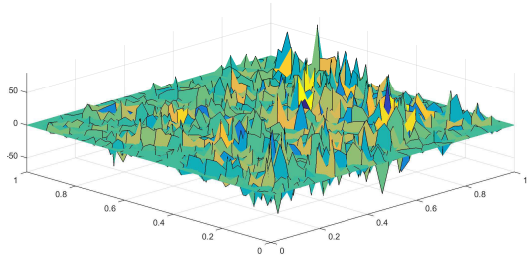

(c) Unstabilized solution

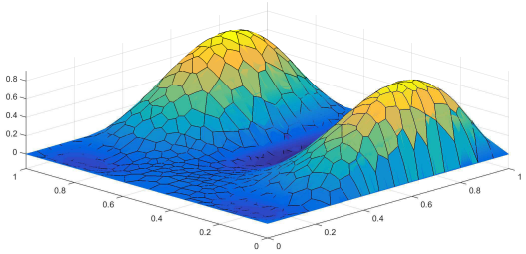

(d) Stabilized solution

Figure 3.2: **Test 2** Sample mesh, exact, unstabilized and stabilized solutions

boundary conditions are prescribed on the whole boundary (see again Figure 3.4), introducing a discontinuity in the inflow boundary that originates an internal boundary as well as an outflow boundary layer due to the null boundary condition at the outflow boundary. Data for the problem is: $\mathsf{K} = 10^{-6}$, and $\beta(x, y) = \big(\cos(\theta), \sin(\theta)\big)$, where $0 \leq \theta \leq \pi/2$ represents the flow direction. We consider the cases $\theta = \arctan(1)$ and $\theta = \arctan(2)$. The problem therefore presents very large Péclet numbers (10^6).

We considered three different mesh types: a regular quadrilateral mesh, a mildly deformed hexagonal mesh (Figure 3.5a), and a randomly generated polygonal mesh (see Figure 3.5b), whose parameters are summarized in Table 3.1. As in the case of standard Finite Elements, the unstabilized solution (not reported here) presents huge oscillations. Results obtained with VEM, with order ranging from 1 to 3 and the different mesh types, are presented in Figures 3.6 and 3.7. For all the orders and the mesh types considered, the results are quite similar to those presented in [17], and are coherent with the expected behavior of the method. Furthermore, higher order elements yield a smoother solution even with coarser meshes. The quadrilateral mesh shows smoother results than the hexagonal mesh, and more so in the case of the highly irregular polygonal mesh.

References for Chapter 3

[1] L. Beirão Da Veiga, F. Brezzi, L. D. Marini, and A. Russo. "The hitchhiker's guide to the Virtual Element method". In: *Math. Models Methods Appl. Sci* 24.8 (2014), pp. 1541–1573.

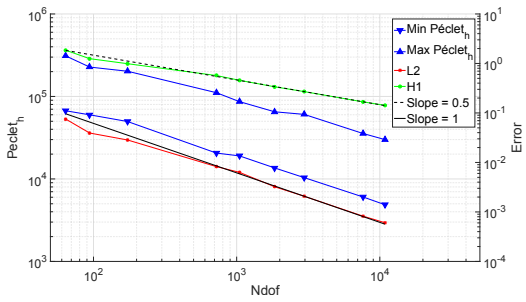

(a) Order 1, triangular mesh

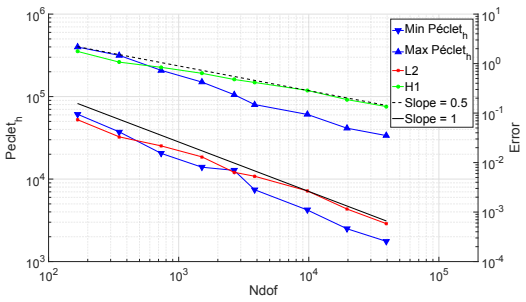

(b) Order 1, polygonal mesh

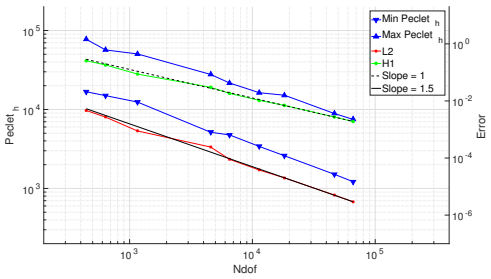

(c) Order 2, triangular mesh

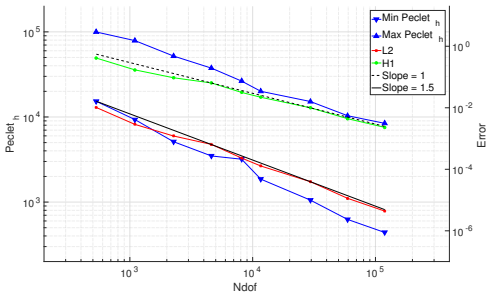

(d) Order 2, polygonal mesh

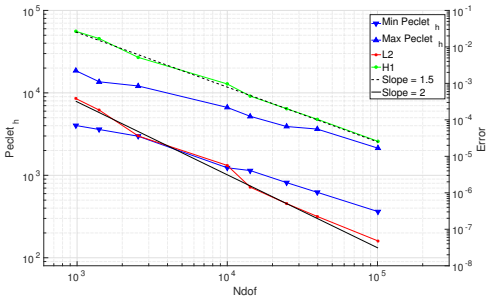

(e) Order 3, triangular mesh

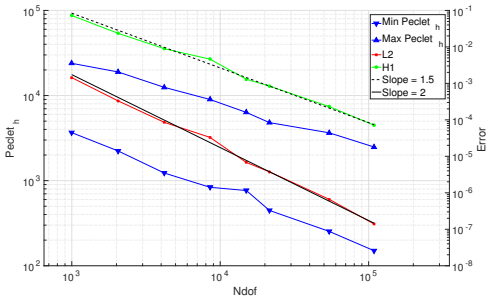

(f) Order 3, polygonal mesh

Figure 3.3: **Test 2** Convergence curves

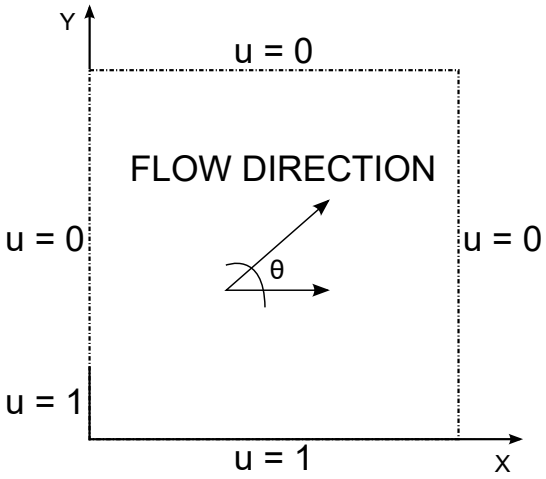

Figure 3.4: **Test 3** Domain and boundary conditions

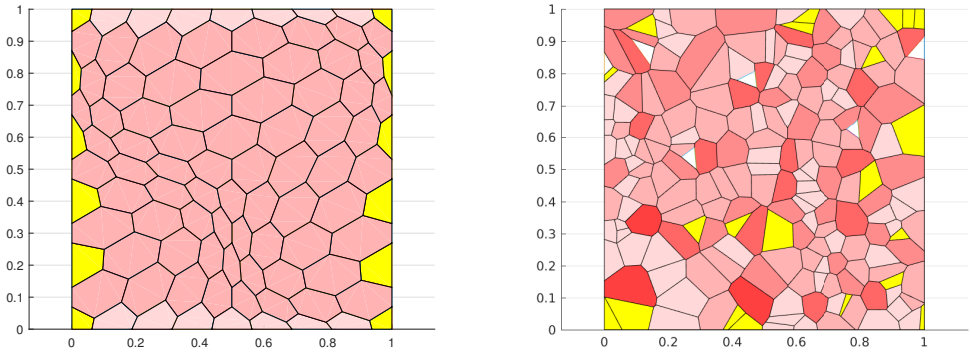

(a) Hexagonal mesh

(b) Random polygonal mesh

Figure 3.5: **Test 3** Examples of mesh used

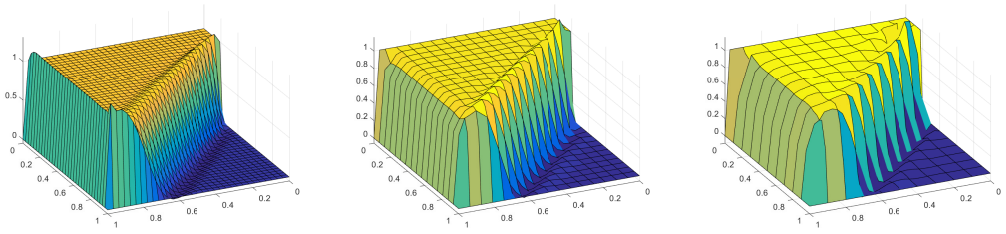

(a) Order 1, quad. mesh (b) Order 2, quad. mesh (c) Order 3, quad. mesh

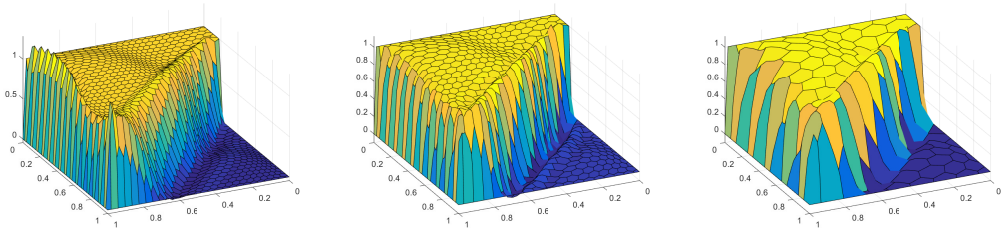

(d) Order 1, hexagonal mesh (e) Order 2, hexagonal mesh (f) Order 3, hexagonal mesh

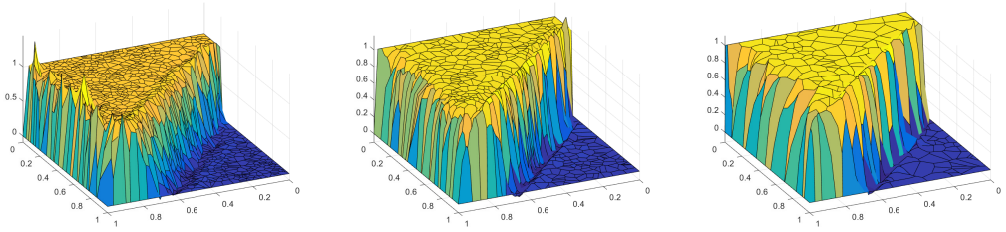

(g) Order 1, polygonal mesh (h) Order 2, polygonal mesh (i) Order 3, polygonal mesh

Figure 3.6: **Test 3** Solutions obtained for $\theta = \arctan(1)$

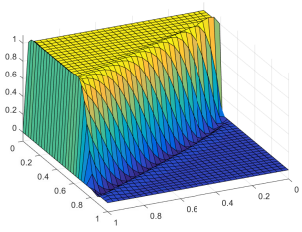

(a) Order 1, quad. mesh

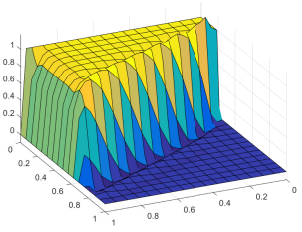

(b) Order 2, quad. mesh

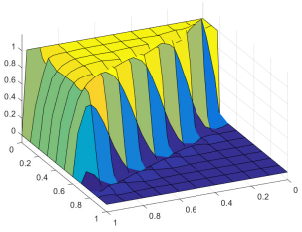

(c) Order 3, quad. mesh

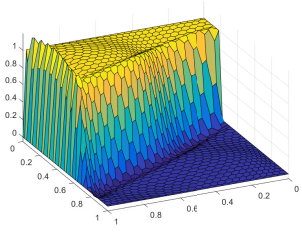

(d) Order 1, hexagonal mesh

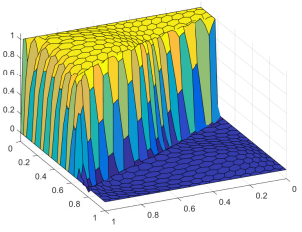

(e) Order 2, hexagonal mesh

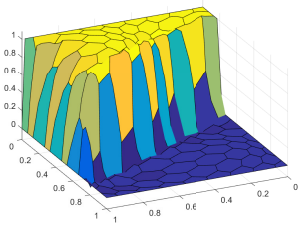

(f) Order 3, hexagonal mesh

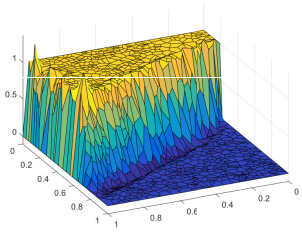

(g) Order 1, polygonal mesh

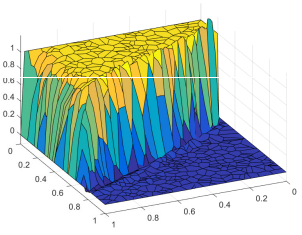

(h) Order 2, polygonal mesh

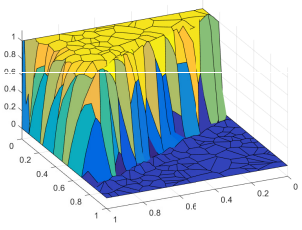

(i) Order 3, polygonal mesh

Figure 3.7: **Test 3** Solutions obtained for $\theta = \arctan(2)$

	Quadrilateral mesh		Hexagonal mesh		Polygonal mesh	
Order	# Polygons	h	# Polygons	h	# Polygons	h
1	1024	0.0312	780	0.044	1000	0.125
2	256	0.0625	360	0.065	500	0.155
3	100	0.1	80	0.139	200	0.192

Table 3.1: **Test 3** Mesh parameters

[2] L. Beirão da Veiga, F. Brezzi, L. D. Marini, and A. Russo. "Virtual Element Methods for General Second Order Elliptic Problems on Polygonal Meshes". In: *Mathematical Models and Methods in Applied Sciences* 26.04 (2015), pp. 729–750. DOI: 10.1142/S0218202516500160.

[3] M. Benedetto, S. Berrone, A. Borio, S. Pieraccini, and S. Scialò. "A Hybrid Mortar Virtual Element Method For Discrete Fracture Network Simulations". In: *J. Comput. Phys.* 306 (2016), pp. 148–166. DOI: 10.1016/j.jcp.2015.11.034.

[4] M. Benedetto, S. Berrone, A. Borio, S. Pieraccini, and S. Scialò. "Order preserving SUPG stabilization for the virtual element formulation of advection-diffusion problems". In: *Computer Methods in Applied Mechanics and Engineering* 311 (2016), pp. 18–40. ISSN: 0045-7825. DOI: 10.1016/j.cma.2016.07.043.

[5] M. Benedetto, S. Berrone, S. Pieraccini, and S. Scialò. "The virtual element method for discrete fracture network simulations". In: *Comput. Methods Appl. Mech. Engrg.* 280.0 (2014), pp. 135–156. ISSN: 0045-7825. DOI: 10.1016/j.cma.2014.07.016.

[6] M. Benedetto, S. Berrone, and S. Scialò. "A Globally Conforming Method For Solving Flow in Discrete Fracture Networks Using the Virtual Element Method". In: *Finite Elem. Anal. Des.* 109 (2016), pp. 23–36. DOI: 10.1016/j.finel.2015.10.003.

[7] S. Berrone and M. Marro. "Numerical investigation of effectivity indices of space-time error indicators for Navier-Stokes equations". In: *Computer Methods in Applied Mechanics and Engineering* 199.25 – 28 (2010), pp. 1764–1782. ISSN: 0045-7825. DOI: 10.1016/j.cma.2010.02.004.

[8] S. Berrone and M. Marro. "Space-time adaptive simulations for unsteady Navier-Stokes problems". In: *Comput. & Fluids* 38.6 (2009), pp. 1132–1144. ISSN: 0045-7930. DOI: 10.1016/j.compfluid.2008.11.004.

[9] S. Berrone. "Adaptive discretization of stationary and incompressible Navier-Stokes equations by stabilized finite element methods". In: *Comput. Methods Appl. Mech. Engrg.* 190.34 (2001), pp. 4435–4455. ISSN: 0045-7825. DOI: 10.1016/S0045-7825(00)00327-3.

[10] S. Berrone. "Robustness in a posteriori error analysis for FEM flow models". In: *Numerische Mathematik* 91.3 (2002), pp. 389–422. ISSN: 0945-3245. DOI: 10.1007/s002110100370.

[11] F. Brezzi, L. Franca, and A. Russo. "Further considerations on residual-free bubbles for advective-diffusive equations". In: *Computer Methods in Applied Mechanics and Engineering* 166.1 – 2 (1998). Advances in Stabilized Methods in Computational Mechanics, pp. 25–33. ISSN: 0045-7825. DOI: 10.1016/S0045-7825(98)00080-2.

[12] A. N. Brooks and T. J. R. Hughes. "Streamline Upwind / Petrov-Galerkin formulation for convective dominated flows with particular emphasis on the incompressible Navier-Stokes equations". In: *Comput. Methods Appl. Engrg.* 32 (1982), pp. 199–259.

[13] E. Burman. "Consistent SUPG-method for transient transport problems: Stability and convergence". In: *Computer Methods in Applied Mechanics and Engineering* 199.17 – 20 (2010), pp. 1114–1123. ISSN: 0045-7825. DOI: 10.1016/j.cma.2009.11.023.

[14] E. Burman and G. Smith. "Analysis of the space semi-discretized SUPG method for transient convection–diffusion equations". In: *Mathematical Models and Methods in Applied Sciences* 21.10 (2011), pp. 2049–2068.

[15] A. Cangiani, E. H. Georgoulis, T. Pryer, and O. J. Sutton. *A posteriori error estimates for the virtual element method.* 2016. arXiv: 1603.05855.

[16] A. Cangiani, G. Manzini, and O. Sutton. *The Conforming Virtual Element Method for the convection-diffusion-reaction equation with variable coefficients.* Techical Report. available online at http://www.osti.gov/scitech/servlets/purl/1159207. Los Alamos National Laboratory, 2014.

[17] L. P. Franca, S. L. Frey, and T. J. Hughes. “Stabilized finite element methods: I. Application to the advective-diffusive model”. In: *Computer Methods in Applied Mechanics and Engineering* 95.2 (1992), pp. 253–276. ISSN: 0045-7825. DOI: 10.1016/0045-7825(92)90143-8.

[18] L. P. Franca and L. Tobiska. “Stability of the residual free bubble method for bilinear finite elements on rectangular grids”. In: *IMA journal of numerical analysis* 22.1 (2002), pp. 73–87.

[19] S. Ganesan and L. Tobiska. “Stabilization by local projection for convection – diffusion and incompressible flow problems”. In: *Journal of Scientific Computing* 43.3 (2010), pp. 326–342.

[20] T. Gelhard, G. Lube, M. A. Olshanskii, and J.-H. Starcke. “Stabilized finite element schemes with LBB - stable elements for incompressible flows”. In: *Journal of Computational and Applied Mathematics* 177.2 (2005), pp. 243–267. ISSN: 0377-0427. DOI: 10.1016/j.cam.2004.09.017.

[21] I. Harari and T. J. Hughes. “What are C and h?: Inequalities for the analysis and design of finite element methods”. In: *Computer Methods in Applied Mechanics and Engineering* 97.2 (1992), pp. 157–192. ISSN: 0045-7825. DOI: 10.1016/0045-7825(92)90162-D.

[22] C. Johnson, U. Nävert, and J. Pitkäranta. “Finite element methods for linear hyperbolic problems”. In: *Computer Methods in Applied Mechanics and Engineering* 45 (1984), pp. 285–312. DOI: 10.1016/0045-7825(84)90158-0.

[23] H.-G. Roos, M. Stynes, and L. Tobiska. *Robust numerical methods for singularly perturbed differential equations: convection-diffusion-reaction and flow problems*. Vol. 24. Springer Science & Business Media, 2008.

[24] C. Talischi, G. H. Paulino, A. Pereira, and I. F. M. Menezes. “PolyMesher: a general-purpose mesh generator for polygonal elements written in Matlab”. In: *Structural and Multidisciplinary Optimization* 45.3 (2012), pp. 309–328. ISSN: 1615-1488. DOI: 10.1007/s00158-011-0706-z.

[25] R. Verfürth. “Robust A Posteriori Error Estimates for Nonstationary Convection-Diffusion Equations”. In: *SIAM Journal on Numerical Analysis* 43.4 (2005), pp. 1783–1802. DOI: 10.1137/040604273.

[26] R. Verfürth. “Robust A Posteriori Error Estimates for Stationary Convection-Diffusion Equations”. In: *SIAM Journal on Numerical Analysis* 43.4 (2005), pp. 1766–1782. DOI: 10.1137/040604261.

Chapter 4

A residual a posteriori error estimate for the Virtual Element Method

In this chapter we develop a residual a posteriori error estimate for Virtual Element Methods, with the focus on avoiding the presence of any terms depending on the VEM stabilization bilinear form. This work is currently submitted for publication.

4.1 Introduction

Since the first investigations on *a posteriori* error analysis [4], many interesting results have been obtained [2, 5, 30, 38] on simple linear models as well as on more complex non-linear equations [16, 21, 24]. In recent years *a posteriori* error analysis and optimality investigations of steady-state adaptive discretizations have been widely tackled for several discretization approaches and model equations, obtaining several interesting results [15, 25, 27, 34]. A large effort has been recently spent on unsteady problems [3, 23, 28, 36], as well as on other interesting issues like, for example, the analysis of stopping criteria during adaptive iterations [31]. Discretization approaches based on traditional simplicial elements are subject to many constraints when mesh refinement and coarsening are applied. These constraints can make reliable and efficient simulations very difficult and computationally demanding. Moreover, in many applications the geometrical complexity of the domain is a relevant issue when partial differential equations have to be solved on a good quality mesh (see, for example, the problem of underground flow simulation in fractured media[17–19]).

In the VEM context, due to the unknown value of the non-polynomial part of the discretization space on each element, the computed discrete solution is immediately known only through the values of its degrees of freedom and cannot be easily evaluated inside the elements. The full discrete solution can, however, be used to compute a piecewise polynomial approximation of the discrete solution that can be easily evaluated at any point of each element.

In this work we address the issue of deriving computable, reliable and efficient residual-based *a posteriori* error estimators for a polynomial projection of the Virtual Element solution to the Poisson problem. This very simple model is, anyway, interesting in several applications like, for example, geological flow simulations [10–12, 17] where the geometrical complexities can be extremely challenging. The *a posteriori* analysis for the same problem was tackled in [9] with a different VEM discretization and with additional terms in the estimates depending

on the VEM stabilization. Moreover, in [26] a more general reaction-advection-diffusion problem is considered for an *a posteriori* error estimate, involving terms depending on the VEM stabilization. Here we show that, using a particular polynomial approximation of the VEM solution, we are able to compute reliable and efficient residual error estimators, overcoming the problem related to the evaluation of the residual of the strong form of the equation and of the values of the co-normal derivatives of the non-polynomial component of the numerical solution. Moreover, we aim at avoiding the inclusion in the error estimators of any VEM stabilization terms. In this approach we establish an equivalence relation between the error with respect to a "post-processing" of the VEM solution and a residual based error estimator. Resorting to post-processed solutions is a quite common practice in proving super-convergence results [40, 42], very common, for example, for the Stokes problem [41]. The equivalence relation we prove involves only the defined error measure and the error estimator, up to classical higher order data oscillation terms. Note that, in the case the estimates were not independent of the VEM stabilization, as are with other approaches, one would have these terms, that are not negligible with respect to the error and the estimator, on the right-hand side of both the upper and lower bound of the error.

The chapter is organized as follows: in Section 4.2 we describe the model problem and we briefly introduce the VEM conforming discretization. In Section 4.3 the *a posteriori* upper bound for the error between the solution of the problem and a suitable projection of the numerical solution is provided, and in Section 4.4, we prove *a posteriori* lower bounds for the chosen error measure. In Section 4.5 we present some numerical results confirming the good agreement of the *a posteriori* error estimates. In particular, we show that the estimates can be effectively applied to a model representing the pressure distribution of a Darcy flow within a fractured medium, modeled by a Discrete Fracture Network approach [10, 12, 14, 17–19]. Finally, in Section 4.7 we discuss a stability issue concerning a fundamental assumption needed in order to have estimates independent of the VEM stabilization terms. For the sake of clarity, we consider the 2D case only, but we remark that all the results concerning the *a posteriori* error estimates presented in Sections 4.3 and 4.4 can be extended to the 3D case as well.

4.2 The model problem and its VEM discretization

In this section we introduce the problem which will be considered herein, followed by its discretization by the Virtual Element Method, that follows the line developed in Chapter 2 and [7].

We consider the simple Poisson problem, that is problem (2.1) with $\beta = (0,0)$ and $\gamma = 0$. Let $\Omega \subset \mathbb{R}^2$ be a bounded open set with Lipschitz boundary $\partial\Omega$; then, for a forcing term f we look for a function u such that,

$$\begin{cases} -\nabla \cdot (\mathsf{K}\nabla u) = f & \text{in } \Omega\,, \\ u = 0 & \text{on } \partial\Omega\,, \end{cases} \tag{4.1}$$

where K is a positive function representing the *diffusivity* coefficient. We consider the classic weak formulation of the problem. Define a: $\mathrm{H}^1_0(\Omega) \times \mathrm{H}^1_0(\Omega) \to \mathbb{R}$ such that

$$a(w,v) := (\mathsf{K}\nabla w, \nabla v) \quad \forall w, v \in \mathrm{H}^1_0(\Omega)\,,$$

where $\mathsf{K} \in \mathrm{L}^\infty(\Omega)$ and $f \in \mathrm{L}^2(\Omega)$. The variational form of (4.1) is: find $u \in \mathrm{H}^1_0(\Omega)$ such that

$$a(u,v) = (f,v) \quad \forall v \in \mathrm{H}^1_0(\Omega)\,. \tag{4.2}$$

We discretize (4.2) by the VEM approach defined in Chapter 2. Let $\mathcal{T}_\delta$ be a polygonal mesh built as described in Section 2.3, with the further assumption that follows.

Assumption 4.1. Let $E \in \mathcal{T}_\delta$. For any two vertices $\mathbf{x}_1, \mathbf{x}_2 \in E$, $\|\mathbf{x}_1 - \mathbf{x}_2\|_{\mathbb{R}^2} \geq \gamma h_E$.

Thanks to Assumption 4.1, it is possible to construct, on each element $E \in \mathcal{T}_\delta$, a uniformly shape regular nested triangulation $\mathcal{T}_{\delta,E}$ whose triangles t are such that

$$\forall E \in \mathcal{T}_\delta, \forall t \in \mathcal{T}_{\delta,E}, \quad h_E \geq h_t \geq \gamma h_E \,, \tag{4.3}$$

and each of these triangles have one edge lying on ∂E. This can be accomplished, for example, by connecting all vertices of E to the center of the ball B_E, whose coordinates are $\mathbf{x}_E = (x_E, y_E)$. Now, consider an edge $e \in \mathcal{E}_\delta$ and let $R, L \in \mathcal{T}_\delta$ be the two polygons sharing e. Let $r \in \mathcal{T}_{\delta,R}$ and $l \in \mathcal{T}_{\delta,L}$ be the two triangles contained in L and R respectively and sharing e, we set $\Omega_e := \{R, L\}$ and $\omega_e := \{r, l\}$.

Let V_δ be defined as in Section 2.4 and let a_δ be defined as in (2.7):

$$a_\delta(w_\delta, v_\delta) = \sum_{E \in \mathcal{T}_\delta} \left(\Pi^0_{k-1} \nabla w_\delta, \Pi^0_{k-1} \nabla v_\delta\right)_E + S^E\left(\left(I - \Pi^\nabla_k\right) w_\delta, \left(I - \Pi^\nabla_k\right) v_\delta\right) \,,$$

with S^E satisfying (2.8). Then, we formulate our Virtual Element method as the solution to the following discrete problem: find $u_\delta \in V_\delta$ such that

$$a_\delta(u_\delta, v_\delta) = (f_\delta, v_\delta) \quad \forall v_\delta \in V_\delta \,, \tag{4.4}$$

where $f_\delta := \Pi^0_{k-1} f$, that is the best approximation of f that allows the computability of the scalar product with a VEM function, since $\left(\Pi^0_{k-1} f, v_\delta\right) = \left(f, \Pi^0_{k-1} v_\delta\right)$ and we can compute $\Pi^0_{k-1} v_\delta$ using the degrees of freedom. The well-posedness of this problem is justified in Section 2.6.

Remark 4.1. As said in Remark 2.1, a possible choice for S^E (see also [6]) is the scalar product between the two vectors containing the degrees of freedom of the two functions involved, i.e., if we indicate by χ_r the operator which associates each function in V_δ to its r-th degree of freedom,

$$S^E(u_\delta, v_\delta) := \sum_{r=1}^{N_E} \chi_r\left(u_\delta\right) \chi_r\left(v_\delta\right) \quad \forall E \in \mathcal{T}_\delta, \forall u_\delta, v_\delta \in V_\delta \,, \tag{4.5}$$

where N_E indicates the number of degrees of freedom on element E.

4.3 A residual a posteriori estimate

In the following we derive *a posteriori* error estimates for a post-processing of the VEM solution to problem (4.4). A common issue when dealing with a VEM solution u_δ is related to the difficulties in getting pointwise values internal to the elements, for example to compute integrals or gradients of the solution for the computation of some physically relevant quantity (maximum or minimum value of the solution, fluxes, stresses). This problem is quite commonly tackled by means of pointwise evaluation of suitable projected solutions [8]. For this reason we have chosen to evaluate the error between the exact solution to the problem u and a polynomial projection of the computed VEM solution in order to have a control on the quality of the solution we are using for the given applicative targets. Indeed, in the following we show that, if a suitable polynomial approximation of u_δ, solution to (4.4), is considered, classical error estimation techniques can be applied to obtain computable, reliable and efficient upper and lower bounds.

Assumption 4.2. From now on we assume that K is piecewise constant on $\mathcal{T}_\delta$ and set $\mathsf{K}_E := \mathsf{K}|_E$, for any given element $E \in \mathcal{T}_\delta$. Furthermore, for a given set of elements ω, we set $\mathsf{K}_\omega^{\max} := \max_\omega \mathsf{K}$ and $\mathsf{K}_\omega^{\vee} := \min_\omega \mathsf{K}$.

4.3.1 Post-processing of the discrete solution and error definition.

For any $v_\delta \in V_\delta$, we define the piecewise discontinuous polynomial function v_δ^π, that, on each $E \in \mathcal{T}_\delta$, is the solution to the local problem

$$(\mathsf{K}\nabla v_\delta^\pi, \nabla p)_E = \left(\mathsf{K}\Pi_{k-1}^0 \nabla v_\delta, \nabla p\right)_E \ \forall p \in \mathbb{P}_k(E) \quad \text{and} \quad (v_\delta^\pi, 1)_{\partial E} = (v_\delta, 1)_{\partial E} \,. \tag{4.6}$$

Remark 4.2. Since here we are considering a piecewise constant diffusivity, we can remove K and Π_{k-1}^0 from (4.6) substantially getting $v_\delta^\pi = \Pi_k^\nabla v_\delta$. In the case of non elementwise constant K, (4.6) has to be used and additional terms will appear in the estimate, as described in Remark 4.10.

We will estimate the error between the exact solution to problem (4.1) and this post-processing of the discrete solution:

$$e_\delta^\pi := u - u_\delta^\pi \,.$$

Since u_δ^π is not continuous, we need to define a broken semi-norm:

$$|\!|\!| v |\!|\!| := \sup_{w \in \mathrm{H}_0^1(\Omega)} \frac{\sum_{E\in\mathcal{T}_\delta} a^E(v,w)}{\left\| \sqrt{\mathsf{K}} \nabla w \right\|} \,. \tag{4.7}$$

Remark 4.3. We point out that the semi-norm $|\!|\!|\cdot|\!|\!|$ is a norm for the error $e_\delta^\pi \in \prod_{E\in\mathcal{T}_\delta} \mathrm{H}^1(E)$ even though u_δ^π does not vanish on the boundary $\partial\Omega$ as u does, because $|\!|\!| e_\delta^\pi |\!|\!| = 0$ implies $e_\delta^\pi = 0$ in Ω. In fact, suppose $|\!|\!| u - u_\delta^\pi |\!|\!| = 0$, then, it must hold $(\nabla u - \nabla u_\delta^\pi)|_E = 0$, $\forall E \in \mathcal{T}_\delta$, implying

$$\forall E \in \mathcal{T}_\delta,\ (u - u_\delta^\pi)|_E = C_E \in \mathbb{R} \Rightarrow u|_E = u_\delta^\pi|_E + C_E \in \mathbb{P}_k(E) \,.$$

Then, it follows that $u|_E \in \mathbb{P}_k(E)$, $\forall E \in \mathcal{T}_\delta$, and $u \in V_\delta$. Then, it must be that $u = u_\delta = u_\delta^\pi$, which means that $C_E = 0$ $\forall E \in \mathcal{T}_\delta$. We conclude that $|\!|\!| u - u_\delta^\pi |\!|\!| = 0 \iff u - u_\delta^\pi = 0$.

We have the following a priori estimate of the error e_δ^π.

Theorem 4.1. *Suppose* K *is piecewise constant on* $\mathcal{T}_\delta$, $u \in \mathrm{H}^{s+1}(\Omega)$ *for some* $s > 0$, *where* k *is the order of the VEM approximation. Then, if* $r = \min\{k, s\}$,

$$\exists C > 0 \colon |\!|\!| u - u_\delta^\pi |\!|\!|^2 \lesssim \sum_{E\in\mathcal{T}_\delta} \mathsf{K}_E h_E^{2r} |u|^2_{\mathrm{H}^{r+1}(E)}$$

Proof. By the triangle inequality, the continuity of Π_k^∇ and VEM convergence estimates, we have

$$|\!|\!| u - u_\delta^\pi |\!|\!|^2 \le \left|\!\left|\!\left| u - \Pi_k^\nabla u \right|\!\right|\!\right|^2 + \left|\!\left|\!\left| \Pi_k^\nabla (u - u_\delta) \right|\!\right|\!\right|^2 \lesssim \sum_{E\in\mathcal{T}_\delta} \mathsf{K}_E h_E^{2r} |u|^2_{\mathrm{H}^{r+1}(E)} \,.$$

□

The above result shows that the error e_δ^π has the same order of convergence as the error $u - u_\delta$. Thus, an efficient a posteriori estimate for e_δ^π will have the same order of convergence as $u - u_\delta$.

4.3.2 A posteriori upper bound.

Before proceeding to the major result, we need to build a locally continuous linear operator that will play the same role as the Clément pseudo-interpolator in the standard FEM context (see [38]).

An oblique projection operator. In the following we focus on the VEM stabilization (4.5) (see [6]).

Let $u_\delta \in V_\delta$ be the solution to (4.4) and let

$$W_\delta := \left\{ v_\delta \in V_\delta \colon S\left(\left(I - \Pi_k^\nabla\right) u_\delta, \left(I - \Pi_k^\nabla\right) v_\delta\right) = 0 \right\} ,$$

Definition 4.1. Let $\mathcal{T}_{\delta,\omega}$ be a partition of Ω such that each element $\omega \in \mathcal{T}_{\delta,\omega}$ is:

1. the union of elements $E \in \mathcal{T}_\delta$, and each element E is contained in one and only one of such ω;
2. the number of elements $E \in \omega$ is uniformly bounded;
3. a Lipschitz set whose diameter scales as the diameter of its elements;
4. either $(I - \Pi_k^\nabla) u_\delta = 0 \ \forall E \in \omega$, or there is at least one degree of freedom of the space V_δ whose corresponding basis function φ_r satisfy $\operatorname{supp} \varphi_r \subseteq \omega$ and

$$\sum_{E \in \omega} S^E\left(\left(I - \Pi_k^\nabla\right) u_\delta, \left(I - \Pi_k^\nabla\right) \varphi_r\right) \neq 0 \,. \tag{4.8}$$

Let us denote by V_δ^ω the space of the restrictions to ω of VEM functions in V_δ. Given $\mathcal{T}_{\delta,\omega}$, we can build an oblique projection as follows.

Definition 4.2. Let $\mathcal{S}_\delta^\omega \colon V_\delta^\omega \to W_\delta^\omega$ be a linear continuous operator, defined locally, such that, for any given $v \in V_\delta^\omega$ and any $\omega \in \mathcal{T}_{\delta,\omega}$,

1. for all the VEM dofs s (Definition 2.1) of the elements E in the patch ω, except for $s = r$ only if $(I - \Pi_k^\nabla) u_\delta\big|_\omega \neq 0$,

$$\chi_s\left(\mathcal{S}_\delta^\omega v\right) = \chi_s\left(v\right) ;$$

2. it holds

$$\sum_{E \in \omega} S^E\left(\left(I - \Pi_k^\nabla\right) u_\delta, \left(I - \Pi_k^\nabla\right) \mathcal{S}_\delta^\omega v\right) = 0 \,, \tag{4.9}$$

   i.e. the r-th degree of freedom $\chi_r\left(\mathcal{S}_\delta^\omega v\right)$ is chosen to satisfy (4.9) if $(I - \Pi_k^\nabla) u_\delta\big|_\omega \neq 0$.

Remark 4.4. Whenever $v \in V_\delta$ is constant on $\omega \in \mathcal{T}_{\delta,\omega}$, condition (4.9) is automatically satisfied and $\mathcal{S}_\delta^\omega$ is the identity on ω. We conclude that the operator $\mathcal{S}_\delta^\omega$ preserves local constant functions on ω.

Definition 4.3. (see [26]) Let $I_\delta \colon \mathrm{H}^1(\Omega) \to V_\delta$ be a VEM interpolation operator such that, $\forall E \in \mathcal{T}_\delta$,

$$\left\| v - I_\delta v \right\|_E \lesssim h_E \left\| \nabla v \right\|_{\tilde{E}} , \tag{4.10}$$

$$\left\| \nabla I_\delta v \right\|_E \lesssim \left\| \nabla v \right\|_{\tilde{E}} , \tag{4.11}$$

where $\tilde{E}$ is the set of polygons with non empty intersection with E.

The existence of such operator is guaranteed by Theorem 11 in [26], see also Remark 2.2.

Definition 4.4. Let $\mathcal{S}_\delta^\omega$ be the operator defined by Definition 4.2, and I_δ be the operator defined by Definition 4.3. We define $P_\delta^\omega \colon \mathrm{H}^1(\Omega) \to W_\delta^\omega$ such that $P_\delta^\omega := \mathcal{S}_\delta^\omega \circ R_\delta^\omega \circ I_\delta$, where R_δ^ω is the restriction operator from V_δ to V_δ^ω. $P_\delta \colon \mathrm{H}^1(\Omega) \to W_\delta$ such that $P_\delta v|_\omega := P_\delta^\omega v$, $\forall v \in \mathrm{H}^1(\Omega)$, $\forall \omega \in \mathcal{T}_{\delta,\omega}$.

Let $\mathcal{E}_\delta^{\text{int}}$ be the set of the edges of the VEM mesh not on the boundary of Ω.

Definition 4.5. For each $E \in \mathcal{T}_\delta$, we indicate by ω_E the patch of elements to which it uniquely belongs, and by $\tilde{\omega}_E$ the patch of elements sharing at least one vertex with ω_E. Moreover, for each $e \in \mathcal{E}_\delta^{\text{int}}$, we set $\tilde{\omega}_e := \cup_{E\in\Omega_e}\tilde{\omega}_E$, where Ω_e is the set of elements sharing e, as defined in Section 4.2.

Definition 4.6. For each internal edge $e \in \mathcal{E}_\delta$ let

$$\mathsf{K}_e := \sum_{E\in\Omega_e} \mathsf{K}_E$$

be the diffusivity associated to this edge.

The operator P_δ satisfies the following important bounds.

Lemma 4.1. *Let P_δ be defined by Definition 4.4. Then, $\forall v \in \mathrm{H}^1_0(\Omega)$,*

$$\|v - P_\delta v\|_E \lesssim h_E \|\nabla v\|_{\tilde{\omega}_E} \qquad \forall E \in \mathcal{T}_\delta\,, \tag{4.12}$$

$$\|\nabla(v - P_\delta v)\|_E \lesssim \|\nabla v\|_{\tilde{\omega}_E} \qquad \forall E \in \mathcal{T}_\delta\,, \tag{4.13}$$

$$\|v - P_\delta v\|_e \lesssim h_e^{\frac{1}{2}} \|\nabla v\|_{\tilde{\omega}_e} \qquad \forall e \in \mathcal{E}_\delta^{\text{int}}\,, \tag{4.14}$$

$$\|v - P_\delta v\|_E \lesssim C_{\mathsf{K},E}\frac{h_E}{\sqrt{\mathsf{K}_E}} \left\|\sqrt{\mathsf{K}}\nabla v\right\|_{\tilde{\omega}_E} \qquad \forall E \in \mathcal{T}_\delta\,, \tag{4.15}$$

$$\|v - P_\delta v\|_e \lesssim C_{\mathsf{K},e}\frac{h_e^{\frac{1}{2}}}{\sqrt{\mathsf{K}_e}} \left\|\sqrt{\mathsf{K}}\nabla v\right\|_{\tilde{\omega}_e} \qquad \forall e \in \mathcal{E}_\delta^{\text{int}}\,, \tag{4.16}$$

$C_{\mathsf{K},E}$ and $C_{\mathsf{K},e}$ being constants depending only on the jumps of K.

Proof. Let $v \in \mathrm{H}^1(\Omega)$ and $v_I := I_\delta v$. First, we observe that, thanks to (4.10), we have

$$\|v - P_\delta v\|_E \lesssim \|v - v_I\|_E + \left\|v_I - \mathcal{S}_\delta^{\omega_E}\, v_I|_{\omega_E}\right\|_E \lesssim h_E \|\nabla v\|_{\tilde{E}} + \left\|v_I - \mathcal{S}_\delta^{\omega_E}\, v_I|_{\omega_E}\right\|_{\omega_E}.$$

We are left to estimate the second norm. Let $\hat{E}$ be a polygon with $h_{\hat{E}} \simeq 1$ such that the element E is obtained by a isotropic rescaling $E = F_E(\hat{E})$, and let $\hat{\omega}_E$ be the Lipschitz set such that $\omega_E = F_E(\hat{\omega}_E)$. Let us prove there exists a constant $C_{\hat{E}}$ such that, for any $v \in V_\delta$ and any $\hat{E}$,

$$\left\|\hat{v} - \mathcal{S}_\delta^{\hat{\omega}_E}\hat{v}\right\|_{\hat{\omega}_E} \le C_{\hat{E}} \|\nabla\hat{v}\|_{\hat{\omega}_E}\,, \tag{4.17}$$

where from now on with $\hat{v}$ we mean $(v \circ F_E)|_{\hat{\omega}_E}$. In order to do that, by contradiction we suppose that for any $C > 0$ there exists a $v \in V_\delta$ such that

$$\left\|\hat{v} - \mathcal{S}_\delta^{\hat{\omega}_E}\hat{v}\right\|_{\hat{\omega}_E} > C \|\nabla\hat{v}\|_{\hat{\omega}_E}\,,$$

in which case we can build a sequence $\hat{w}_k$ of functions in V_δ such that

$$\left\|\hat{w}_k - \mathcal{S}_\delta^{\hat{\omega}_E}\hat{w}_k\right\|_{\mathrm{L}^2(\hat{\omega}_E)} \ge k \|\nabla\hat{w}_k\|_{\mathrm{L}^2(\hat{\omega}_E)}\,, \quad \left\|\hat{w}_k - \mathcal{S}_\delta^{\hat{\omega}_E}\hat{w}_k\right\|_{\mathrm{L}^2(\hat{\omega}_E)} = 1,$$

which means that

$$\|\nabla\hat{w}_k\|_{\mathrm{L}^2(\hat{\omega}_E)} \le \frac{1}{k} \Rightarrow \|\nabla\hat{w}_k\|_{\mathrm{L}^2(\hat{\omega}_E)} \to 0\,.$$

Then, if we define $\hat{u}_k = \hat{w}_k - \mathcal{S}_\delta^{\hat{\omega}_E}\hat{w}_k$, we have, by the continuity of $\mathcal{S}_\delta^{\hat{\omega}_E}$ for any given patch and u_h, and the fact that it preserves constants, that, if $\hat{w}_k$ tends to a constant, also $\mathcal{S}_\delta^{\hat{\omega}_E}\hat{w}_k$ tends to the same constant. Then,

$$\|\nabla \hat{u}_k\|_{\mathrm{L}^2(\hat{\omega}_E)} \to 0\,. \tag{4.18}$$

The sequence $\hat{u}_k \circ F_E^{-1} \in V_\delta^{\omega_E} \cap \mathrm{H}_0^1(\omega_E)$ and $\|\hat{u}_k\|_{\mathrm{L}^2(\hat{\omega}_E)} = 1$, thus it converges to a function $\hat{u}^\star$ up to sub-sequences. By (4.18), $\nabla\hat{u}^\star = 0$, thus $\hat{u}^\star$ is constant and it must be $\hat{u}^\star = 0$ being $\hat{u}^\star|_{\partial\hat{\omega}_E} = 0$. This is a contraddiction since $\|\hat{u}^\star\|_{\hat{\omega}_E} = 1$. We conclude that (4.17) must hold and, by scaling arguments exploiting the fact that we can build uniformly shape regular triangulations on the polygons and (4.11), we get

$$\left\|v_I - \mathcal{S}_\delta^{\omega_E}\, v_I|_{\omega_E}\right\|_{\omega_E} \lesssim h_E \left\|\nabla v_I\right\|_{\tilde{\omega}_E} \lesssim h_E \left\|\nabla v\right\|_{\tilde{\omega}_E}\,.$$

By similar arguments we get also (4.13). Considering

$$\|\nabla v\|_{\tilde{\omega}_E} \lesssim \frac{1}{\sqrt{\mathsf{K}^\vee_{\tilde{\omega}_E}}}\left\|\sqrt{\mathsf{K}}\nabla v\right\|_{\omega_E} \lesssim \frac{\sqrt{\mathsf{K}_E}}{\sqrt{\mathsf{K}^\vee_{\tilde{\omega}_E}}}\frac{1}{\sqrt{\mathsf{K}_E}}\left\|\sqrt{\mathsf{K}}\nabla v\right\|_{\tilde{\omega}_E} \leq$$
$$\leq \frac{\sqrt{\mathsf{K}^{\max}_\omega}}{\sqrt{\mathsf{K}^\vee_{\tilde{\omega}_E}}}\frac{1}{\sqrt{\mathsf{K}_E}}\left\|\sqrt{\mathsf{K}}\nabla v\right\|_{\tilde{\omega}_E},$$

we get (4.15).

Regarding (4.14) and (4.16), we apply a trace inequality, (4.12) and (4.13). Let $e \in \mathcal{E}_\delta^{\mathrm{int}}$ and $E \in \Omega_e$:

$$\|v - P_\delta v\|_e^2 \lesssim h_e^{-1}\|v - P_\delta v\|_E^2 + h_e\|\nabla(v - P_\delta v)\|_E^2 \lesssim h_e^{-1}h_E^2\|\nabla v\|^2_{\tilde{\omega}_E}$$
$$+ h_e\|\nabla v\|^2_{\tilde{\omega}_E} \lesssim h_e\|\nabla v\|^2_{\tilde{\omega}_E} \lesssim \frac{\mathsf{K}^{\max}_\omega}{\mathsf{K}^\vee_{\tilde{\omega}_E}}\frac{h_e}{\mathsf{K}_E}\left\|\sqrt{\mathsf{K}}\nabla v\right\|^2_{\tilde{\omega}_E},$$

because $h_E \lesssim h_e$ by mesh regularity assumptions. To complete the proof of (4.16), we denote $\Omega_e = \{R, L\}$ and use the above estimate, bearing in mind that K is constant on both R and L:

$$\mathsf{K}_R\|v - P_\delta v\|_e^2 \lesssim \frac{\mathsf{K}^{\max}_\omega}{\mathsf{K}^\vee_{\tilde{\omega}_R}}h_e\left\|\sqrt{\mathsf{K}}\nabla v\right\|^2_{\tilde{\omega}_R}, \quad \mathsf{K}_L\|v - P_\delta v\|_e^2 \lesssim \frac{\mathsf{K}^{\max}_\omega}{\mathsf{K}^\vee_{\tilde{\omega}_L}}h_e\left\|\sqrt{\mathsf{K}}\nabla v\right\|^2_{\tilde{\omega}_L}$$
$$\Rightarrow (\mathsf{K}_R + \mathsf{K}_L)\|v - P_\delta v\|_e^2 \lesssim \max\left\{\frac{\mathsf{K}^{\max}_\omega}{\mathsf{K}^\vee_{\tilde{\omega}_R}}, \frac{\mathsf{K}^{\max}_\omega}{\mathsf{K}^\vee_{\tilde{\omega}_L}}\right\}h_e\left\|\sqrt{\mathsf{K}}\nabla v\right\|^2_{\tilde{\omega}_e}$$
$$\Rightarrow \|v - P_\delta v\|_e^2 \lesssim \max\left\{\frac{\mathsf{K}^{\max}_\omega}{\mathsf{K}^\vee_{\tilde{\omega}_R}}, \frac{\mathsf{K}^{\max}_\omega}{\mathsf{K}^\vee_{\tilde{\omega}_L}}\right\}\frac{h_e}{\mathsf{K}_e}\left\|\sqrt{\mathsf{K}}\nabla v\right\|^2_{\tilde{\omega}_e}.$$

□

Remark 4.5. $\forall e \in \mathcal{E}_\delta^{\mathrm{int}}$, if $C_{\mathsf{K},E} = 1$, for all $E \in \tilde{\omega}_e$, then $C_{\mathsf{K},e} = 1$.

Remark 4.6. We remark that Definition 4.4 is one of the possible definitions of a local operator with the property of preserving a.e. constant functions for which Lemma 4.1 holds true. In the following analysis we just use the existence of such operator and the computation of the error estimator does not require any evaluation of such operator.

Remark 4.7. In the proof of Lemma 4.1 we have used the continuity of the local operator $\mathcal{S}_\delta^\omega$, its stability constant does not appear explicitly in the proof of (4.12). Nevertheless, the constants appearing in Lemma 4.1 can depend on this stability constant that can be relevant for example in an adaptive algorithm based on the derived a posteriori error estimates. For this reason we discuss the stability of the operator and its relation with the choice of the patches in Appendix.

Remark 4.8. Whenever the solution u_δ on each element is not a polynomial, being the local stability matrix $(\mathbf{I}-\mathbf{\Pi}^{\nabla})^{\intercal}(\mathbf{I}-\mathbf{\Pi}^{\nabla})$ symmetric positive definite, we have that there is at least a basis function φ_r on that element that satisfies condition 4 of Definition 4.1. In fact $(I-\Pi_k^{\nabla})u_\delta$ cannot be orthogonal to $(I-\Pi_k^{\nabla})\varphi_i$ for all the VEM basis functions of the element.

Remark 4.9. In the definition of I_δ in [26], under a quasi-monotonicity condition for the distribution of coefficients K, we can resort to a modified Clément quasi interpolator as in [13, 29, 32] in case of discontinous diffusivity coefficient in order to bound the constants $C_{\mathsf{K},E}$ and $C_{\mathsf{K},e}$.

A posteriori upper bound. The following result states the Galerkin orthogonality for those function which are the image of a $\mathrm{H}_0^1(\Omega)$ function through the operator P_δ defined by Definition 4.4.

Lemma 4.2. *Let u_δ be the solution to (4.4), u_δ^π be defined by (4.6), $f\in \mathrm{L}^2(\Omega)$ be the forcing term in (4.1), $f_\delta=\Pi_{k-1}^0 f$, K the diffusivity coefficient, piecewise constant on the elements of $\mathcal{T}_\delta$, and P_δ the operator defined by Definition 4.4, then we have*

$$\sum_{E\in\mathcal{T}_\delta} a^E(u_\delta^\pi, P_\delta w) = (f_\delta, P_\delta w) \quad \forall w\in \mathrm{H}_0^1(\Omega)\ . \tag{4.19}$$

Proof. Since K is constant on each element and $\nabla u_\delta^\pi \in \left[\mathbb{P}_{k-1}(\mathcal{T}_\delta)\right]^2$, we have that

$$(\mathsf{K}\nabla u_\delta^\pi, \nabla(P_\delta w))_E = \left(\mathsf{K}\nabla u_\delta^\pi, \Pi_{k-1}^0\nabla(P_\delta w)\right)_E \quad \forall E\in\mathcal{T}_\delta\,.$$

Then, using the VEM discrete variational formulation (4.4), the definition of u_δ^π in (4.6) and the definition of P_δ we obtain

$$\begin{aligned}\sum_{E\in\mathcal{T}_\delta} a^E(u_\delta^\pi, P_\delta w) &= \sum_{E\in\mathcal{T}_\delta}(\mathsf{K}\nabla u_\delta^\pi, \nabla(P_\delta w))_E = \sum_{E\in\mathcal{T}_\delta}\left(\mathsf{K}\nabla u_\delta^\pi, \Pi_{k-1}^0\nabla(P_\delta w)\right)_E = \\ &= \sum_{E\in\mathcal{T}_\delta}\left(\mathsf{K}\Pi_{k-1}^0\nabla u_\delta, \Pi_{k-1}^0\nabla(P_\delta w)\right)_E = \sum_{E\in\mathcal{T}_\delta}\left(\mathsf{K}\Pi_{k-1}^0\nabla u_\delta, \Pi_{k-1}^0\nabla(P_\delta w)\right)_E + \\ &\quad + S^E\left(\left(I-\Pi_k^{\nabla}\right)u_\delta, \left(I-\Pi_k^{\nabla}\right)P_\delta w\right) = a_\delta(u_\delta, P_\delta w) = (f_\delta, P_\delta w)\ .\end{aligned}$$

□

Remark 4.10. If we admit a non-constant diffusivity on each polygon, we have that, on any given $E\in\mathcal{T}_\delta$,

$$(\mathsf{K}\nabla u_\delta^\pi, \nabla(P_\delta w))_E = \left(\mathsf{K}\nabla u_\delta^\pi, \Pi_{k-1}^0\nabla(P_\delta w)\right)_E + \left(\mathsf{K}\nabla u_\delta^\pi, \nabla(P_\delta w) - \Pi_{k-1}^0\nabla(P_\delta w)\right)_E\ ,$$

and it follows that

$$\sum_{E\in\mathcal{T}_\delta} a^E(u_\delta^\pi, P_\delta w) = (f_\delta, P_\delta w) + \left(\mathsf{K}\nabla u_\delta^\pi, \nabla\left(P_\delta w\right) - \Pi_{k-1}^0\nabla\left(P_\delta w\right)\right)_E \leq (f_\delta, P_\delta w)$$
$$+ \sum_{E\in\mathcal{T}_\delta} \left\|\mathsf{K}\nabla u_\delta^\pi\right\|_E \left\|\nabla\left(P_\delta w\right) - \Pi_{k-1}^0\nabla\left(P_\delta w\right)\right\|_E \leq (f_\delta, P_\delta w)$$
$$+ \sum_{E\in\mathcal{T}_\delta} h_E \left\|\mathsf{K}\nabla u_\delta^\pi\right\|_E \left\|\nabla\left(P_\delta w\right)\right\|_E \leq (f_\delta, P_\delta w) + \sum_{E\in\mathcal{T}_\delta} h_E \left\|\mathsf{K}\nabla u_\delta^\pi\right\|_E \left\|\nabla w\right\|_E .$$

If we do not assume K to be piecewise constant on the polygons of $\mathcal{T}_\delta$ other terms appear in the estimates.

In the proof of the following major result, we will use the following estimate (see[7] and (4.15)):

$$\forall E \in \mathcal{T}_\delta,\ \forall w \in \mathrm{H}^1(E),\ \left\|w - \Pi_k^0 w\right\|_E \lesssim \frac{h_E}{\sqrt{\mathsf{K}_E}} \left\|\sqrt{\mathsf{K}}\nabla w\right\|_E . \tag{4.20}$$

Definition 4.7. For any internal edge $e \in \mathcal{E}_\delta^{\mathrm{int}}$ let us define a unit normal vector $\mathbf{n}_e$ as the outward unit normal vector for the element on the right of e ($\mathbf{n}_e = \mathbf{n}_R$) and the jump of the co-normal derivative of u_δ^π

$$\left[\!\left[\frac{\partial u_\delta^\pi}{\partial \hat{n}_e^{\mathsf{K}}}\right]\!\right]_e = \mathsf{K}_R\nabla u_{\delta\,|_R}^\pi \cdot \mathbf{n}_R + \mathsf{K}_L\nabla u_{\delta\,|_L}^\pi \cdot \mathbf{n}_L = \mathsf{K}_R\nabla u_{\delta\,|_R}^\pi \cdot \mathbf{n}_e - \mathsf{K}_L\nabla u_{\delta\,|_L}^\pi \cdot \mathbf{n}_e.$$

Theorem 4.2. *Let u be the solution to (4.1), u_δ^π be defined by (4.6), and $f_\delta = \Pi_{k-1}^0 f$. Then,*

$$|\!|\!| u - u_\delta^\pi |\!|\!| \lesssim \left\{ C_{\mathsf{K}}^2 \left[\sum_{E\in\mathcal{T}_\delta} \frac{h_E^2}{\mathsf{K}_E} \left\|f_\delta + \nabla\cdot(\mathsf{K}\nabla u_\delta^\pi)\right\|_E^2 + \sum_{e\in\mathcal{E}_\delta^{\mathrm{int}}} \frac{h_e}{\mathsf{K}_e} \left\| \left[\!\left[\frac{\partial u_\delta^\pi}{\partial \hat{n}_e^{\mathsf{K}}}\right]\!\right]_e \right\|_e^2 \right] + \right.$$
$$\left. \sum_{E\in\mathcal{T}_\delta} \frac{h_E^2}{\mathsf{K}_E} \left\|f - f_\delta\right\|_E^2 \right\}^{\frac{1}{2}} ,$$

being C_{K} a constant dependent on the constants in Lemma 4.1.

Proof. Let P_δ be the operator defined by Definition 4.4. Let $w \in \mathrm{H}_0^1(\Omega)$. Using (4.19), the problem (4.1), the fact that $\left(f_\delta, \Pi_k^0 w\right) = \left(\Pi_k^0 f, \Pi_k^0 w\right) = \left(f, \Pi_k^0 w\right)$ and by Green's formula, we have

$$\sum_{E\in\mathcal{T}_\delta} a^E(u - u_\delta^\pi, w) = (f, w)_E - \sum_{E\in\mathcal{T}_\delta} \left(\mathsf{K}\nabla u_\delta^\pi, \nabla w\right)_E = \left(f_\delta, w\right)_E$$
$$- \sum_{E\in\mathcal{T}_\delta} \left(\mathsf{K}\nabla u_\delta^\pi, \nabla w\right)_E + \left(f - f_\delta, w\right)_E = \left(f_\delta, w - P_\delta w\right)_E$$
$$- \sum_{E\in\mathcal{T}_\delta} \left(\mathsf{K}\nabla u_\delta^\pi, \nabla\left(w - P_\delta w\right)\right)_E + \left(f - f_\delta, w - \Pi_k^0 w\right)_E ,$$

then, by Green's formula,the Cauchy-Schwarz inequality and by estimates (4.15), (4.16) and

(4.20),

$$\sum_{E\in\mathcal{T}_\delta} a^E(u-u_\delta^\pi,w) = \sum_{E\in\mathcal{T}_\delta} \left(f_\delta+\nabla\cdot(\mathsf{K}\nabla u_\delta^\pi), w-P_\delta w\right)_E - \sum_{e\in\mathcal{E}_\delta^{\text{int}}} \left(\left[\!\left[\frac{\partial u_\delta^\pi}{\partial \hat{n}_e^{\mathsf{K}}}\right]\!\right]_e, w-P_\delta w\right)_e$$
$$+\left(f-f_\delta, w-\Pi_k^0 w\right) \leq \sum_{E\in\mathcal{T}_\delta} \|f+\nabla\cdot(\mathsf{K}\nabla u_\delta^\pi)\|_E \|w-P_\delta w\|_E + \sum_{e\in\mathcal{E}_\delta^{\text{int}}} \left\|\left[\!\left[\frac{\partial u_\delta^\pi}{\partial \hat{n}_e^{\mathsf{K}}}\right]\!\right]_e\right\|_e \times$$
$$\times \|w-P_\delta w\|_e + \sum_{E\in\mathcal{T}_\delta} \|f-f_\delta\|_E \left\|w-\Pi_k^0 w\right\|_E \lesssim \sum_{E\in\mathcal{T}_\delta} C_{\mathsf{K},E}\frac{h_E}{\sqrt{\mathsf{K}_E}} \|f+\nabla\cdot(\mathsf{K}\nabla u_\delta^\pi)\|_E \times$$
$$\times \left\|\sqrt{\mathsf{K}}\nabla w\right\|_{\tilde{\omega}_E} + \sum_{e\in\mathcal{E}_\delta^{\text{int}}} C_{\mathsf{K},e}\frac{h_e^{\frac{1}{2}}}{\sqrt{\mathsf{K}_e}} \left\|\left[\!\left[\frac{\partial u_\delta^\pi}{\partial \hat{n}_e^{\mathsf{K}}}\right]\!\right]_e\right\|_e \left\|\sqrt{\mathsf{K}}\nabla w\right\|_{\tilde{\omega}_e}$$
$$+ \sum_{E\in\mathcal{T}_\delta} \frac{h_E}{\sqrt{\mathsf{K}_E}} \|f-f_\delta\|_E \left\|\sqrt{\mathsf{K}}\nabla w\right\|_E.$$

Finally, we obtain

$$\sum_{E\in\mathcal{T}_\delta} a^E(u-u_\delta^\pi,w) \lesssim \left\{ C_{\mathsf{K}}^2 \left[\sum_{E\in\mathcal{T}_\delta} \frac{h_E^2}{\mathsf{K}_E}\|f+\nabla\cdot(\mathsf{K}\nabla u_\delta^\pi)\|_E^2 + \sum_{e\in\mathcal{E}_\delta^{\text{int}}} \frac{h_e}{\mathsf{K}_e}\left\|\left[\!\left[\frac{\partial u_\delta^\pi}{\partial \hat{n}_e^{\mathsf{K}}}\right]\!\right]_e\right\|_e^2\right]\right.$$
$$\left. + \sum_{E\in\mathcal{T}_\delta} \frac{h_E^2}{\mathsf{K}_E}\|f-f_\delta\|^2 \right\}^{\frac{1}{2}} \left\|\sqrt{\mathsf{K}}\nabla w\right\|,$$

where C_{K} depends on $\max\{\max_{E\in\mathcal{T}_\delta} C_{\mathsf{K},E}, \max_{e\in\mathcal{E}_\delta^{\text{int}}} C_{\mathsf{K},e}\}$ and the maximum number of elements in each patch. The thesis is obtained by the definition of the $|||\cdot|||$-norm in (4.7). □

4.4 Efficiency of the a posteriori estimate

This section is devoted to obtain lower bounds for the error measured in terms of the following error estimator:

$$\eta_R := \left\{\sum_{E\in\mathcal{T}_\delta} \eta_{R,E}^2\right\}^{\frac{1}{2}}, \tag{4.21}$$

where, for all $E\in\mathcal{T}_\delta$, we define

$$\eta_{R,E}^2 := \frac{h_E^2}{\mathsf{K}_E}\|f_\delta+\nabla\cdot(\mathsf{K}\nabla u_\delta^\pi)\|_E^2 + \frac{1}{2}\sum_{e\in\mathcal{E}_\delta^{\text{int}}\cap\partial E} \frac{h_e}{\mathsf{K}_e}\left\|\left[\!\left[\frac{\partial u_\delta^\pi}{\partial \hat{n}_e^{\mathsf{K}}}\right]\!\right]_e\right\|_e^2. \tag{4.22}$$

4.4.1 Auxiliary results. The aim of this subsection is to extend the techniques based on triangle-bubble functions used in [38] to general polygons.

Consider a polygon $E\in\mathcal{T}_\delta$ and a triangle $t\in\mathcal{T}_{\delta,E}$. Let $\lambda_{t,i}$, $i=1,2,3$, be the barycentric coordinates of t. Define the *triangle-bubble function* of t, $\mathfrak{b}_t\in \mathrm{H}_0^1(t)$, as the function with support on t whose expression on t is $\mathfrak{b}_t|_t := 27\lambda_{t,1}\lambda_{t,2}\lambda_{t,3}$. Using the above definition we can define the *polygon-bubble function* $\mathfrak{b}_E\in\mathrm{H}_0^1(E)$ as the function with support on E such that $\mathfrak{b}_E|_t := \mathfrak{b}_t\ \forall t\in\mathcal{T}_{\delta,E}$. Note that $\mathfrak{b}_E|_{\partial t}=0\ \forall t\in\mathcal{T}_{\delta,E}$. Next, consider an edge $e\in\mathcal{E}_\delta^{\text{int}}$ and

define the *edge bubble-function* of e, $\mathfrak{b}_e \in \mathrm{H}^1_0(\omega_e)$, as the function with support on ω_e and such that $\mathfrak{b}_e|_r := 4\lambda_{r,1}\lambda_{r,2} \quad \forall r \in \omega_e$ if we enumerate the vertices of r such that the vertices of e are numbered first. The following useful properties of the polygon-bubble functions follow from the classic estimates in [37, Lemma 4.1] combined with (4.3).

Lemma 4.3. *Let $E \in \mathcal{T}_\delta$ and $\mathfrak{b}_E$ be the polygon-bubble function of E. Let $\mathcal{P}(E)$ be a polynomial space defined on E. Then, for any $v \in \mathcal{P}(E)$,*

$$\|v\|_E^2 \lesssim (v, v\mathfrak{b}_E)_E \,, \qquad \|\mathfrak{b}_E v\|_E \leq \|v\|_E \,, \tag{4.23}$$

$$\|\nabla(\mathfrak{b}_E v)\|_E \lesssim h_E^{-1} \|v\|_E \,. \tag{4.24}$$

Proof. (4.23) follows immediately from the fact that

$$\|v\|_t^2 \lesssim (v, v\mathfrak{b}_t)_t \,, \ \|\mathfrak{b}_t v\|_t \leq \|v\|_E \qquad \forall t \in \mathcal{T}_{\delta,E}$$

where the inequality constants are independent on any scale parameter of t (see [38]). Regarding (4.24), classical results give us the inequality on each $t \in \mathcal{T}_{\delta,E}$, i.e. $\forall E \in \mathcal{T}_\delta$, $\forall t \in \mathcal{T}_{\delta,E}$, $\|\nabla(\mathfrak{b}_E v)\|_t = \|\nabla(\mathfrak{b}_t v)\|_t \lesssim C h_t^{-1} \|v\|_t$. Using (4.3), that implies $h_t \sim h_E$ and $\|\nabla(\mathfrak{b}_E v)\|_E \lesssim h_E^{-1} \|v\|_E$, with an equivalence constant depending on γ. □

In order to state some useful properties of the edge-bubble functions, we first recall the concept of continuation of a function[38] from an edge to a triangle.

Definition 4.8 (Continuation operator)**.** Let t be a triangle, σ one of its sides and $v \in \mathrm{C}^\infty(\sigma)$. Let $\hat{t}$ be the unitary triangle and let F be the mapping from $\hat{t}$ to t such that $F([0,1] \times \{0\}) = \sigma$. Let $\mathcal{C}_{\hat{t}} \colon \mathrm{C}^\infty([0,1] \times \{0\}) \to \mathrm{C}^\infty(\hat{t})$ be the reference continuation operator, such that

$$\forall \hat{v} \in \mathrm{C}^\infty([0,1] \times \{0\}), \quad \mathcal{C}_{\hat{t}}(\hat{v})(\hat{x}, \hat{y}) = \hat{v}(\hat{x}, 0) \quad \forall (\hat{x}, \hat{y}) \in \hat{t}\,.$$

Then the *continuation* of v to t is $\mathcal{C}_t := \mathcal{C}_{\hat{t}} \circ F^{-1}$

Using classic estimates[38] and (4.3) we have the following properties for edge-bubble functions.

Lemma 4.4. *Let $e \in \mathcal{E}_\delta^{\mathrm{int}}$ and $\mathfrak{b}_e$ be the edge-bubble function of e. Let $\mathcal{P}(e)$ be a polynomial space defined on e. Then, for any $v \in \mathcal{P}(e)$,*

$$\begin{aligned} \|v\|_e^2 &\lesssim (v, v\mathfrak{b}_e)_e \,, \\ \|\mathfrak{b}_e v\|_e &\leq \|v\|_e \,, \\ \|\mathcal{C}_t(v)\,\mathfrak{b}_e\|_t &\lesssim h_t^{\frac{3}{2}} \|v\|_e \quad \forall t \in \omega_e \,, \\ \|\nabla(\mathcal{C}_t(v)\,\mathfrak{b}_e)\|_t &\lesssim h_t^{-\frac{1}{2}} \|v\|_e \quad \forall t \in \omega_e \,. \end{aligned} \tag{4.25}$$

Proof. The proof is analogous to the one of Lemma 4.3: classical results [38] give us the desired inequalities on sub-triangles, while (4.3) allows to extend them to the whole polygon with constants independent of the meshsize, but depending on the quality of the element.

In particular, regarding (4.25), we recall from [38] that, given the regularity assumptions and since $\mathfrak{b}_e$ is a positive function and $\max \mathfrak{b}_e = 1$,

$$\forall t \in \omega_e,\ \|\mathfrak{b}_e\|_t^2 = (\mathfrak{b}_e, \mathfrak{b}_e)_t \leq (\mathfrak{b}_e, 1)_t = \frac{1}{3}|t| \sim h_e^2 \Rightarrow \|\mathfrak{b}_e\|_{\omega_e} \lesssim h_e \,. \tag{4.26}$$

Let $V := \mathcal{C}_t(v)$. First of all, using (4.26), we see that

$$\|V\,\mathfrak{b}_e\|_{\omega_e} \leq \|\mathfrak{b}_e\|_{\omega_e} \|V\|_{\omega_e} \lesssim h_e \|V\|_{\omega_e} \leq h_e \sum_{t\in\omega_e} \|V\|_t \,. \tag{4.27}$$

Let $t \in \omega_e$. Indicating by $\hat{t}$ the unitary triangle, by F the map from $\hat{t}$ to t and setting $\hat{V} := V \circ F$,

$$\|V\|_t^2 = \int_t V^2 = 2\,|t| \int_{\hat{t}} \hat{V}^2 = 2\,|t| \int_0^1 \int_0^{1-x} \hat{v}(\hat{x})^2 \mathrm{d}\hat{y}\mathrm{d}\hat{x} = 2\,|t| \int_0^1 (1-\hat{x})\hat{v}(\hat{x})^2 \leq$$
$$\leq 2\,|t| \int_0^1 \hat{v}(\hat{x})^2 = 2\,|t|\, h_e^{-1} \|v\|_e^2 \lesssim h_e \|v\|_e^2 \,,$$

where $\hat{v} := v \circ F = (V \circ F)|_{\hat{y}=0}$. It follows that $\|V\|_t \lesssim h_e^{\frac{1}{2}} \|v\|_e$ and, using (4.27), we obtain (4.25). □

4.4.2 Lower bounds. By standard techniques[38] and suitable global bubble functions [20, 22] we are able to prove the following lower bound.

Theorem 4.3. *Let u be the solution to (4.1), u_δ^π be defined by (4.6), f be the right-hand side of (4.1), $f_\delta = \Pi_{k-1}^0 f$. Then, $\forall E \in \mathcal{T}_\delta$*

$$\eta_R \lesssim \left\{ |\!|\!| u - u_\delta^\pi |\!|\!|^2 + \sum_{E\in\mathcal{T}_\delta} \frac{h_E^2}{\mathsf{K}_E} \|f - f_\delta\|_E^2 \right\}^{\frac{1}{2}} , \tag{4.28}$$

where h is the maximum diameter of the discretization.

Proof. Let $E \in \mathcal{T}_\delta$ and let $\mathfrak{b}_E$ be the bubble function of E. Let

$$w_E := \frac{h_E}{\sqrt{\mathsf{K}_E}} \left(f_\delta + \nabla\cdot(\mathsf{K}\nabla u_\delta^\pi)\right) \mathfrak{b}_E \in \mathrm{H}_0^1(E) \,,$$
$$w := \sum_{E\in\mathcal{T}_\delta} w_E \in \mathrm{H}_0^1(\Omega) \,.$$

Then, using Lemma 4.3, we prove that

$$\sqrt{\sum_{E\in\mathcal{T}_\delta} \frac{h_E^2}{\mathsf{K}_E} \|f_\delta + \nabla\cdot(\mathsf{K}\nabla u_\delta^\pi)\|_E^2} \lesssim \sqrt{|\!|\!| u - u_\delta^\pi |\!|\!|^2 + \sum_{E\in\mathcal{T}_\delta} \frac{h_E^2}{\mathsf{K}_E} \|f - f_\delta\|_E^2} \,,$$

indeed,

$$\sum_{E\in\mathcal{T}_\delta}\frac{h_E^2}{\mathsf{K}_E}\left\|f_\delta+\nabla\cdot(\mathsf{K}\nabla u_\delta^\pi)\right\|_E^2\lesssim\sum_{E\in\mathcal{T}_\delta}\left(f_\delta+\nabla\cdot(\mathsf{K}\nabla u_\delta^\pi),\frac{h_E}{\sqrt{\mathsf{K}_E}}w_E\right)_E=$$
$$=\sum_{E\in\mathcal{T}_\delta}\left(f,\frac{h_E}{\sqrt{\mathsf{K}_E}}w_E\right)_E-\left(\mathsf{K}\nabla u_\delta^\pi,\frac{h_E}{\sqrt{\mathsf{K}_E}}\nabla w_E\right)_E+\left(f_\delta-f,\frac{h_E}{\sqrt{\mathsf{K}_E}}w_E\right)_E=$$
$$=\sum_{E\in\mathcal{T}_\delta}a^E\left(u-u_\delta^\pi,\frac{h_E}{\sqrt{\mathsf{K}_E}}w_E\right)+\sum_{E\in\mathcal{T}_\delta}\left(f_\delta-f,\frac{h_E}{\sqrt{\mathsf{K}_E}}w_E\right)_E\lesssim$$
$$\lesssim|\!|\!|u-u_\delta^\pi|\!|\!|\sqrt{\sum_{E\in\mathcal{T}_\delta}\frac{h_E^2}{\mathsf{K}_E}\left\|\sqrt{\mathsf{K}}\nabla w\right\|_E^2}+\sum_{E\in\mathcal{T}_\delta}\frac{h_E}{\sqrt{\mathsf{K}_E}}\left\|f_\delta-f\right\|_E\left\|w_E\right\|_E\lesssim$$
$$\lesssim\sqrt{\sum_{E\in\mathcal{T}_\delta}\left\|w\right\|_E^2}\left(|\!|\!|u-u_\delta^\pi|\!|\!|_E^2+\frac{h_E^2}{\mathsf{K}_E}\left\|f-f_\delta\right\|_E^2\right)^{\frac{1}{2}}.$$

Now, consider an edge $e\in\mathcal{E}_\delta^{\mathrm{int}}$ and let $\mathfrak{b}_e$ be the edge-bubble function of e. Define $w_e\in\mathrm{H}_0^1(\omega_e)$ such that

$$w_e|_t:=\mathcal{C}_t\left(\frac{\sqrt{h_e}}{\sqrt{\mathsf{K}_e}}\left[\!\left[\frac{\partial u_\delta^\pi}{\partial\hat{n}_e^{\mathsf{K}}}\right]\!\right]_e\right)\mathfrak{b}_e\quad\forall t\subset\omega_e\,,$$
$$w:=\sum_{e\in\mathcal{E}_\delta^{\mathrm{int}}}w_e\in\mathrm{H}_0^1(\Omega)\,.$$

From the properties in Lemma 4.4 and regularity assumptions on the elements $E\in\mathcal{T}_\delta$ it follows that

$$\sqrt{\sum_{e\in\mathcal{E}_\delta^{\mathrm{int}}}\frac{h_e}{\mathsf{K}_e}\left\|\left[\!\left[\frac{\partial u_\delta^\pi}{\partial\hat{n}_e^{\mathsf{K}}}\right]\!\right]_e\right\|_e^2}\lesssim\sqrt{(1+h^2)\,|\!|\!|u-u_\delta^\pi|\!|\!|^2+\sum_{E\in\mathcal{T}_\delta}\frac{h_E^4}{\mathsf{K}_E}\left\|f-f_\delta\right\|_E^2},$$

indeed,

$$\sum_{e\in\mathcal{E}_\delta^{\text{int}}}\frac{h_e}{\mathsf{K}_e}\left\|\left[\!\left[\frac{\partial u_\delta^\pi}{\partial\hat{n}_e^{\mathsf{K}}}\right]\!\right]_e\right\|_e^2\lesssim\sum_{e\in\mathcal{E}_\delta^{\text{int}}}\left(\left[\!\left[\frac{\partial u_\delta^\pi}{\partial\hat{n}_e^{\mathsf{K}}}\right]\!\right]_e,\sqrt{\frac{h_e}{\mathsf{K}_e}}w_e\right)_e=\sum_{e\in\mathcal{E}_\delta^{\text{int}}}\sum_{t\in\omega_e}\left(\mathsf{K}\nabla u_\delta^\pi,\sqrt{\frac{h_e}{\mathsf{K}_e}}\nabla w_e\right)_t$$
$$+\left(\nabla\cdot(\mathsf{K}\nabla u_\delta^\pi),\sqrt{\frac{h_e}{\mathsf{K}_e}}w_e\right)_t=\sum_{E\in\mathcal{T}_\delta}a^E\left(u_\delta^\pi-u,\sum_{e\in\mathcal{E}_\delta^{\text{int}}}\sqrt{\frac{h_e}{\mathsf{K}_e}}w_e\right)$$
$$+\sum_{e\in\mathcal{E}_\delta^{\text{int}}}\sum_{t\in\omega_e}\left(f+\nabla\cdot(\mathsf{K}\nabla u_\delta^\pi),\sqrt{\frac{h_e}{\mathsf{K}_e}}w_e\right)_t\lesssim|\!|\!|u-u_\delta^\pi|\!|\!|\sqrt{\sum_{e\in\mathcal{E}_\delta^{\text{int}}}\frac{h_e}{\mathsf{K}_e}\left\|\sqrt{\mathsf{K}}\nabla w_e\right\|_{\omega_e}^2}$$
$$+\sum_{e\in\mathcal{E}_\delta^{\text{int}}}\sum_{t\in\omega_e}\sqrt{\frac{h_e}{\mathsf{K}_e}}\left\|(f+\nabla\cdot(\mathsf{K}\nabla u_\delta^\pi))\right\|_t\|w_e\|_t\lesssim\left(|\!|\!|u-u_\delta^\pi|\!|\!|^2+\sum_{E\in\mathcal{T}_\delta}\left(\frac{h_E^4}{\mathsf{K}_E}\|f-f_\delta\|_E^2\right.\right.$$
$$\left.\left.+\frac{h_E^4}{\mathsf{K}_E}\|f_\delta+\nabla\cdot(\mathsf{K}\nabla u_\delta^\pi)\|_E^2\right)\right)^{\frac{1}{2}}\sqrt{\sum_{e\in\mathcal{E}_\delta^{\text{int}}}\frac{h_e}{\mathsf{K}_e}\left\|\left[\!\left[\frac{\partial u_\delta^\pi}{\partial\hat{n}_e^{\mathsf{K}}}\right]\!\right]_e\right\|_e^2}\lesssim$$
$$\lesssim\sqrt{\sum_{e\in\mathcal{E}_\delta^{\text{int}}}\frac{h_e}{\mathsf{K}_e}\left\|\left[\!\left[\frac{\partial u_\delta^\pi}{\partial\hat{n}_e^{\mathsf{K}}}\right]\!\right]_e\right\|_e^2}\left(\left(1+h^2\right)|\!|\!|u-u_\delta^\pi|\!|\!|^2+\sum_{E\in\mathcal{T}_\delta}\frac{h_E^4}{\mathsf{K}_E}\|f-f_\delta\|_E^2\right)^{\frac{1}{2}}.$$

The proof is concluded by the definition of η_R, given by (4.21), and neglecting higher order terms. □

4.5 Numerical results

In the following we present some numerical tests performed in order to numerically evaluate the *effectivity index*, defined as

$$\epsilon:=\frac{err}{\eta_R}\quad\text{where}\quad err:=\left\{\sum_{E\in\mathcal{T}_\delta}\left\|\sqrt{\mathsf{K}}\nabla(u-u_\delta^\pi)\right\|_E^2\right\}^{\frac{1}{2}}.\tag{4.29}$$

A constant behaviour of the effectivity index shows that the constants of equivalence between exact and estimated error are independent of the meshsize, element distortion and diffusivity jumps. Several VEM orders are considered.

In order to test the behaviour of the effectivity index we first perform several tests on the simple domain $\Omega=[0,1]\times[0,1]$, as shown in Figure 4.1, possibly split in subregions (Figures 4.1a to 4.1c: 1 subdomain, Figure 4.1d: 2 subdomains, Figure 4.1e: 4 subdomains) with different diffusivity coefficients on each subdomain. Several meshes are considered to test the behaviour of the estimators on a quasi uniform mesh (Figures 4.1a and 4.1b), as well as on a highly distorted Voronoi mesh (Figure 4.1c).

4.5.1 Test 1: Robustness with respect to mesh distortion. We consider a constant diffusivity $\mathsf{K}(x,y)=1$ and we set the loading term f in such a way that the solution of the problem is $u(x,y)=\sin(2\pi x)\sin(2\pi y)$. We are interested in testing the independence of the effectivity index of the meshsize and observe its variation on different mesh shapes. First, we consider two families of good quality meshes made up of mildly distorted squares

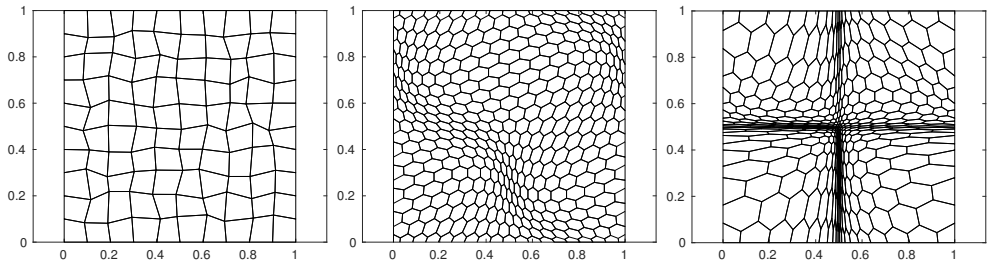

(a) **Test 1** distorted square mesh.

(b) **Test 1** distorted Voronoi mesh.

(c) **Test 1** highly distorted Voronoi mesh.

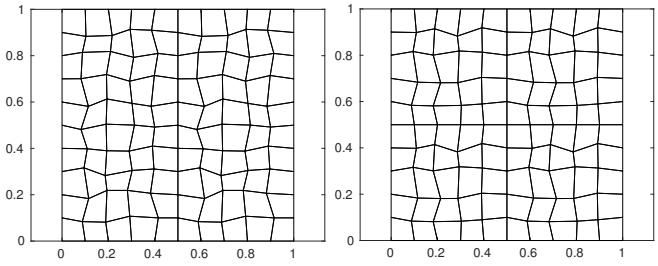

(d) **Test 2** Mesh conforming to the discontinuity of the diffusivity.

(e) **Test 3** Mesh conforming to the discontinuities of the diffusivity.

Figure 4.1: Examples of the meshes used.

	$k=1$		$k=2$		$k=3$		$k=4$	
Mesh	err	η_R	err	η_R	err	η_R	err	η_R
Figure 4.1a	1.0228	1.0275	2.0581	2.0578	3.0790	3.0777	4.1177	4.1149
Figure 4.1b	0.9876	0.9983	1.9707	1.9688	2.9784	2.9848	3.9772	3.9658
Figure 4.1c	1.0667	1.1105	2.0860	1.9827	3.2413	3.2719	-	-

Table 4.1: **Test 1** Convergence rates.

and Voronoi polygons [35] (Figures 4.1a and 4.1b). In Figures 4.2 and 4.3 we compare the exact error err defined by (4.29) and the error estimator η_R defined by (4.21). We see that the two quantities have the same rate of convergence (see also Table 4.1). This agreement is confirmed by Tables 4.2 and 4.3, where we see that the effectivity indices are essentially independent of the meshsize. Moreover, comparing the two tables we see that the effectivity indices corresponding to the same VEM order are quite comparable, thus showing that the efficiency of the estimate is not affected by the type of polygons we choose to discretize the domain.

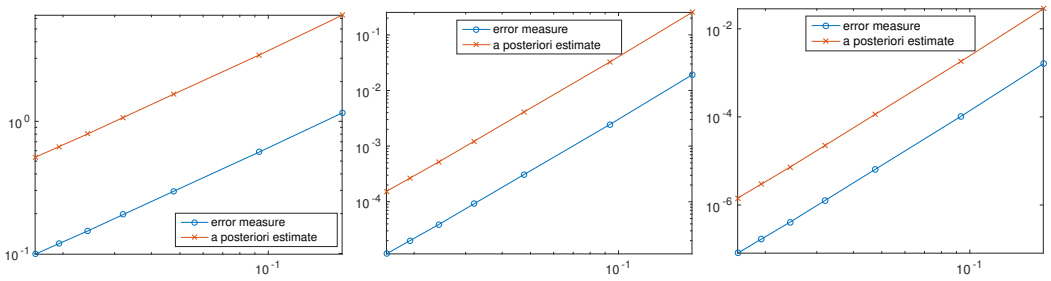

(a) Order 1. (b) Order 3. (c) Order 4.

Figure 4.2: **Test 1**, distorted square mesh Error measure and error estimator vs. maximum diameter of the discretization.

$k=1$		$k=2$		$k=3$		$k=4$	
h	ϵ	h	ϵ	h	ϵ	h	ϵ
0.1784	0.1821	0.1784	0.1106	0.1784	0.0752	0.1784	0.0567
0.0933	0.1843	0.0933	0.1104	0.0933	0.0752	0.0933	0.0566
0.0475	0.1841	0.0475	0.1106	0.0475	0.0749	0.0475	0.0565
0.0321	0.1844	0.0321	0.1106	0.0321	0.0751	0.0321	0.0563
0.0243	0.1843	0.0243	0.1106	0.0243	0.0750	0.0243	0.0563
0.0194	0.1846	0.0194	0.1105	0.0194	0.0750	0.0194	0.0563
0.0161	0.1847	0.0161	0.1105	0.0161	0.0750	0.0161	0.0563

Table 4.2: **Test 1**, distorted square mesh Effectivity indices.

To test the robustness of the estimate in presence of bad quality polygons, we solve the same problem on the mesh in Figure 4.1c, using VEM of order 1 to 3. We do not use larger values for the VEM order as the resulting linear systems turn to out to be too ill conditioned. From Figure 4.4 we see the good agreement between the exact error and

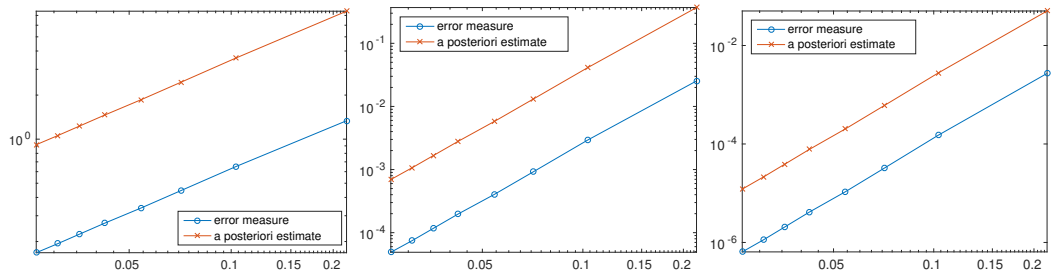

(a) Order 1. (b) Order 3. (c) Order 4.

Figure 4.3: **Test 1**, distorted Voronoi mesh Error measure and error estimator vs. maximum diameter of the discretization.

$k=1$		$k=2$		$k=3$		$k=4$	
h	ϵ	h	ϵ	h	ϵ	h	ϵ
0.2190	0.1786	0.2190	0.1005	0.2190	0.0687	0.2190	0.0539
0.1033	0.1814	0.1033	0.1026	0.1033	0.0712	0.1033	0.0544
0.0711	0.1820	0.0711	0.1012	0.0711	0.0703	0.0711	0.0535
0.0542	0.1822	0.0542	0.1004	0.0542	0.0698	0.0542	0.0530
0.0423	0.1827	0.0423	0.1013	0.0423	0.0706	0.0423	0.0534
0.0357	0.1827	0.0357	0.1008	0.0357	0.0702	0.0357	0.0530
0.0308	0.1827	0.0308	0.1004	0.0308	0.0700	0.0308	0.0528
0.0266	0.1830	0.0266	0.1010	0.0266	0.0704	0.0266	0.0531

Table 4.3: **Test 1**, distorted Voronoi mesh Effectivity indices.

the a posteriori estimate (see also Table 4.1 for the computed convergence rates). These results are confirmed by Table 4.4, from which we can observe that the effectivity index is not significantly affected by the presence of oddly shaped polygons. In particular, the effectivity indices do not depend significantly on the meshsize, mesh distortion, and they are comparable to the ones corresponding to the same order k computed on the previous two meshes (Tables 4.2 and 4.3). The dependence on the mesh regularity parameter is more evident from the effectivity indices shown in Table 4.5, which are computed only on the elements belonging to $\omega_{\text{vd}} = (0.475, 0.525)\times(0,1)\cup(0,1)\times(0.475, 0.525)$, where very distorted elements concentrate. We see that the effectivity index is still asymptotically constant, but its values are influenced by the distortion of the elements.

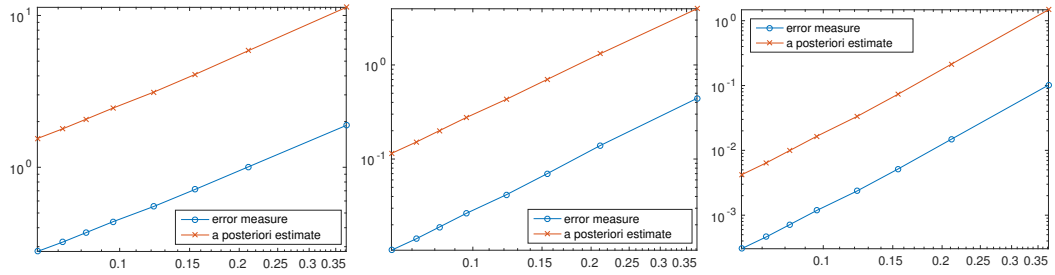

(a) Order 1. (b) Order 2. (c) Order 3.

Figure 4.4: **Test 1**, highly distorted Voronoi mesh Error measure and error estimator vs. maximum diameter of the discretization.

$k=1$		$k=2$		$k=3$	
h	ϵ	h	ϵ	h	ϵ
0.3720	0.1668	0.3720	0.1115	0.3720	0.0688
0.2111	0.1718	0.2111	0.1058	0.2111	0.0695
0.1547	0.1748	0.1547	0.0996	0.1547	0.0702
0.1217	0.1765	0.1217	0.0967	0.1217	0.0708
0.0962	0.1785	0.0962	0.0958	0.0962	0.0717
0.0822	0.1790	0.0822	0.0946	0.0822	0.0719
0.0718	0.1795	0.0718	0.0937	0.0718	0.0721
0.0621	0.1803	0.0621	0.0936	0.0621	0.0724

Table 4.4: **Test 1**, highly distorted Voronoi mesh Effectivity indices.

4.5.2 Test 2: Robustness with respect to diffusivity jumps.

We consider here two further tests featuring discontinuous piecewise constant diffusivities $\mathsf{K}_1(x,y)$ and $\mathsf{K}_2(x,y)$ satisfying a quasi-monotonicity condition (see Remark 4.9) defined on $\Omega = [0,1]\times[0,1]$ as follows:

$$\mathsf{K}_1(x,y) := \begin{cases} 10 & \text{in } \Omega_1 = [0,0.5]\times[0,1], \\ 1 & \text{in } \Omega_2 = (0.5,1]\times[0,1]. \end{cases}$$

$$\mathsf{K}_2(x,y) := \begin{cases} 10^{-3} & \text{in } \Omega_1 = [0,0.5]\times[0,1], \\ 1 & \text{in } \Omega_2 = (0.5,1]\times[0,1]. \end{cases}$$

$k=1$		$k=2$		$k=3$	
h	ϵ	h	ϵ	h	ϵ
0.3720	0.6171	0.3720	0.3150	0.3720	0.1602
0.2111	0.3445	0.2111	0.3280	0.2111	0.1859
0.1547	0.3009	0.1547	0.2984	0.1547	0.2049
0.1217	0.2825	0.1217	0.2787	0.1217	0.2156
0.0962	0.2847	0.0962	0.2781	0.0962	0.2295
0.0822	0.2774	0.0822	0.2697	0.0822	0.2363
0.0718	0.2714	0.0718	0.2643	0.0718	0.2371
0.0621	0.2727	0.0621	0.2664	0.0621	0.2412

Table 4.5: **Test 1**, highly distorted Voronoi mesh Effectivity indices computed on highly distorted polygons only.

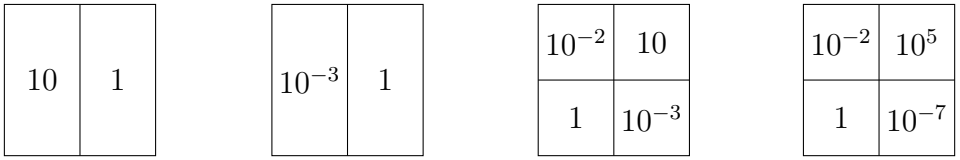

(a) K_1 (b) K_2 (c) K_3 (d) K_4

Figure 4.5: **Test 2**: subfigures a and b, **Test 3**: subfigures c and d; distributions of diffusivity coefficients considered in Sections 4.5.2 and 4.5.3, respectively.

See Figures 4.5a and 4.5b for a representation of these coefficients. In both cases, the loading term is chosen in such a way that the solution corresponding to $\mathsf{K}_i(x,y)$ is $u_i(x,y) = \xi_i(x)Y(y)$, where

$$\xi_i(x) := \begin{cases} -\dfrac{1}{\mathsf{K}_i|_{\Omega_1}}\left(\dfrac{x^2}{2} + c_i x\right) & \text{if } x \in \left[0, \tfrac{1}{2}\right], \\ -\dfrac{1}{\mathsf{K}_i|_{\Omega_2}}\left(\dfrac{x^2}{2} + c_i x - c_i - \dfrac{1}{2}\right) & \text{if } x \in \left(\tfrac{1}{2}, 1\right], \end{cases} \tag{4.30}$$

$$Y(y) := y\,(1-y)\left(y - \frac{1}{2}\right)^2, \tag{4.31}$$

and $c_i := -\frac{3\,\mathsf{K}_i|_{\Omega_1} + \mathsf{K}_i|_{\Omega_2}}{4\left(\mathsf{K}_i|_{\Omega_1} + \mathsf{K}_i|_{\Omega_2}\right)}$ is chosen in such a way that $-\mathsf{K}_i \frac{\mathrm{d}^2\xi_i}{\mathrm{d}x^2} = 1$. In Figure 4.6a we show the solution u_1. We used Virtual Elements of order 1 to 4 with meshes made up of deformed squares conforming to the discontinuity (central vertical line), as in Figure 4.1d. To compare the error estimate and the exact error, we show in Table 4.6 the rates of convergence computed from the tests performed, which are optimal. Tables 4.7 and 4.8 contain the computed effectivity indices. These are stable with respect to the meshsize and we observe that their values are comparable to the ones obtained for the other cases with the same VEM order. Moreover, we notice a very weak dependence of the effectivity indices on the jump of the diffusivity coefficient denoting a good robustness with respect to this property.

Remark 4.11. In the definition of the projection operator P_δ provided in Section 4.3.2 we do not consider any particular strategy to contain the jumps of the diffusivity coefficients within the patches ω_E, and consequently the constants $C_{\mathsf{K},E}$. In this example, the diffusivity distribution satisfies the *quasi-monotonicity* condition and consequently the definition of the

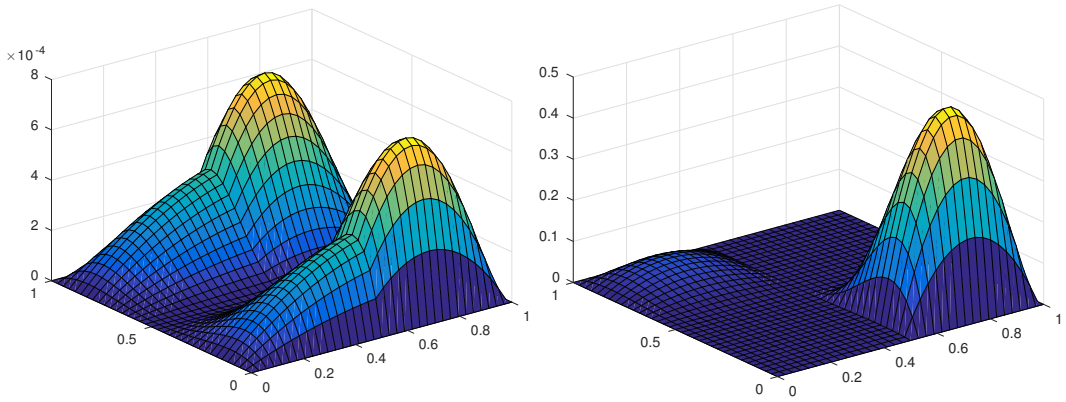

(a) **Test 2**, diffusivity K_1 Exact solution (b) **Test 3**, diffusivity K_3 Exact solution

Figure 4.6: Two solutions with diffusivity jumps

	$k=1$		$k=2$		$k=3$		$k=4$	
Diffusivity	err	η_R	err	η_R	err	η_R	err	η_R
K_1	1.0567	1.0076	2.0792	2.0700	3.0811	3.0666	4.1207	4.1128
K_2	1.0433	1.0112	2.0463	2.0378	3.0579	3.0466	4.1165	4.1077

Table 4.6: **Test 2** Convergence rates.

Clément quasi-interpolator used in the definition of the operator I_δ (Definition 4.3 and [26]) can be replaced by the modified versions in [13, 29, 32] leading to robust estimates (4.15) and (4.16).

$k=1$		$k=2$		$k=3$		$k=4$	
h	ϵ	h	ϵ	h	ϵ	h	ϵ
0.1784	0.1821	0.1784	0.1291	0.1784	0.1113	0.1784	0.0873
0.1449	0.2281	0.1449	0.1403	0.1449	0.1173	0.1449	0.0891
0.0741	0.2272	0.0741	0.1401	0.0741	0.1152	0.0741	0.0881
0.0379	0.2263	0.0379	0.1412	0.0379	0.1156	0.0379	0.0885
0.0194	0.1805	0.0194	0.1312	0.0194	0.1097	0.0194	0.0860
0.0097	0.1801	0.0097	0.1312	0.0097	0.1099		
0.0049	0.1798						

Table 4.7: **Test 2**, diffusivity K_1 Effectivity indices.

4.5.3 Test 3: Checkerboard discontinuous diffusivity. A further test is performed in order to investigate problems with not quasi-monotone diffusivity coefficients [32]

$k=1$		$k=2$		$k=3$		$k=4$	
h	ϵ	h	ϵ	h	ϵ	h	ϵ
0.1784	0.1825	0.1784	0.1630	0.1784	0.1290	0.1784	0.0925
0.1449	0.2135	0.1449	0.1729	0.1449	0.1285	0.1449	0.0931
0.0741	0.2121	0.0741	0.1712	0.0741	0.1257	0.0741	0.0918
0.0379	0.2119	0.0379	0.1733	0.0379	0.1254	0.0379	0.0921
0.0194	0.1823	0.0194	0.1639	0.0194	0.1250	0.0194	0.0908
0.0097	0.1820	0.0097	0.1638	0.0097	0.1248		
0.0049	0.1818						

Table 4.8: **Test 2**, diffusivity K_2 Effectivity indices.

	$k=1$		$k=2$		$k=3$		$k=4$	
	err	η_R	err	η_R	err	η_R	err	η_R
K_3	1.0032	1.0075	2.0211	2.0353	3.0351	3.0316	4.0757	4.0634
K_4	1.0022	1.0075	2.0194	2.0345	3.0328	3.0292	4.0731	4.0594

Table 4.9: **Test 3** Convergence rates.

(see Figures 4.5c and 4.5d):

$$\mathsf{K}_3(x,y) := \begin{cases} 1 & \text{in } \Omega_{11} = [0,0.5)^2, \\ 10^{-3} & \text{in } \Omega_{12} = [0.5,1]\times[0,0.5), \\ 10^{-2} & \text{in } \Omega_{21} = [0,0.5)\times[0.5,1], \\ 10 & \text{in } \Omega_{22} = [0.5,1]^2. \end{cases} \qquad \mathsf{K}_4 := \begin{cases} 1 & \text{in } \Omega_{11}, \\ 10^{-7} & \text{in } \Omega_{12}, \\ 10^{-2} & \text{in } \Omega_{21}, \\ 10^{5} & \text{in } \Omega_{22}. \end{cases}$$

This kind of distributions of the diffusivity coefficient are usually a limitation in deriving efficient a posteriori error estimators based on Clément type quasi interpolation operators [32], nonetheless the numerical results which follow show that the estimates here derived are robust with respect to diffusivity jumps and distribution. The forcing terms are defined in such a way that the exact solutions are

$$u_i(x,y) := \begin{cases} \xi_i(x)Y(y) & \text{in } \Omega_{11}\cup\Omega_{21}, \\ \xi_i(1-x)Y(y) & \text{in } \Omega_{12}\cup\Omega_{22}, \end{cases}$$

$$\text{where} \quad c_i := \begin{cases} -\frac{3\,\mathsf{K}_i|_{\Omega_{11}}+\mathsf{K}_i|_{\Omega_{12}}}{4\left(\mathsf{K}_i|_{\Omega_{11}}+\mathsf{K}_i|_{\Omega_{12}}\right)} & \text{in } \Omega_{11}\cup\Omega_{12}, \\ -\frac{3\,\mathsf{K}_i|_{\Omega_{21}}+\mathsf{K}_i|_{\Omega_{22}}}{4\left(\mathsf{K}_i|_{\Omega_{21}}+\mathsf{K}_i|_{\Omega_{22}}\right)} & \text{in } \Omega_{21}\cup\Omega_{22}, \end{cases} \qquad i\in\{3,4\}\,.$$

In Figure 4.6b we show the solution u_3. As done for the test in Section 4.5.2, we show in Table 4.9 the computed convergence rates for the exact error err and the a posteriori estimate η_R, proving to be optimal. In addition, Tables 4.10 and 4.11 report the computed effectivity indices, which prove that the estimate is robust even though the diffusivity lacks quasi-monotonicity condition. Again, the values of the effectivity indices are comparable to those obtained for the other tests for the same VEM order. Finally, we can see that the effectivity indices are not significantly affected by the jumps of K, although the effectivity indices could be affected by these jumps by Lemma 4.1.

$k=1$		$k=2$		$k=3$		$k=4$	
h	ϵ	h	ϵ	h	ϵ	h	ϵ
0.1799	0.1761	0.1799	0.1538	0.1799	0.1240	0.1799	0.0938
0.0892	0.1840	0.0892	0.1671	0.0892	0.1292	0.0892	0.0917
0.0466	0.1827	0.0466	0.1639	0.0466	0.1261	0.0466	0.0914
0.0238	0.1817	0.0238	0.1646	0.0238	0.1249	0.0238	0.0911
0.0190	0.1815	0.0190	0.1641	0.0190	0.1252	0.0190	0.0909
0.0097	0.1816	0.0097	0.1637	0.0097	0.1246		
0.0049	0.1819						

Table 4.10: **Test 3**, diffusivity K_3 Effectivity indices.

$k=1$		$k=2$		$k=3$		$k=4$	
h	ϵ	h	ϵ	h	ϵ	h	ϵ
0.1799	0.1753	0.1799	0.1545	0.1799	0.1242	0.1799	0.0942
0.0892	0.1841	0.0892	0.1687	0.0892	0.1297	0.0892	0.0917
0.0466	0.1828	0.0466	0.1652	0.0466	0.1265	0.0466	0.0915
0.0238	0.1817	0.0238	0.1660	0.0238	0.1251	0.0238	0.0911
0.0190	0.1815	0.0190	0.1654	0.0190	0.1256	0.0190	0.0909
0.0097	0.1817	0.0097	0.1650	0.0097	0.1249		
0.0049	0.1820						

Table 4.11: **Test 3**, diffusivity K_4 Effectivity indices.

4.5.4 Test 4: irregular solution. Here we test the behaviour of the a posteriori estimate on a problem whose exact solution displays a bounded smoothness [33, 39]. Let

$$\mathsf{K}_5(x,y) := \begin{cases} 100 & \text{in } \Omega_{11} = [0,0.5)^2, \\ 1 & \text{in } \Omega_{12} = [0.5,1] \times [0,0.5), \\ 1 & \text{in } \Omega_{21} = [0,0.5) \times [0.5,1], \\ 100 & \text{in } \Omega_{22} = [0.5,1]^2. \end{cases}$$

Let $\Lambda : \Omega \to \mathbb{R}$ be the function whose expression in polar coordinates with center in $(\frac{1}{2}, \frac{1}{2})$ and with axes parallel to the standard axes is

$$u_5(\rho,\theta) := \rho^\alpha \left(a_{ij}\sin(\alpha\theta) + b_{ij}\cos(\alpha\theta)\right) .$$

This function satisfies $-\nabla \cdot (\mathsf{K}_5 \nabla u_5) = 0$ non-trivially for certain choices of the coefficients, in which case it belongs to $\mathrm{H}^{1+\alpha}(\Omega)$. We present here tests with the choices in Tables 4.12 and 4.13, done with VEM of order 1 to 3 on a triangular mesh conforming to the discontinuites of the diffusivity function. In Tables 4.14 and 4.15 we see how the effectivity indices are subject to bounded oscillations as we refine the mesh. Finally, in Table 4.16 we report the computed rates of convergence for both the choices of coefficients, we can notice a very good agreement with the expected theoretical values $\min\{k, \alpha\}$.

4.5.5 Test DFN: A test on a Discrete Fracture Network. As a final, more general test, we consider a Discrete Fracture Network (DFN, Figure 4.7), that is a possible way to model an impervious fractured medium, consisting in a set of planar rectangles intersecting in space (see [1]). In [12], the flexibility of the Virtual Element Method in handling

$\alpha = 1.873097930277786$		
Ω_{ij}	a_{ij}	b_{ij}
Ω_{11}	0.480354867169885	-0.882756592490932
Ω_{12}	-7.701564882495475	-6.456461752439308
Ω_{21}	9.603960396039620	2.960396039603962
Ω_{22}	-0.100000000000000	1.000000000000000

Table 4.12: **Test 4** First choice for the coefficients

$\alpha = 0.126902069722214$		
Ω_{ij}	a_{ij}	b_{ij}
Ω_{11}	-0.480354867169885	-0.882756592490932
Ω_{12}	7.701564882495503	-6.456461752439336
Ω_{21}	-9.603960396039598	2.960396039603959
Ω_{22}	0.100000000000000	1.000000000000000

Table 4.13: **Test 4** Second choice for the coefficients

$k=1$		$k=2$		$k=3$	
h	ϵ	h	ϵ	h	ϵ
0.1976	0.4014	0.1976	0.1951	0.1976	0.1040
0.0699	0.3897	0.0699	0.1833	0.0699	0.0963
0.0217	0.3877	0.0217	0.1854	0.0217	0.0969
0.0071	0.3904	0.0071	0.1869	0.0159	0.0973

Table 4.14: **Test 4**, First choice Effectivity indices

$k=1$		$k=2$		$k=3$	
h	ϵ	h	ϵ	h	ϵ
0.1976	0.7870	0.1976	0.4221	0.1976	0.2208
0.0699	0.8493	0.0699	0.4380	0.0699	0.2270
0.0217	0.8604	0.0217	0.4341	0.0217	0.2244
0.0159	0.9176	0.0159	0.4654	0.0159	0.2368
0.0050	0.8832	0.0050	0.4391		

Table 4.15: **Test 4**, Second choice Effectivity indices

	$k=1$		$k=2$		$k=3$	
coefficients	err	η_R	err	η_R	err	η_R
Table 4.12	0.9991	0.9998	1.7641	1.7727	1.7443	1.7509
Table 4.13	0.1435	0.1475	0.1312	0.1233	0.1598	0.1778

Table 4.16: **Test 4** Convergence rates.

$k=1$		$k=2$	
err	η_R	err	η_R
1.0302	1.0341	2.0810	2.0813

Table 4.17: **Test DFN** Convergence rates.

hanging nodes as vertices of a polygon that correspond to a flat angle is used to obtain a mesh which is globally conforming to the intersections, allowing the application of domain decomposition techniques. On such domain, the hydraulic head distribution satisfies equation (4.1) on each of the rectangles, with coupling conditions given by the continuity of the solution and balance of incoming and outgoing fluxes at each intersection. The numerical tools developed in the present work can be easily applied to this framework, giving a slightly modified a posteriori error estimator:

$$\tilde{\eta}^2_{R,E} := \frac{h_E^2}{\mathsf{K}_E}\left\|f_\delta + \nabla\cdot(\mathsf{K}\nabla u^\pi_\delta)\right\|^2_E + \frac{1}{2}\sum_{e\in\mathcal{E}^{\mathrm{int}}_\delta\cap\partial E}\frac{h_e}{\mathsf{K}_e}\left\|\left[\!\left[\frac{\partial u^\pi_\delta}{\partial \hat{n}^{\mathsf{K}}_e}\right]\!\right]_e\right\|^2_e + \frac{1}{4}\sum_{e\in\mathcal{E}^{\mathrm{tr}}_\delta\cap\partial E}\frac{h_e}{\mathsf{K}_e}\left\|\left[\!\left[\frac{\partial u^\pi_{hi_e}}{\partial \hat{n}^{\mathsf{K}}_e}\right]\!\right]_e + \left[\!\left[\frac{\partial u^\pi_{hj_e}}{\partial \hat{n}^{\mathsf{K}}_e}\right]\!\right]_e\right\|^2_e,$$

where $\mathcal{E}^{\mathrm{tr}}_\delta$ is the set of edges which lie on some of the rectangle intersections, $\mathcal{E}^{\mathrm{int}}_\delta$ the other internal edges of the fracture, and $u^\pi_{hi_e}$ and $u^\pi_{hj_e}$ are the restrictions of the projection of the discrete solution to the two fractures intersecting at e.

The geometry of the DFN we consider for the numerical tests is shown in Figure 4.7, the diffusivity coefficient is $\mathsf{K}(x,y)=1$, more details on this test problem can be found in [10], Subsection 6.1. In Table 4.18 we show the effectivity indices computed on progressively refined grids for linear and quadratic VEM, whereas in Figure 4.8 the a posteriori estimate is compared to the error measure. The convergence rates of err and η_R are shown in Table 4.17 for $k=1,2$.

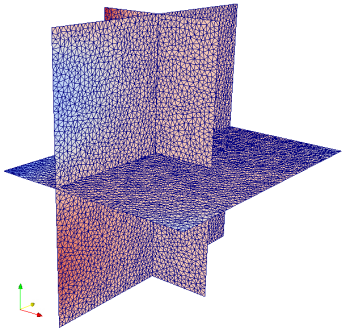

Figure 4.7: **Test DFN** The Discrete Fracture Network considered.

4.6 Conclusions

We have considered the issue of deriving an a posteriori error estimate for the Virtual Element Method formulation of a simple Poisson problem with discontinuous viscosity coefficient com-

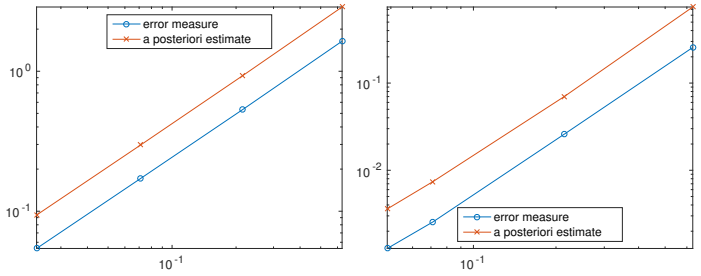

(a) Order 1. (b) Order 2.

Figure 4.8: **Test DFN** Error measure and error estimator vs. maximum diameter of the discretization.

$k=1$		$k=2$	
h	ϵ	h	ϵ
0.6305	0.5699	0.6305	0.3438
0.2144	0.5725	0.2144	0.3702
0.0712	0.5764	0.0712	0.3449
0.0231	0.5770	0.0485	0.3522

Table 4.18: **Test DFN** Effectivity indices.

pletely independent of the particular choice of the VEM stabilization. The numerical solution obtained with a VEM discretization is usually provided through some degrees of freedom that do not allow an easy and direct evaluation of the solution on all the domain. We have introduced a suitable projection of the solution onto a piecewise polynomial space on each element, which can be used for solution evaluation and to define an error measure between such projection and the exact solution. An equivalence relation between the error and the analyzed error estimator can be provided avoiding terms related to the VEM stabilization in the error estimator.

Numerical results clearly show a very good agreement between the error estimator and the exact error, with an almost constant effectivity index confirming that the constants involved in the equivalence relation are independent of the meshsize and the diffusivity jump distribution. In the numerical results we also naturally address a DFN flow problem introducing in the estimates the effect of the flux balance at the fracture intersections; again, an almost constant effectivity index is found.

The proposed approach to the a posteriori error analysis of the error of a polynomial approximation can be extended to more complex problems and is currently under investigation.

4.7 Appendix: stability of the operator $\mathcal{S}_h^\omega$

In this section we provide a short discussion of the stability properties of the operator $\mathcal{S}_h^\omega$.

Lemma 4.5. *Let $v_h \in V_h$, ω be a patch such that the degree of freedom r satisfies condition (4) in Definition 4.2. Let $\mathbf{w} = \frac{\mathbf{u_h}^\intercal(\mathbf{I}-\mathbf{\Pi}^\nabla)^\intercal(\mathbf{I}-\mathbf{\Pi}^\nabla)}{\left\|\mathbf{u_h}^\intercal(\mathbf{I}-\mathbf{\Pi}^\nabla)^\intercal(\mathbf{I}-\mathbf{\Pi}^\nabla)\right\|_\infty}$, where $\mathbf{\Pi}^\nabla \in \mathbb{R}^{N_\omega \times N_\omega}$ is the matrix representing the operator Π_k^∇ on the degrees of freedom of ω, N_ω is the total number of degrees*

of freedom in ω and $\mathbf{u_h}$ is the vector of the degrees of freedom of ω, ordered in such a way that the last one is r. Then,

$$\|\mathcal{S}_h^\omega v_h\| \lesssim \max\left\{1, \frac{1}{|w_{N_\omega}|}\right\} \|v_h\| \ , \tag{4.32}$$

Proof. Let $\mathbf{s_v}$, $\mathbf{v_h}$ be the vectors of degrees of freedom of $\mathcal{S}_h^\omega v_h$ and v_h, respectively, ordered in such a way that the last one is r. Then, condition (4.9) is equivalent to $\frac{\mathbf{w}}{w_{N_\omega}} \cdot \mathbf{s_v} = 0$. Then, $\mathbf{s_v}$ is obtained from $\mathbf{v_h}$ by

$$\mathbf{s_v} = \mathbf{M}^{-1} \begin{pmatrix} \tilde{\mathbf{v}}_\mathbf{h} \\ 0 \end{pmatrix} , \tag{4.33}$$

where $\tilde{\mathbf{v}}_\mathbf{h} \in \mathbb{R}^{N_\omega - 1}$ is the vector of all the degrees of freedom of v_h except the last one (corresponding to the index r in the original numbering), and

$$\mathbf{M} = \begin{pmatrix} \tilde{\mathbf{I}} & \mathbf{0} \\ \frac{\tilde{\mathbf{w}}}{w_{N_\omega}} & 1 \end{pmatrix} ,$$

where $\tilde{\mathbf{I}} \in \mathbb{R}^{N_\omega - 1 \times N_\omega - 1}$ is the identity matrix of order $N_\omega - 1$. From (4.33), we have

$$\|\mathbf{s_v}\|_{\mathbb{R}^{N_\omega}} \leq \left\|\mathbf{M}^{-1}\right\|_{\mathbb{R}^{N_\omega \times N_\omega}} \|\tilde{\mathbf{v}}_\mathbf{h}\|_{\mathbb{R}^{N_\omega - 1}} \leq \left\|\mathbf{M}^{-1}\right\|_{\mathbb{R}^{N_\omega \times N_\omega}} \|\mathbf{v}_h\|_{\mathbb{R}^{N_\omega}} \ , \tag{4.34}$$

We choose as matrix norm the ∞-norm. The matrix $\mathbf{M}^{-1}$ can be written

$$\mathbf{M}^{-1} = \begin{pmatrix} \tilde{\mathbf{I}} & \mathbf{0} \\ -\frac{\tilde{\mathbf{w}}}{w_{N_\omega}} & 1 \end{pmatrix} = \begin{pmatrix} \tilde{\mathbf{I}} & \mathbf{0} \\ \mathbf{0} & \frac{1}{w_{N_\omega}} \end{pmatrix} \begin{pmatrix} \tilde{\mathbf{I}} & \mathbf{0} \\ -\tilde{\mathbf{w}} & w_{N_\omega} \end{pmatrix} \tag{4.35}$$

$$\left\|\mathbf{M}^{-1}\right\|_\infty \leq \max\left\{1, \frac{1}{|w_{N_\omega}|}\right\} \max\left\{1, \|\mathbf{w}\|_1\right\} .$$

Equation (4.32) comes from the equivalence between $\|\mathbf{w}\|_1$ and $\|\mathbf{w}\|_\infty$ in which appears the dimension N_ω that is bounded by the assumption of a bounded number of element in each patch ω. □

A possible algorithm for the construction of the patches can be set up quite easily for $k \geq 2$, resorting to the presence of basis functions whose support is contained in the polygonal elements.

In the following we numerically investigate the value of the stability factor in the case of Test 1 (Section 4.5.1). Namely, we devise a simple possible strategy to build a set of patches that minimizes the stability constant and apply it to different families of progressively refined meshes. We then compute the maximum stability constant for each of the resulting constructed sets and then consider its behaviour with respect to refinement, VEM order and mesh quality.

For a given patch $\omega \in \mathcal{T}_{\delta,\omega}$ let us define the smallest stability constant

$$C_{\mathcal{S}_h^\omega} = \max\left\{1, \frac{1}{|w_r|}\right\} , \tag{4.36}$$

corresponding to all the possible choices of the internal dofs as the dof satisfying (4.8) used to impose (4.9). In order to construct patches we start computing the stability constant for each basis function considering as patch its support. Then, a first set of possible patches

Table 4.19: **Test 1**, order 2 Behaviour of the maximum stability constants of the patches built as described in Section 4.7, and percentage of patches with only one polygon.

distorted square mesh			distorted Voronoi mesh			highly distorted Voronoi mesh		
h	$C_{\mathcal{S}_h^\omega}$	%	h	$C_{\mathcal{S}_h^\omega}$	%	h	$C_{\mathcal{S}_h^\omega}$	%
0.0161	1.03	99.9	0.0266	1.81	13.3	0.0621	2.35	11.6
0.0194	1.00	99.9	0.0308	1.64	15.5	0.0718	2.10	13.0
0.0243	1.00	99.7	0.0357	1.39	17.6	0.0822	1.91	14.8
0.0321	1.00	99.6	0.0423	1.19	21.2	0.0962	1.67	16.0
0.0475	1.00	99.0	0.0542	1.00	0.1	0.1217	1.00	0.1
0.0933	1.00	99.1	0.0711	1.00	0.1	0.1547	1.00	0.1

is built applying a greedy approach. We sort the stability constants in an increasing order and we start to select the patches choosing the support of the basis functions with smallest stability constant that do not contain in the support element already included in a patch. Every time we create a patch we mark the elements around it as elements possibly included in this patch if not included by the process in a different patch. We end the process when all the elements are included in a patch or marked as candidates to be included in a neighboring patch. In a second step we consider the created patches with the largest stability constants for a possible gluing with neighboring patches and elements marked for gluing, considering if this gluing can reduce the stability constant. In this gluing step we consider all the basis functions that become internal after the gluing and compute for all of them the stability constant of the patch and set as stability constant of the new patch the smallest one.

In Tables 4.19 to 4.21 we show the maximum values of constants $C_{\mathcal{S}_h^\omega}$ obtained with this process on different meshes for the test in Section 4.5.1 and different VEM orders k. In Table 4.19 we report the value of the computed stability constants and the percentage of the patches that are constituted by one polygon for $k = 2$, that means that the function φ_r is one of the internal basis functions. We can observe that the estimated stability constants can be considered quite stable with respect to refinement and mesh quality. In Table 4.20 we report the same data for $k = 3$, and the previous conclusions are confirmed in an even more clear way. Results reported for $k = 3$ are obtained with no gluing step. This confirms the assumption that the presence of several internal basis functions simplifies the construction of patches satisfying condition (4) in Definition 4.2. Finally, in Table 4.21 we report the outcome of the algorithm for $k = 1$. The stability of the projection operator $\mathcal{S}_h^\omega$ corresponding to the patches given by the previous algorithm with respect to mesh refinement and patch changes is less evident. A different strategy that considers from the beginning patches with a number of internal basis functions larger than one could probably yield better results.

References for Chapter 4

[1] P. M. Adler. *Fractures and Fracture Networks*. Kluwer Academic, Dordrecht, 1999.

[2] M. Ainsworth and J. T. Oden. "A unified approach to a posteriori error estimation using element residual methods". In: *Numer. Math.* 65.1 (1993), pp. 23–50. ISSN: 0029-599X. DOI: 10.1007/BF01385738.

[3] G. Akrivis, C. Makridakis, and R. H. Nochetto. "A posteriori error estimates for the Crank-Nicolson method for parabolic equations". In: *Math. Comp.* 75.254 (2006), pp. 511–531. ISSN: 0025-5718. DOI: 10.1090/S0025-5718-05-01800-4.

Table 4.20: **Test 1**, order 3 Behaviour of the maximum stability constants of the patches built as described in Section 4.7, and percentage of patches with only one polygon.

distorted square mesh			distorted Voronoi mesh			highly distorted Voronoi mesh		
h	$C_{\mathcal{S}_h^\omega}$	%	h	$C_{\mathcal{S}_h^\omega}$	%	h	$C_{\mathcal{S}_h^\omega}$	%
0.0194	1.00	100.0	0.0266	1.00	22.2	0.0621	1.00	79.3
0.0243	1.00	100.0	0.0308	1.00	24.5	0.0718	1.00	82.5
0.0321	1.00	100.0	0.0357	1.00	35.9	0.0822	1.00	87.3
0.0475	1.00	100.0	0.0423	1.00	32.3	0.0962	1.00	90.6
0.0933	1.00	100.0	0.0542	1.00	31.9	0.1217	1.00	96.6
0.1784	1.00	100.0	0.0711	1.00	52.4	0.1547	1.00	100.0

Table 4.21: **Test 1**, order 1 Behaviour of the maximum stability constants of the patches built as described in Section 4.7.

distorted square mesh		distorted Voronoi mesh		highly distorted Voronoi mesh	
h	$C_{\mathcal{S}_h^\omega}$	h	$C_{\mathcal{S}_h^\omega}$	h	$C_{\mathcal{S}_h^\omega}$
0.0161	8.41e+01	0.0266	2.12e+02	0.0621	6.53e+01
0.0194	5.64e+02	0.0308	1.57e+02	0.0718	4.32e+01
0.0243	1.25e+01	0.0357	8.82e+01	0.0822	4.45e+01
0.0321	1.82	0.0423	7.81e+01	0.0962	4.34e+01
0.0475	1.53	0.0542	4.71e+01	0.1217	8.71e+01
0.0933	1.06	0.0711	3.60e+01	0.1547	9.21e+00

[4] I. Babuška and W. C. Rheinboldt. "Error estimates for adaptive finite element computations". In: *SIAM J. Numer. Anal.* 15.4 (1978), pp. 736–754. ISSN: 0036-1429.

[5] R. Becker and R. Rannacher. "A feed-back approach to error control in finite element methods: basic analysis and examples". In: *East-West J. Numer. Math.* 4.4 (1996), pp. 237–264. ISSN: 0928-0200.

[6] L. Beirão da Veiga, F. Brezzi, A. Cangiani, G. Manzini, L. D. Marini, and A. Russo. "Basic principles of virtual element methods". In: *Mathematical Models and Methods in Applied Sciences* 23.01 (2013), pp. 199–214.

[7] L. Beirão da Veiga, F. Brezzi, L. D. Marini, and A. Russo. "Virtual Element Methods for General Second Order Elliptic Problems on Polygonal Meshes". In: *Mathematical Models and Methods in Applied Sciences* 26.04 (2015), pp. 729–750. DOI: 10.1142/S0218202516500160.

[8] L. Beirão da Veiga, C. Lovadina, and D. Mora. "A Virtual Element Method for elastic and inelastic problems on polytope meshes". In: *Computer Methods in Applied Mechanics and Engineering* 295 (2015), pp. 327–346. ISSN: 0045-7825. DOI: 10.1016/j.cma.2015.07.013.

[9] L. Beirão da Veiga and G. Manzini. "Residual a posteriori error estimation for the Virtual Element Method for elliptic problems". In: *ESAIM: Mathematical Modelling and Numerical Analysis* 49.2 (2015), pp. 577–599.

[10] M. Benedetto, S. Berrone, A. Borio, S. Pieraccini, and S. Scialò. "A Hybrid Mortar Virtual Element Method For Discrete Fracture Network Simulations". In: *J. Comput. Phys.* 306 (2016), pp. 148–166. DOI: 10.1016/j.jcp.2015.11.034.

[11] M. Benedetto, S. Berrone, S. Pieraccini, and S. Scialò. "The virtual element method for discrete fracture network simulations". In: *Comput. Methods Appl. Mech. Engrg.* 280.0 (2014), pp. 135–156. ISSN: 0045-7825. DOI: 10.1016/j.cma.2014.07.016.

[12] M. Benedetto, S. Berrone, and S. Scialò. "A Globally Conforming Method For Solving Flow in Discrete Fracture Networks Using the Virtual Element Method". In: *Finite Elem. Anal. Des.* 109 (2016), pp. 23–36. DOI: 10.1016/j.finel.2015.10.003.

[13] C. Bernardi and R. Verfürth. "Adaptive finite element methods for elliptic equations with non-smooth coefficients". In: *Numerische Mathematik* 85.4 (2000), pp. 579–608.

[14] S. Berrone, A. Borio, and S. Scialò. "A posteriori error estimate for a PDE-constrained optimization formulation for the flow in DFNs". In: *SIAM J. Numer. Anal.* 54.1 (2016), pp. 242–261. DOI: 10.1137/15M1014760.

[15] S. Berrone and T. Kozubek. "An Adaptive WEM Algorithm for Solving Elliptic Boundary Value Problems in Fairly General Domains". In: *SIAM Journal on Scientific Computing* 28.6 (2006), pp. 2114–2138. DOI: 10.1137/04062014X.

[16] S. Berrone and M. Marro. "Space-time adaptive simulations for unsteady Navier-Stokes problems". In: *Comput. & Fluids* 38.6 (2009), pp. 1132–1144. ISSN: 0045-7930. DOI: 10.1016/j.compfluid.2008.11.004.

[17] S. Berrone, S. Pieraccini, and S. Scialò. "A PDE-constrained optimization formulation for discrete fracture network flows". In: *SIAM J. Sci. Comput.* 35.2 (2013), B487–B510. ISSN: 1064-8275. DOI: 10.1137/120865884.

[18] S. Berrone, S. Pieraccini, and S. Scialò. "Towards effective flow simulations in realistic discrete fracture networks". In: *J. Comput. Phys.* 310 (2016), pp. 181–201. DOI: 10.1016/j.jcp.2016.01.009.

[19] S. Berrone, S. Pieraccini, S. Scialò, and F. Vicini. "A parallel solver for large scale DFN flow simulations". In: *SIAM J. Sci. Comput.* 37.3 (2015), pp. C285–C306. DOI: 10.1137/140984014.

[20] S. Berrone. "A Local-in-Space-Timestep Approach to a Finite Element Discretization of the Heat Equation with a Posteriori Estimates". In: *SIAM Journal on Numerical Analysis* 47.4 (2009), pp. 3109–3138. DOI: 10.1137/080737058.

[21] S. Berrone. "Adaptive discretization of stationary and incompressible Navier-Stokes equations by stabilized finite element methods". In: *Comput. Methods Appl. Mech. Engrg.* 190.34 (2001), pp. 4435–4455. ISSN: 0045-7825. DOI: 10.1016/S0045-7825(00)00327-3.

[22] S. Berrone. "Robust a posteriori error estimates for finite element discretizations of the heat equation with discontinuous coefficients". In: *ESAIM: Mathematical Modelling and Numerical Analysis* 40.06 (2006), pp. 991–1021.

[23] S. Berrone. "Skipping transition conditions in a posteriori error estimates for finite element discretizations of parabolic equations". In: *M2AN Math. Model. Numer. Anal.* 44.3 (2010), pp. 455–484. ISSN: 0764-583X. DOI: 10.1051/m2an/2010009.

[24] S. Berrone and E. Süli. "Two-sided a posteriori error bounds for incompressible quasi-Newtonian flows". In: *IMA J. Numer. Anal.* 28.2 (2008), pp. 382–421. ISSN: 0272-4979. DOI: 10.1093/imanum/drm017.

[25] P. Binev, W. Dahmen, and R. DeVore. "Adaptive finite element methods with convergence rates". In: *Numer. Math.* 97.2 (2004), pp. 219–268. ISSN: 0029-599X. DOI: 10.1007/s00211-003-0492-7.

[26] A. Cangiani, E. H. Georgoulis, T. Pryer, and O. J. Sutton. *A posteriori error estimates for the virtual element method*. 2016. arXiv: 1603.05855.

[27] L. Diening, C. Kreuzer, and R. Stevenson. "Instance Optimality of the Adaptive Maximum Strategy". English. In: *Foundations of Computational Mathematics* (2015), pp. 1–36. ISSN: 1615-3375. DOI: 10.1007/s10208-014-9236-6.

[28] V. Dolejší, A. Ern, and M. Vohralík. "A framework for robust a posteriori error control in unsteady nonlinear advection-diffusion problems". In: *SIAM J. Numer. Anal.* 51.2 (2013), pp. 773–793. ISSN: 0036-1429. DOI: 10.1137/110859282.

[29] M. Dryja, V. M. Sarkis, and B. O. Widlund. "Multilevel Schwarz methods for elliptic problemswith discontinuous coefficients in three dimensions". In: *Numerische Mathematik* 72.3 (1996), pp. 313–348. ISSN: 0945-3245. DOI: 10.1007/s002110050172.

[30] A. Ern and M. Vohralík. "Flux reconstruction and a posteriori error estimation for discontinuous Galerkin methods on general nonmatching grids". In: *C. R. Math. Acad. Sci. Paris* 347.7-8 (2009), pp. 441–444. ISSN: 1631-073X. DOI: 10.1016/j.crma.2009.01.017.

[31] P. Jiránek, Z. Strakoš, and M. Vohralík. "A posteriori error estimates including algebraic error and stopping criteria for iterative solvers". In: *SIAM J. Sci. Comput.* 32.3 (2010), pp. 1567–1590. ISSN: 1064-8275. DOI: 10.1137/08073706X.

[32] M. Petzoldt. "A posteriori error estimators for elliptic equations with discontinuous coefficients". In: *Advances in Computational Mathematics* 16.1 (2002), pp. 47–75.

[33] B. Rivière and M. Wheeler. "A Posteriori error estimates for a discontinuous galerkin method applied to elliptic problems". In: *Computers & Mathematics with Applications* 46.1 (2003), pp. 141–163. DOI: 10.1016/S0898-1221(03)90086-1.

[34] R. Stevenson. "Optimality of a standard adaptive finite element method". In: *Found. Comput. Math.* 7.2 (2007), pp. 245–269. ISSN: 1615-3375. DOI: 10.1007/s10208-005-0183-0.

[35] C. Talischi, G. H. Paulino, A. Pereira, and I. F. M. Menezes. "PolyMesher: a general-purpose mesh generator for polygonal elements written in Matlab". In: *Structural and Multidisciplinary Optimization* 45.3 (2012), pp. 309–328. ISSN: 1615-1488. DOI: 10.1007/s00158-011-0706-z.

[36] R. Verfürth. "A posteriori error estimates for finite element discretizations of the heat equation". In: *Calcolo* 40.3 (2003), pp. 195–212. ISSN: 0008-0624. DOI: 10.1007/s10092-003-0073-2.

[37] R. Verfürth. "A posteriori error estimation and adaptive mesh-refinement techniques". In: *Journal of Computational and Applied Mathematics* 50 (1994), pp. 67–83.

[38] R. Verfürth. *A Review of a Posteriori Error Estimation and Adaptive Mesh-Refinement Techniques*. Advances in Numerical Mathematics Series. Teubner B.G. GmbH, 1996. ISBN: 9783519026051.

[39] M. Vohralík. "A Posteriori Error Estimates for Lowest-Order Mixed Finite Element Discretizations of Convection-Diffusion-Reaction Equations". In: *SIAM Journal on Numerical Analysis* 45.4 (2007), pp. 1570–1599. DOI: 10.1137/060653184.

[40] J. Wang. "Superconvergence analysis for finite element solutions by the least-squares surface fitting on irregular meshes for smooth problems". In: *J. Math. Study* 33.3 (2000), pp. 229–243. ISSN: 1006-6837.

[41] T. Zhang and L. Tang. "Superconvergence of the stable $P_1 - P_1$ finite element pair for Stokes problem". English. In: *Calcolo* (2015), pp. 1–15. ISSN: 0008-0624. DOI: 10.1007/s10092-014-0134-8.

[42] O. C. Zienkiewicz and J. Z. Zhu. "The superconvergent patch recovery and a posteriori error estimates. Part 2: Error estimates and adaptivity". In: *International Journal for Numerical Methods in Engineering* 33.7 (1992), pp. 1365–1382. ISSN: 1097-0207. DOI: 10.1002/nme.1620330703.

Chapter 5

The Virtual Element Method for Discrete Fracture Network simulations

In this chapter we introduce a general framework for the use of Virtual Element Methods coupled with domain decomposition techniques to perform numerical simulations on general Discrete Fracture Networks. The content that follows was published in [7].

5.1 Introduction

The simulation of the flow in underground formations is a complex and challenging task, involving multiple physical phenomena on different scales and intricate computational domains. Among the different models available in the literature, Discrete Fracture Network (DFN) [2, 21] models aim at a simplified representation of the network of fractures in the underground, but still reflecting the fracture pattern of the peculiar geological site under investigation and its key hydrological and geometrical characteristics [1, 22–24, 28]. A DFN is a stochastically generated network of fracture-resembling planar polygons in the 3D space. This model is valid under the assumption that the surrounding rock matrix is impervious, and thus the fluid flows along fractures and through fractures intersections. Size, orientation, density and hydrological properties of the fractures, such as the hydraulic transmissivity, are determined using probability distributions based on probing data and laboratory tests on soil specimens. Due to the stochastic nature of input data uncertainty quantification methods are then used to describe the flow properties [14, 33, 39]. The quantity of interest is the hydraulic head in the whole system of fractures, given by the sum of pressure head and elevation. This is ruled by the Darcy law on each fracture with additional constraints of continuity and flux conservation at fracture intersections, called traces. Uncertainty quantification strategies for DFN problems require the repeated computation of the hydraulic head on stochastically generated networks, therefore reliability and efficiency of numerical tools are of paramount importance in this context. The major source of complexity lies in the intricate nature of the domain, characterized by intersecting fractures possibly with extremely narrow angles, almost overlapping parallel traces [19], and, due to the multi-scale nature of the problem, the simultaneous presence of very small and very large fractures intersecting each other. As a consequence, the generation of a conforming mesh suitable for the resolution of the problem with finite element based discretizations might result very hard or even impossible [33, 34], though it is needed in order to ensure a correct representation of the flux exchange between

fractures. A variety of strategies is available in the literature in order to overcome these difficulties, mainly suggesting the use of Mortar methods to relax the conformity constraint at fracture intersections [25, 32, 44, 45], sometimes coupled with mixed [26, 48], domain decomposition methods [46] or Boundary Element Methods [27, 38]; these geometrical difficulties may be even more relevant for more complex flow models such as multiphase flows. In other papers the conformity requirement is accomplished through modification of the geometry of the DFN [33, 40]. An approach not involving mesh generation is described in [24, 42, 43]. More complex models on the fractures can be found in [29–31, 35, 36]. In [15–18], an optimization based method was proposed, capable to remove all conformity constraints and obtain good quality solutions with optimal rates of convergence; this method was further investigated in [9, 13, 19].

In the present chapter, we discuss the use of the rather new Virtual Element Method for performing simulations in fracture networks, building an unified framework for the methods developed in [8, 10]. In Section 5.2 we introduce some notation regarding Discrete Fracture Networks, which will also be used in the upcoming chapters; in Section 5.3 we describe the problem formulation on a DFN; in Section 5.4 we discuss the use of VEM in this framework, focusing on the two possible cited approaches. Finally, we propose in Section 5.5 some numerical results aimed at comparing the two approaches.

5.2 Discrete Fracture Networks

Each fracture in the underground is represented as a 2D open polygon. In what follows, we will identify the geological fracture and its representing polygon, and we will refer also to the polygons as fractures. Accordingly, a DFN Ω is represented as a (3D) set given by the union of N fractures F_i, with $i \in \mathcal{I} = \{1, \dots, N\}$. We also introduce the set $\partial\Omega = \cup_{i\in\mathcal{I}}\partial F_i$. Fractures intersections are called *traces* and denoted by Γ_m, with $m \in \mathcal{M} = \{1, \dots, M\}$ (see Figure 5.1). Without loss of generality, we assume that the set $\bar{\Omega}$ is connected. For the sake of simplicity, we also assume that each trace is given by the intersection of precisely two fractures. For future reference, we introduce the following notation:

- $\forall i \in \mathcal{I}$, we introduce the subset $\mathcal{M}_i \subset \mathcal{M}$ of the indices of traces lying on F_i; each subset $\mathcal{M}_i$ is assumed to be ordered, and we will denote by $\mathcal{M}_i(k)$ the k-th index of a trace in $\mathcal{M}_i$;
- $\forall m \in \mathcal{M}$, we introduce the couple $\mathcal{I}_m = (i, j)$ of indices such that $\Gamma_m = F_i \cap F_j$; the couple is assumed to be ordered in such a way that $i \leq j$;
- for each $i \in \mathcal{I}$ and each $m \in \mathcal{M}_i$, we fix a unit vector $\hat{n}_m^i$ normal to Γ_m on F_i.

For any function defined on Ω, we use a subscript i to indicate its restriction to fracture F_i. Let $\Gamma^D \subseteq \partial\Omega$ be the portion of boundary on which Dirichlet conditions are imposed, and let h^D be the Dirichlet condition defined on Γ^D. We define the functional spaces

$$
\begin{aligned}
V_i &:= \left\{v \in \mathrm{H}^1(F_i) : \gamma_{\Gamma^D}(v) = 0\right\} && \forall i \in \mathcal{I}, \\
V_i^D &:= \left\{v \in \mathrm{H}^1(F_i) : \gamma_{\Gamma^D}(v) = h_i^D\right\} && \forall i \in \mathcal{I}, \\
V &:= \left\{v \colon v_i \in V_i \quad \forall i \in \mathcal{I}\right\}, \\
V^D &:= \left\{v \colon v_i \in V_i^D \quad \forall i \in \mathcal{I}\right\}.
\end{aligned}
$$

For any given segment $\sigma \subset F_i$, $i \in \mathcal{I}$, $\gamma_\sigma^i : \mathrm{H}_0^1(F_i) \to \mathrm{H}^{\frac{1}{2}}(\sigma)$ is the trace operator and

$$
\langle \mu, \beta \rangle_\sigma := {}_{\mathrm{H}^{-\frac{1}{2}}(\sigma)}\langle \mu, \beta \rangle_{\mathrm{H}^{\frac{1}{2}}(\sigma)} \quad \forall \mu \in \mathrm{H}^{-\frac{1}{2}}(\sigma), \forall \beta \in \mathrm{H}^{\frac{1}{2}}(\sigma)
$$

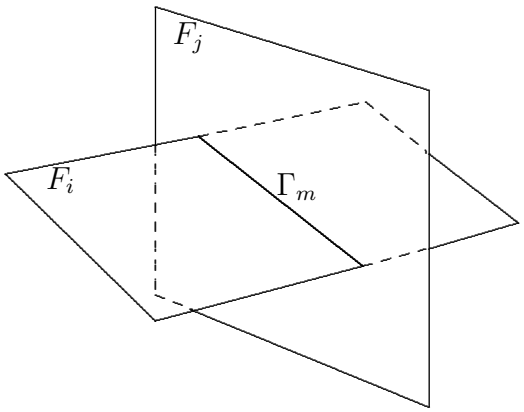

Figure 5.1: Example of two fractures (F_i and F_j) intersecting and generating a trace (Γ_m).

is the duality between $\mathrm{H}^{\frac{1}{2}}(\sigma)$ and $\mathrm{H}^{-\frac{1}{2}}(\sigma)$. For any given function $v \in \mathrm{H}^1_0(F_i)$, $\gamma_{\mathcal{M}_i}(v) \in \prod_{m\in\mathcal{M}_i} \mathrm{H}^{\frac{1}{2}}(\Gamma_m)$ is the tuple of functions $\gamma^i_{\Gamma_m}(v)$, $m \in \mathcal{M}_i$ ordered by increasing trace index m, and we denote the duality between product spaces on the set of the traces of a fracture as

$$\forall \mu \in \prod_{m\in\mathcal{M}_i} \mathrm{H}^{-\frac{1}{2}}(\Gamma_m), \forall \beta \in \prod_{m\in\mathcal{M}_i} \mathrm{H}^{\frac{1}{2}}(\Gamma_m), \quad \langle \mu, \beta\rangle_{\mathcal{M}_i} := \sum_{m\in\mathcal{M}_i} \langle \mu_m, \beta_m\rangle_{\Gamma_m} .$$

For any function $g \in V$, we define the jump operator across a trace Γ_m as $[\![g]\!]_{\Gamma_m} := \gamma^i_{\Gamma_m}(g_i) - \gamma^j_{\Gamma_m}(g_j)$, $\forall m \in \mathcal{M}$ and $(i,j) = \mathcal{I}_m$. Then $[\![g]\!]_{\mathcal{M}_i}$ is the vector of jumps of g across the traces in $\mathcal{M}_i$, ordered according to trace index: $[\![g]\!]_{\mathcal{M}_i} := \left([\![g]\!]_{\Gamma_{\mathcal{M}_i(1)}}, \ldots, [\![g]\!]_{\Gamma_{\mathcal{M}_i(M_i)}}\right)$. Similarly, given a function $g_i \in V_i$, $\left[\!\left[\frac{\partial g_i}{\partial \hat{n}^i_m}\right]\!\right]_{\Gamma_m}$ is the jump of the co-normal derivative across Γ_m on F_i, and we define the tuple

$$\left[\!\left[\frac{\partial g_i}{\partial \hat{n}_{\mathcal{M}_i}}\right]\!\right]_{\mathcal{M}_i} := \left(\left[\!\left[\frac{\partial g_i}{\partial \hat{n}^i_{\mathcal{M}_i(1)}}\right]\!\right]_{\Gamma_{\mathcal{M}_i(1)}}, \ldots, \left[\!\left[\frac{\partial g_i}{\partial \hat{n}^i_{\mathcal{M}_i(M_i)}}\right]\!\right]_{\Gamma_{\mathcal{M}_i(M_i)}}\right).$$

For any segment $\sigma \subset F_i$, $i \in \mathcal{I}$, we introduce the trace operator $\gamma_\sigma \colon \mathrm{H}^1(F_i) \to \mathrm{H}^{\frac{1}{2}}(\sigma)$ and the notation

$$\langle \mu, \beta\rangle_\sigma := {}_{\mathrm{H}^{-\frac{1}{2}}(\sigma)}\langle \mu, \beta\rangle_{\mathrm{H}^{\frac{1}{2}}(\sigma)}, \quad \forall \mu \in \mathrm{H}^{-\frac{1}{2}}(\sigma), \beta \in \mathrm{H}^{\frac{1}{2}}(\sigma),$$

to denote the duality product between $\mathrm{H}^{-\frac{1}{2}}(\sigma)$ and $\mathrm{H}^{\frac{1}{2}}(\sigma)$. Finally, we denote

$$(\mu, \beta)_{\mathcal{M}_i} := \sum_{m\in\mathcal{M}_i} (\mu, \beta)_{\Gamma_m} \quad \forall \mu, \beta \in \prod_{m\in\mathcal{M}_i} \mathrm{L}^2(\Gamma_m) .$$

5.3 Problem formulation

We are interested in computing the hydraulic head $h = \pi/(\rho g) + z \in V^D$, where π is the fluid pressure, g the gravitational acceleration, ρ the fluid density and z the elevation. The hydraulic head, on each fracture F_i, is modeled by means of the Darcy law as follows. Let K_i

denote the transmissivity on F_i, which we assume to be constant, and $f_i = f_i(x)$ denote the source term on F_i; notice that both K_i and f_i are functions of the local tangential coordinate system.

The problem on each fracture is: find $h_i \in V_i^D$ such that, $\forall v_i \in V_i$,

$$(\mathsf{K}_i \nabla h_i, \nabla v_i)_{F_i} = (f_i, v_i)_{F_i} + \left\langle h_i^N, \gamma_{\Gamma_i^N}^i(v_i) \right\rangle_{\Gamma_i^N} + \left\langle \left[\!\left[\frac{\partial h_i}{\partial \hat{n}_{\mathcal{M}_i}} \right]\!\right]_{\mathcal{M}_i}, \gamma_{\mathcal{M}_i}(v_i) \right\rangle_{\mathcal{M}_i} \tag{5.1}$$

where $\left[\!\left[\frac{\partial h_i}{\partial \hat{n}_m^i} \right]\!\right]_{\Gamma_m}$ is the jump of the co-normal derivative $\frac{\partial h_i}{\partial \hat{n}_m^i} = \mathsf{K}_i \nabla h_i \cdot \hat{n}_m^i$ along $\hat{n}_m^i$; furthermore, $\Gamma_i^N \subseteq \partial F_i$ is the Neumann boundary on F_i and $h_i^N \in \mathrm{H}^{-\frac{1}{2}}\left(\Gamma_i^N\right)$ is the Neumann boundary condition. For future reference, we set $\Gamma^N = \cup_{i \in \mathcal{I}} \Gamma_i^N \subset \partial\Omega$ and define h^N such that h_i^N is the restriction of h^N to F_i.

The problems on each fracture are coupled by the imposition of suitable matching conditions which guarantee the continuity of the solution and balance of incoming and outgoing fluxes at each trace: $\forall m \in \mathcal{M}$, with $\mathcal{I}_m = (i, j)$, we have

$$[\![h]\!]_{\Gamma_m} = \gamma_{\Gamma_m}(h_i) - \gamma_{\Gamma_m}(h_j) = 0, \tag{5.2}$$

$$\left[\!\left[\frac{\partial h_i}{\partial \hat{n}_m^i} \right]\!\right]_{\Gamma_m} + \left[\!\left[\frac{\partial h_j}{\partial \hat{n}_m^j} \right]\!\right]_{\Gamma_m} = 0. \tag{5.3}$$

5.4 The Virtual Element Method for DFN simulations

We will use the Virtual Element space defined in Section 2.4 on each fracture, exploiting in particular the fact that the Virtual Element Method allows the use of any kind of non-degenerate star-shaped polygon to mesh the spatial domain, even including the possibility of straight angles. In the present framework, we take advantage from this flexibility to easily build a mesh which, on each fracture, is locally conforming to the traces. In the following of this section, we review the use of VEM, focusing on the framework of DFN simulations.

5.4.1 The VEM setting in the DFN framework. Let us fix a fracture F_i. To obtain a locally conforming mesh, we first introduce on F_i a triangular mesh built independently of trace positions; the triangles are then cut into polygons by the traces, possibly prolonging the trace segment up to the nearest mesh edge if it happens to end in the interior of a triangle. Note that in this latter case the trace tip is kept as a node of the discretization, a new node is created at the intersection between the prolongation of the trace and the mesh edge, and therefore two edges are created, with a 180° angle between them. Let $\mathcal{T}_{\delta,i}$ be the resulting local mesh. Referring to the configuration already depicted in Figure 5.1, we report in Figures 5.2a and 5.2b an example of the VEM meshes $\mathcal{T}_{\delta,i}$ and $\mathcal{T}_{\delta,j}$ obtained on the two fractures F_i and F_j, respectively. Furthermore, we notice that all polygons created with the above procedure are convex, thus satisfying the assumptions in [3], that require the elements to be star-shaped with respect to a ball. Let $\mathcal{T}_\delta = \cup_{i \in \mathcal{I}} \mathcal{T}_{\delta,i}$, being δ a global mesh parameter, e.g. the maximum element diameter. We will use the symbols $\mathcal{E}_{\delta,i}$ and $\mathcal{V}_{\delta,i}$ to denote the sets of edges and vertices on fracture F_i, respectively; similarly, $\mathcal{E}_{\delta,i}^E$ and $\mathcal{V}_{\delta,i}^E$ denote sets of edges and vertices on the element $E \in \mathcal{T}_{\delta,i}$, and define $\mathcal{E}_\delta = \cup_{i \in \mathcal{I}} \mathcal{E}_{\delta,i}$, $\mathcal{V}_\delta = \cup_{i \in \mathcal{I}} \mathcal{V}_{\delta,i}$.

On each fracture F_i, we consider the local VEM spaces defined on $\mathcal{T}_{\delta,i}$:

$$V_{\delta i}^E := \big\{ v_h \in \mathrm{H}^1(E) : \Delta v_h \in \mathbb{P}_k(E),\, v_h \in \mathbb{P}_k(e)\ \forall e \subset \partial E,\, \gamma_{\partial E}(v_h) \in \mathrm{C}^0(\partial E), \\ (v_h, p)_E = \left(\Pi_k^\nabla v_h, p\right)_E\ \forall p \in \mathbb{P}_k(E)/\mathbb{P}_{k-2}(E) \big\} \quad E \in \mathcal{T}_{\delta,i}, \tag{5.4}$$

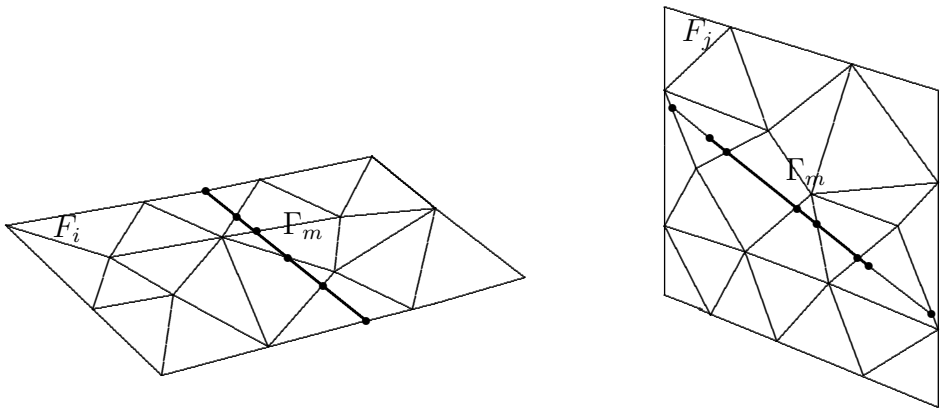

(a) VEM mesh $\mathcal{T}_{\delta,i}$ on F_i

(b) VEM mesh $\mathcal{T}_{\delta,j}$ on F_j

and let the VEM space on F_i be

$$V_{\delta i} := \left\{ v_\delta \in \mathrm{C}^0\left(F_i\right) : v \in V_{\delta i}^E \quad \forall E \in \mathcal{T}_{\delta,i} \right\} . \tag{5.5}$$

Finally, we introduce the following global discrete subspace of V:

$$V_\delta := \left\{ v_\delta \in V \colon v \in V_{\delta i} \quad \forall i \in \mathcal{I} \right\} . \tag{5.6}$$

As seen in Chapter 2, a possible set of degrees of freedom that uniquely define a function $v_\delta \in V_\delta$ is given by:

- the values of v_δ at each vertex $V \in \mathcal{V}_\delta$;
- if $k > 1$, the values of v_δ at $k-1$ internal points (e.g. internal Gauss-Lobatto quadrature nodes) on each edge $e \in \mathcal{E}_\delta$;
- if $k > 1$ the moments $\frac{1}{|E|} \int_E v_h m_{\boldsymbol{\alpha}}$ for $|\boldsymbol{\alpha}| \leq k-2$, where $\boldsymbol{\alpha} = (\alpha_1, \alpha_2) \in \mathbb{N}^2$ and

$$m_{\boldsymbol{\alpha}}(x,y) := \left(\frac{x - x_E}{h_E} \right)^{\alpha_1} \left(\frac{y - y_E}{h_E} \right)^{\alpha_2} ,$$

where (x_E, y_E) and h_E are the centroid and the diameter of the element E, respectively. As a basis of V_δ, we consider the functions ϕ_k, $k \in \{1, \ldots, N\}$ which are lagrangian with respect to the above degrees of freedom.

We now turn our attention to equation (5.1), assuming that the transmissivity coefficient is constant on each element of the mesh. Following [3, 5], in order to discretize this equation using functions in V_δ, since the virtual functions are not known in the interior of the elements, we introduce the operator $\Pi_{k,E}^\nabla \colon V_{\delta i}^E \to \mathbb{P}_k\left(E\right)$ that associates, for each $i \in \mathcal{I}$, $E \in \mathcal{T}_{\delta,i}$, and each $\phi \in V_{\delta i}^E$, the polynomial $\Pi_k^\nabla(\phi)$ such that

$$\begin{cases} \left(\mathsf{K}_i \nabla \Pi_k^\nabla(\phi), \nabla p\right)_E = \left(\mathsf{K}_i \nabla \phi, \nabla p\right)_E & \forall p \in \mathbb{P}_k\left(E\right), \\ \sum_{V \in \mathcal{V}_{\delta,i}^E} \Pi_k^\nabla(\phi)\left(V\right) = \sum_{V \in \mathcal{V}_{\delta,i}^E} \phi(V) & \text{if } k = 1, \\ \int_E \Pi_k^\nabla(\phi) = \int_E \phi & \text{if } k > 1. \end{cases}$$

We remark that the application of this operator only requires the knowledge of the degrees of freedom of ϕ, through the application of Green's formula (see [4]). In addition to Π_k^∇, for

each $E \in \mathcal{T}_{\delta,i}$, let S^E: $V_{\delta i}^E \times V_{\delta i}^E \to \mathbb{R}$ be a symmetric bilinear form defined in such a way that there exist two positive constants c_* and c^* independent on E and i such that $\forall \phi \in V_{\delta i}^E$, if $\Pi_{k,E}^\nabla(\phi) = 0$, then

$$c_* \left(\mathsf{K}_i \nabla\phi, \nabla\phi\right)_E \leq S^E(\phi,\phi) \leq c^* \left(\mathsf{K}_i \nabla\phi, \nabla\phi\right)_E . \tag{5.7}$$

With the above ingredients, we define the discrete bilinear form a_δ^i: $V_\delta \times V_\delta \to \mathbb{R}$ such that, $\forall v, w \in V_\delta$,

$$a_\delta^E(v,w) := \left(\mathsf{K}_i \Pi_{k-1}^0 \nabla v, \Pi_{k-1}^0 \nabla w\right)_E + S^E\left(v - \Pi_k^\nabla v, w - \Pi_k^\nabla w\right) .$$

Thanks to (5.7), we easily find that $a_\delta^E(v,v)$ scales like $\left(\mathsf{K}_i \nabla v, \nabla v\right)_E$, with scaling constants independent of E and of the fracture index i. Thus, if we introduce the fracture-wide bilinear form $a_{\delta i}$: $V_{\delta i} \times V_{\delta i} \to \mathbb{R}$ such that

$$a_{\delta i}(v,w) := \sum_{E \in \mathcal{T}_{\delta,i}} a_\delta^E(v,w) ,$$

we have the following property:

$$\exists \alpha_*, \alpha^* > 0 \colon \alpha_* \left(\mathsf{K}_i \nabla v, \nabla v\right)_{F_i} \leq a_{\delta i}(v,v) \leq \alpha^* \left(\mathsf{K}_i \nabla v, \nabla v\right)_{F_i} . \tag{5.8}$$

Moreover, since the scalar product (f, v_δ) is not computable in general if v_δ is a virtual function, we define the discrete scalar product

$$(f_i, v_{\delta i})_{\delta, F_i} := \left(f_i, \Pi_{k-1}^0 v_{\delta i}\right)_{F_i} \quad \forall i \in \mathcal{I} .$$

Finally, to ease the notation in the following it is convenient to define the global discrete products

$$a_\delta(v_\delta, w_\delta) := \sum_{i \in \mathcal{I}} a_{\delta i}(v_\delta, w_\delta) \qquad \forall v_\delta, w_\delta \in V_\delta,$$
$$(f, v_\delta)_\delta := \sum_{i \in \mathcal{I}} (f_i, v_{\delta i})_{\delta, F_i} \qquad \forall v_\delta \in V_\delta.$$

Remark 5.1. As suggested in [3, 5], a possible choice for the stabilization term S^E is given by the scalar product between the vectors containing the degrees of freedom of the two arguments on the element. This choice guarantees property (5.7) under some basic regularity assumptions on the triangulation. This choice has been adopted in [9].

5.4.2 Formulation of the problem towards domain decomposition.

For each $m \in \mathcal{M}$, with $\mathcal{I}_m = (i,j)$, we define the function $s_{\Gamma_m} \colon \mathcal{I}_m \to \{0,1\}$ such that

$$s_{\Gamma_m}(i) = 1, \quad s_{\Gamma_m}(j) = 0,$$

and the bilinear form $b_i^{\mathcal{M}}$: $M_i := V_i \times \prod_{m \in \mathcal{M}_i} \mathrm{H}^{-\frac{1}{2}}(\Gamma_m) \to \mathbb{R}$ such that

$$b_i^{\mathcal{M}}(v,\psi) := \sum_{m \in \mathcal{M}_i} (-1)^{s_{\Gamma_m}(i)} \left\langle \psi_m, \gamma_{\Gamma_m}(v_i) \right\rangle_{\Gamma_m} ,$$

in such a way that

$$b^{\mathcal{M}}(v,\psi) := \sum_{i \in \mathcal{I}} b_i^{\mathcal{M}}(v,\psi) = \sum_{m \in \mathcal{M}} \left\langle \psi_m, [\![v]\!]_{\Gamma_m} \right\rangle_{\Gamma_m} .$$

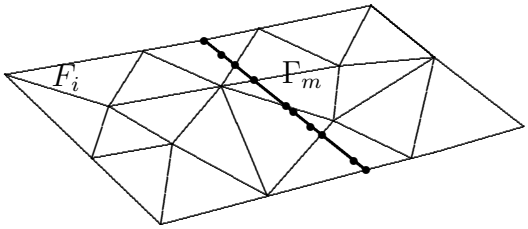

Figure 5.3: Globally conforming VEM mesh on F_i

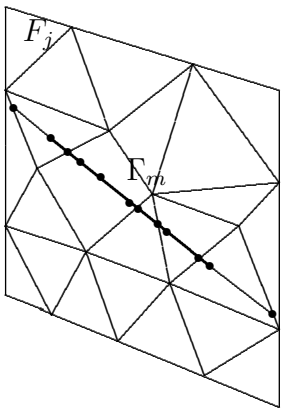

Figure 5.4: Globally conforming VEM mesh on F_j

We define the functional $\mathcal{F}\colon V \times M := \prod_{m\in\mathcal{M}} \mathrm{H}^{-\frac{1}{2}}(\Gamma_m)$ such that

$$\mathcal{F}(v,\psi) := \sum_{i\in\mathcal{I}} \frac{1}{2}\left(\mathsf{K}_i\nabla v_i, \nabla v_i\right)_{F_i} - \left(f_i, v_i\right)_{F_i} - \left\langle h_i^N, \gamma^i_{\Gamma_i^N}(v_i)\right\rangle_{\Gamma_i^N} + \left(\nabla\mathcal{R}_i\left(h_i^D\right), \nabla v_i\right)_{F_i} + b_i^{\mathcal{M}}(v,\psi) + b_i^{\mathcal{M}}\left(\mathcal{R}_i\left(h^D\right),\psi\right), \quad (5.9)$$

where $\mathcal{R}_i$ is the lift operator from $\mathrm{H}^{\frac{1}{2}}\left(\Gamma_i^D\right)$ to $\mathrm{H}^1(F_i)$, $i\in\mathcal{I}$. It is well known (see [47]) that solving problem (5.1)–(5.3) is equivalent to solve the problem of finding $(h,\lambda)\in V^D\times M$ such that $h_i = h_i^0 + \mathcal{R}_i\left(h^D\right)$, $h_i^0\in V_i$, $i\in\mathcal{I}$ and

$$\mathcal{F}\left(h^0,\lambda\right) = \min_{v\in V}\max_{\psi\in M}\mathcal{F}(v,\psi), \quad (5.10)$$

that, by uniqueness of the solution, implies

$$\lambda_m = \left[\!\left[\frac{\partial h_i}{\partial\hat{n}_m^i}\right]\!\right]_{\Gamma_m} = -\left[\!\left[\frac{\partial h_j}{\partial\hat{n}_m^j}\right]\!\right]_{\Gamma_m},$$

with $\mathcal{I}_m = (i,j)$. Notice that the functional $\mathcal{F}$ is made up of local contributions from each fracture. We will now present two different approaches for discretizing problem (5.10).

5.4.3 A globally conforming approach.

A first approach to tackle problem (5.10), introduced in [10], is to strongly impose the matching conditions by building a globally conforming mesh. This is easily achieved by exploiting the capability of the Virtual Element Method to handle straight angles. Consider the mesh $\mathcal{T}_\delta$ constructed as depicted in Section 5.4.1 and let us consider an arbitrary trace Γ_m, with $m\in\mathcal{M}$ and $\mathcal{I}_m = (i,j)$. Then, we add to $\mathcal{T}_{\delta,i}$ the nodes generated by $\mathcal{T}_{\delta,j}$ on Γ_m, and vice-versa. Some polygons belonging to mesh $\mathcal{T}_{\delta,i}$ ($\mathcal{T}_{\delta,j}$, respectively) having an edge lying on Γ_m, will possibly have such edges split by the new nodes, the new edges forming a straight angle at their intersection. In the same configuration of Figures 5.1, 5.2a and 5.2b, we show in Figures 5.3 and 5.4 the globally conforming VEM meshes on F_i and F_j, respectively.

We will call $\mathcal{T}_\delta^{gc}$ this new set of globally conforming polygons and discretize problem (5.10) with the Virtual Element Method as previously described. Let $V_\delta^{\mathrm{gc}}\subset V$ be the

Virtual Element space defined on $\mathcal{T}_\delta^{gc}$ considering, for each trace node, two different degrees of freedom, each one associated with one of the two fractures intersecting there. In other words, we admit that functions in V_δ^{gc} could be discontinuous on each trace, even though on each trace their degrees of freedom correspond to the same geometrical point. To discretize the space M we define, for each $i \in \mathcal{I}$ and on each trace Γ_m such that $m \in \mathcal{M}_i$, the finite dimensional space

$$M_{\delta m,i}^{\mathrm{gc}} = \operatorname{span}\left\{\mu_{ki}^m,\ k = 1, \dots, N_{\Gamma_m}\right\},$$

where N_{Γ_m} is the number of interior nodes on Γ_m and μ_{ki}^m is a continuous linear operator such that

$$\left\langle \mu_{ki}^m, \gamma_{\Gamma_m}(v_{\delta j})\right\rangle_{\Gamma_m} = \delta_{ij} v_{\delta i}(\mathbf{x}_k^m) \quad \forall v_\delta \in V_\delta^{\mathrm{gc}}, \tag{5.11}$$

being δ_{ij} the Kroneker delta and $\mathbf{x}_k^m$ the k-th node on trace Γ_m. The space that discretizes M is $M_\delta^{\mathrm{gc}} = \prod_{m\in\mathcal{M}} M_{\delta m}^{\mathrm{gc}}$, where

$$M_{\delta m}^{\mathrm{gc}} := \left\{\mu_k^m \colon \mu_k^m = \mu_{ki}^m - \mu_{kj}^m \text{ if } \mathcal{I}_m = (i,j)\,,\ k = 1, \dots, N_{\Gamma_m}\right\}.$$

With this definition we have, for any $m \in \mathcal{M}$, if $\mathcal{I}_m = (i,j)$, $\forall k \in \{1, \dots, N_{\Gamma_m}\}$,

$$\left\langle \mu_k^m, [\![v_\delta]\!]_{\Gamma_m}\right\rangle_{\Gamma_m} = \left\langle \mu_{ki}^m, \gamma_{\Gamma_m}(v_{\delta i})\right\rangle_{\Gamma_m} - \left\langle \mu_{kj}^m, \gamma_{\Gamma_m}(v_{\delta j})\right\rangle_{\Gamma_m} = v_{\delta i}(\mathbf{x}_k^m) - v_{\delta j}(\mathbf{x}_k^m),$$

and therefore, enforcing orthogonality of the jumps on traces with respect to M_δ^{gc} is enough to obtain continuity on V_δ^{gc}. Indeed,

$$b^{\mathcal{M}}(v_\delta, \psi_\delta) = 0 \quad \forall \psi_\delta \in M_\delta^{\mathrm{gc}} \iff [\![v_\delta]\!]_{\mathcal{M}} = 0\,.$$

Let us define, for $i \in \mathcal{I}$

$$h_\delta = h_\delta^0 + \mathcal{R}_\delta\big(h^D\big),$$

where $h_\delta^0 \in V_\delta^{\mathrm{gc}}$ and $\mathcal{R}_\delta\big(h^D\big)$ is the discrete lifting of the boundary conditions. For the sake of simplicity we neglect the approximation error of the Dirichlet boundary condition. The globally conforming discrete solution $(h_\delta^0, \lambda_\delta) \in V_\delta^{\mathrm{gc}} \times M_\delta^{\mathrm{gc}}$ satisfies the virtual element discretization of (5.10):

$$\mathcal{F}\left(h_\delta^0, \lambda_\delta\right) = \min_{v_\delta \in V_\delta^{\mathrm{gc}}} \max_{\psi_\delta \in M_\delta^{\mathrm{gc}}} \mathcal{F}\left(v_\delta, \psi_\delta\right),$$

which leads us to the following saddle point formulation:

$$\begin{cases} a_\delta\big(h_\delta^0, v_\delta\big) + b^{\mathcal{M}}(v_\delta, \lambda_\delta) = (f, v_\delta)_\delta + \left\langle h^N, \gamma_{\Gamma^N}(v_{\delta i})\right\rangle_{\Gamma^N} \\ \qquad\qquad\qquad\qquad + a_\delta\big(\mathcal{R}_\delta\big(h^D\big), v_\delta\big) & \forall v_\delta \in V_\delta^{\mathrm{gc}}, \\ b^{\mathcal{M}}\big(h_\delta^0, \psi_\delta\big) = -b^{\mathcal{M}}\big(\mathcal{R}_\delta\big(h^D\big), \psi_\delta\big) & \forall \psi_\delta \in M_\delta^{\mathrm{gc}}. \end{cases}$$

The above problem has a unique solution because $v_\delta \mapsto \sum_{i\in\mathcal{I}} \left(\mathsf{K}_i \nabla v_{\delta i}, \nabla v_{\delta i}\right)_{F_i}$ is a norm on

$$W_\delta^{\mathrm{gc}} = \left\{v_\delta \in V_\delta^{\mathrm{gc}} \colon b^{\mathcal{M}}(v_\delta, \psi_\delta) = 0\ \forall \psi_\delta \in M_\delta^{\mathrm{gc}}\right\} = \left\{v_\delta \in V_\delta^{\mathrm{gc}} \colon [\![v_\delta]\!]_{\Gamma_m} = 0\ \forall m \in \mathcal{M}\right\},$$

and therefore a_δ is coercive on W_δ^{gc} thanks to (5.8), and that

$$\forall \psi_\delta \in M_\delta^{\mathrm{gc}}, \quad \sup_{v_\delta \in V_\delta^{\mathrm{gc}}} \frac{b^{\mathcal{M}}(v_\delta, \psi_\delta)}{\|v_\delta\|_{V_\delta}} = \|\psi_\delta\|_{M_\delta^{\mathrm{gc}}},$$

since M_δ is a space of linear operators.

Implementation. Let $\{\phi_k^{\mathrm{gc}}\}_{k=1}^{\dim V_\delta^{\mathrm{gc}}}$ be the Lagrangian basis of V_δ^{gc} and define, for each $i \in \mathcal{I}$, the fracture stiffness matrix A_i, such that

$$(A_i)_{kl} = a_{\delta i}(\phi_{ki}^{\mathrm{gc}}, \phi_{li}^{\mathrm{gc}}) \ .$$

We note that, by (5.11), if ϕ_l^{gc} is a basis function associated to an internal node of the mesh (always placed on the boundary of a VEM element),

$$b_i^{\mathcal{M}}(\phi_l^{\mathrm{gc}}, \mu_k^m) = \begin{cases} (-1)^{s_{\Gamma_m}(i)} & \text{if } \mathbf{x}_l = \mathbf{x}_k^m, \\ 0 & \text{otherwhise,} \end{cases}$$

where $\mathbf{x}_l$ is the node associated to ϕ_l^{gc}. If ϕ_l^{gc} is a basis function associated to one of the polygon internal degrees of freedom, $b_i^{\mathcal{M}}(\phi_l, \mu_k^m) = 0 \ \forall i \in \mathcal{I}, m \in \mathcal{M}_i, k \in \{1, \dots, N_{\Gamma_m}\}$. To collect the terms coming from the bilinear form $b^{\mathcal{M}}$, we define a global numbering of the degrees of freedom on all the traces and, for each $m \in \mathcal{M}$, with $\mathcal{I}_m = (i, j)$, we identify the row vector B_m such that $(B_m)_k = 1$ if the k-th trace degree of freedom is on trace m and fracture i and $(B_m)_k = -1$ if the k-th trace degree of freedom is on trace m and fracture j. Then the vector $\mathbf{h}$ containing the degrees of freedom of h_δ is the solution of

$$\begin{pmatrix} A & B^T \\ B & 0 \end{pmatrix} \begin{pmatrix} \mathbf{h} \\ \boldsymbol{\lambda} \end{pmatrix} = \begin{pmatrix} \mathbf{f} \\ \mathbf{d} \end{pmatrix} , \tag{5.12}$$

where $\boldsymbol{\lambda}$ is a vector of Lagrange multipliers, $\mathbf{f}$ is the vector containing the right-hand-side terms, $\mathbf{d}$ the vector of nodal values of h^D on the traces and

$$A := \begin{pmatrix} A_1 & & & \\ & A_2 & & \\ & & \ddots & \\ & & & A_N \end{pmatrix} , \qquad B := \begin{pmatrix} B_1 \\ \vdots \\ B_M \end{pmatrix} .$$

Using classical results (see e.g. [41]) it is easily proven that system (5.12) has a unique solution. Moreover, this reformulation falls into the framework of domain decomposition methods [50]; this property is exploited in [10] to devise a preconditioned one-level FETI method [37] for its solution.

5.4.4 A Hybrid Mortar Virtual Element approach.

The second approach we present here, developed in [8], consists in imposing a weak continuity of the solution, by applying the mortar element method [6, 11, 12].

We consider the locally conforming mesh $\mathcal{T}_\delta$ defined in Section 5.4.1 and, for each $m \in \mathcal{M}$, with $\mathcal{I}_m = (i, j)$, we introduce a finite dimensional space $M_{\delta m} \subset \mathrm{L}^2(\Gamma_m)$ defined on the discretization of the trace induced by $\mathcal{T}_{\delta,i}$. We discretize (5.10) on $V_\delta \times M_\delta = \prod_{m \in \mathcal{M}} M_{\delta m}$, where V_δ is the Virtual Element space defined by (5.4)-(5.6). The mortar formulation of the problem is: find $h_\delta = h_\delta^0 + \mathcal{R}_\delta(h^D)$, with $h_\delta^0 \in V_\delta$ and $\lambda_\delta \in M_\delta$ such that,

$$\begin{cases} a_\delta(h_\delta^0, v_\delta) + b^{\mathcal{M}}(v_\delta, \lambda_\delta) = (f, v_\delta)_\delta + \left(h^N, v_\delta\right)_{\Gamma^N} - a_\delta\left(\mathcal{R}_\delta(h^D), v_\delta\right) & \forall v_\delta \in V_\delta , \\ b^{\mathcal{M}}(h_\delta^0, \psi_\delta) = -b^{\mathcal{M}}\left(\mathcal{R}_\delta(h^D), \psi_\delta\right) & \forall \psi_\delta \in M_\delta . \end{cases} \tag{5.13}$$

In practical implementations, $M_{\delta m}$ will be a piecewise polynomial space (see [11, 49]). The well-posedness of (5.13) is proved in [8] under the hypothesis that M_δ contains the constant functions and under the following regularity assumption.

Assumption 5.1. There exists a constant $\sigma > 0$ independent of δ such that, $\forall E \in \mathcal{T}_\delta$, the distance between any two vertices of E is larger than or equal to σh_E, where h_E is the diameter of E.

Indeed, since $v_\delta \mapsto \sum_{i\in\mathcal{I}} \left(\mathsf{K}_i \nabla v_{\delta i}, \nabla v_{\delta i}\right)_{F_i}$ is a norm on

$$W_\delta := \left\{ v_\delta \in V_\delta \colon b^{\mathcal{M}}(v_\delta, \psi_\delta) = 0 \quad \forall \psi_\delta \in M_\delta \right\} ,$$

by (5.8), a_δ is coercive of W_δ. Moreover, by classical arguments (see [20, 47]), since VEM functions are piecewise polynomials on traces and Assumption 5.1 allows us to build a regular triangulation inside each polygon, there exists a constant $\beta > 0$ independent of δ such that the following *inf-sup* condition holds:

$$\inf_{\psi_\delta \in M_\delta} \sup_{v_\delta \in V_\delta} \frac{b^{\mathcal{M}}(v_\delta, \psi_\delta)}{\|v_\delta\|_{V_\delta} \|\psi_\delta\|_{M_\delta}} \geq \beta \, .$$

An advantage of the present method, as opposite to the globally conforming case, is that $\lambda_{\delta m}$ is now a piecewise polynomial approximation of $\left[\!\left[\frac{\partial h_i}{\partial \hat{n}_m^i} \right]\!\right]_{\Gamma_m}$, whereas in the previous case the latter is obtained by evaluating the gradient of the numerical solution, and this may yield less accurate approximations.

Implementation. As previously sketched, the space $M_{\delta m}$, $m \in \mathcal{M}$, will contain piecewise polynomial (not necessarily continuous) functions, defined on the discretization of the trace Γ_m induced by $\mathcal{T}_{\delta,i}$, with $\mathcal{I}_m = (i, j)$. Let N_h and N_λ be the total number of degrees of freedom of h_δ^0 and λ_δ, respectively. The vectors $\mathbf{h}$ and $\boldsymbol{\lambda}$ containing the degrees of freedom are the solution of the system

$$\begin{pmatrix} A & B^T \\ B & 0 \end{pmatrix} \begin{pmatrix} \mathbf{h} \\ \boldsymbol{\lambda} \end{pmatrix} = \begin{pmatrix} \mathbf{f} \\ \mathbf{d} \end{pmatrix} ,$$

where $A \in \mathbb{R}^{N_h \times N_h}$ is defined, as in Section 5.4.3, as the block-diagonal matrix of the local stiffness matrices and $B \in \mathbb{R}^{N_\lambda \times N_h}$ collects the terms coming from $b^{\mathcal{M}}$:

$$B_{lk} := b^{\mathcal{M}}(\phi_k, \psi_l) \quad \forall l \in \{1, \dots, N_\lambda\},\, k \in \{1, \dots, N_h\},$$

being ϕ_k the k-th basis function of V_δ and μ_l the l-th basis function of M_δ. Regarding the right-hand-side, we have

$$\begin{aligned} f_k &:= (f, \phi_k)_\delta + \left(h^N, \phi_k\right)_{\Gamma^N} - a_\delta\left(\mathcal{R}_\delta\left(h^D\right), \phi_l\right) && \forall k \in \{1, \dots, N_h\}, \\ d_l &:= -b^{\mathcal{M}}\left(\mathcal{R}_\delta\left(h^D\right), \psi_l\right) && \forall l \in \{1, \dots, N_\lambda\}. \end{aligned}$$

5.5 Numerical results

While referring the reader to [8, 10] for numerical results that validate the two proposed approaches, here we focus on a comparison between the two.

We consider two DFNs. The first example is a more simple DFN (Figure 5.5a) presenting all possible configurations (tips, three fractures intersection point and traces spanning all the fracture) for which we have an analytical solution, reported in [8]. The second one (Figure 5.5b) is a more complex DFN stochastically generated, containing 27 fractures and all common geometrical complexities. More details can be found in [10].

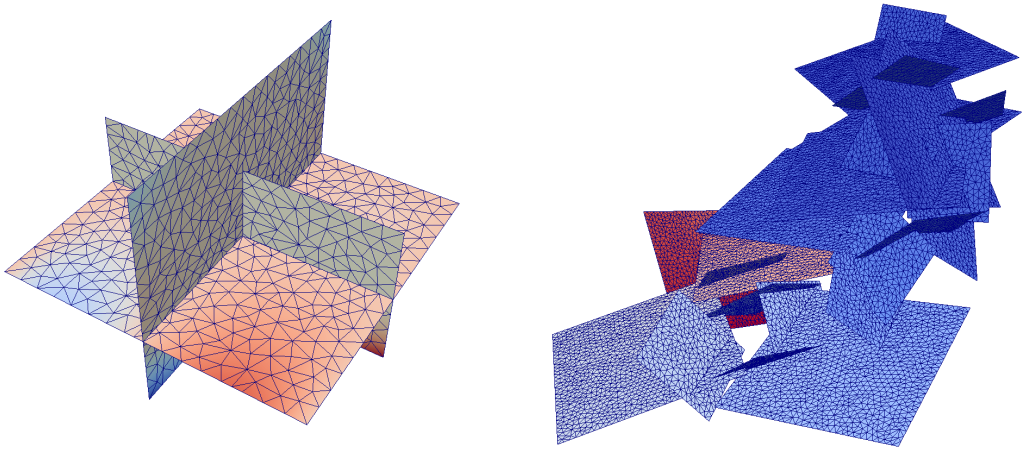

(a) Geometry of the 3 fracture DFN (b) Geometry of the 27 fracture DFN

Figure 5.5

Figure 5.6a displays a possible mesh configuration on the DFN in Figure 5.5b. In Figure 5.6b a detail of the previous mesh is reported. We highlight that, as said in Section 5.4.1, a triangular mesh is built independently on each fracture and then triangles are cut in along the traces, thus obtaining convex polygons. In the case of the globally conforming approach (Section 5.4.3), all the mesh points on the traces become degrees of freedom of the VEM spaces defined on each fracture (each physical point corresponds to two different degrees of freedom, one for each fracture). Instead, the VEM-Mortar approach (Section 5.4.4) requires that the points on the traces become degrees of freedom of the VEM space defined only on the fracture which they belong to.

To compare the results obtained by the two methods, we focus on the fluxes computed on traces. Using the Mortar approach with piecewise linear Lagrange multipliers, we obtain an approximation of the flux at each trace from the solution λ_δ of the problem. In the globally

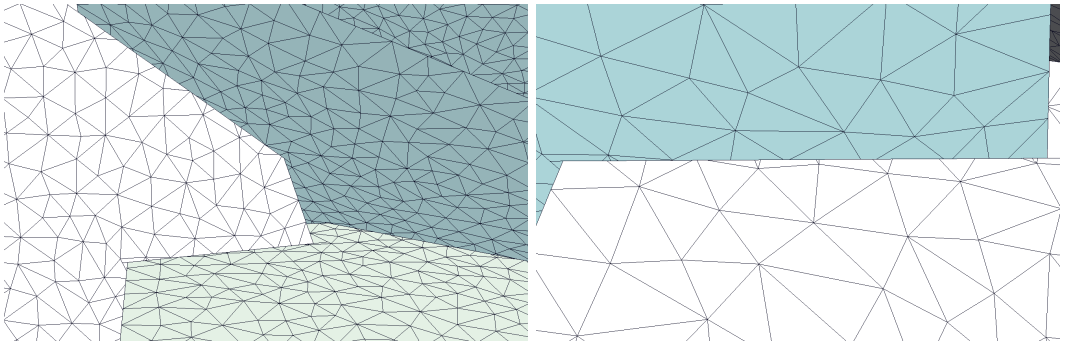

(a) (b)

Figure 5.6: Detail of the non-conformity of the fracture meshes to traces

conforming case, we obtain an approximation of the flux by post-processing the discrete solution, first projecting it on polynomials on each VEM element and then computing the jump of the co-normal derivative of the projection.

In Figure 5.7 we compare the fluxes obtained by the conforming and the Mortar approaches to the exact solution for the trace with the tip (the vertical one) of the DFN in Figure 5.5a. We can see a good agreement between the fluxes.

In Figure 5.8 we show this comparison on three different traces of the DFN in Figure 5.5b, from which we see that the two proposed approaches give comparable results.

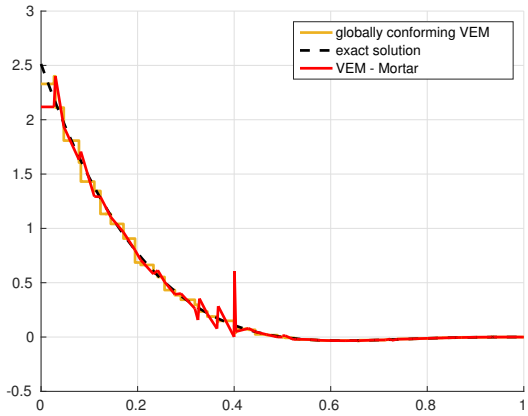

Figure 5.7: Superposition of the fluxes computed by the two methods and the exact solution on a trace of the DFN in Figure 5.5a.

In the Mortar approach the plot of the fluxes displays evident oscillations, due to the fact that convergence to the exact solution is proven in the $\mathrm{H}^{-\frac{1}{2}}(\Gamma_m)$-norm, $\forall m \in \mathcal{M}$. Nevertheless, the quality of the approximation is usually more accurate and reliable being the result of a direct computation and not of a post-processing process.

References for Chapter 5

[1] P. M. Adler. *Fractures and Fracture Networks*. Kluwer Academic, Dordrecht, 1999.

[2] J. Bear and A. H.-D. Cheng. *Modeling Groundwater Flow and Contaminant Transport*. Theory and Applications of Transport in Porous Media 23. Springer, 2010.

[3] L. Beirão da Veiga, F. Brezzi, A. Cangiani, G. Manzini, L. D. Marini, and A. Russo. "Basic principles of virtual element methods". In: *Mathematical Models and Methods in Applied Sciences* 23.01 (2013), pp. 199–214.

[4] L. Beirão Da Veiga, F. Brezzi, L. D. Marini, and A. Russo. "The hitchhiker's guide to the Virtual Element method". In: *Math. Models Methods Appl. Sci* 24.8 (2014), pp. 1541–1573.

[5] L. Beirão da Veiga, F. Brezzi, L. D. Marini, and A. Russo. "Virtual Element Methods for General Second Order Elliptic Problems on Polygonal Meshes". In: *Mathematical Models and Methods in Applied Sciences* 26.04 (2015), pp. 729–750. DOI: 10.1142/S0218202516500160.

[6] F. B. Belgacem. "The mortar finite element method with Lagrange multipliers". In: *Numerische Mathematik* 84.2 (1999), pp. 173–197.

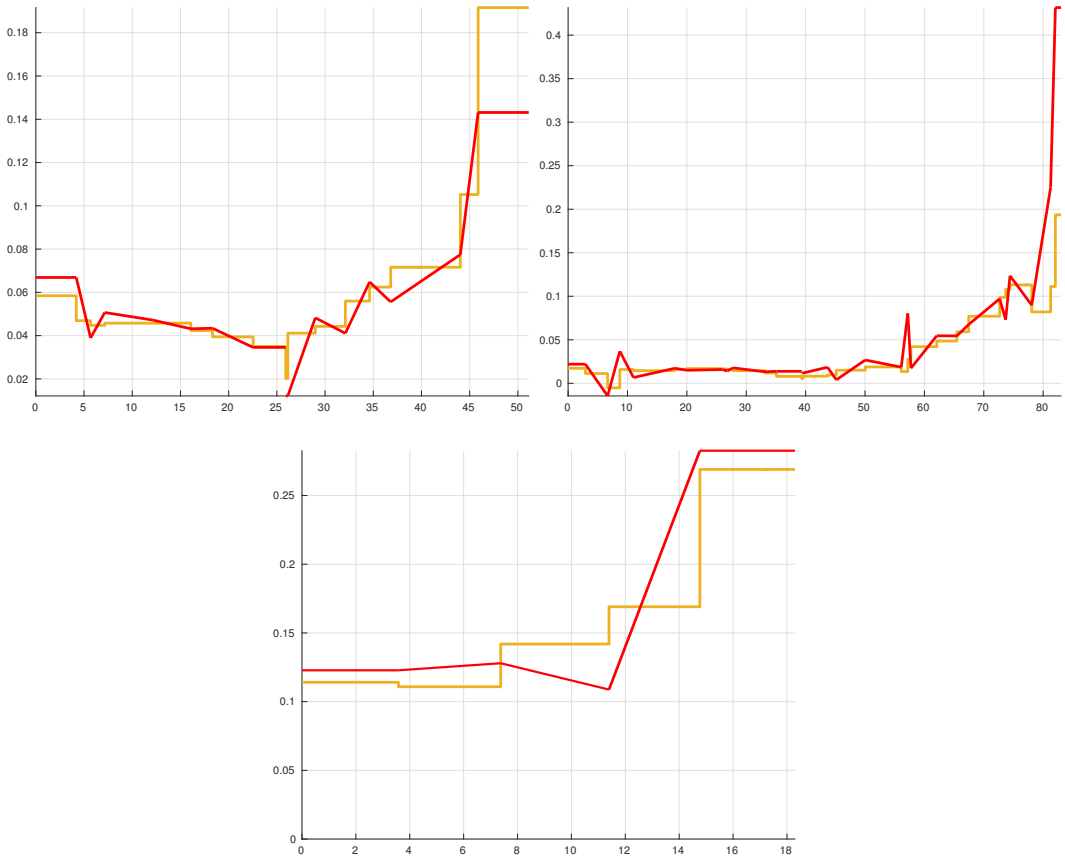

Figure 5.8: Superposition of the fluxes computed by the two methods on three traces of the 27 fracture DFN in Figure 5.5b.

[7] M. Benedetto, S. Berrone, and A. Borio. "The Virtual Element Method for underground flow simulations in fractured media". In: *Advances in Discretization Methods*. Vol. 12. SEMA SIMAI Springer Series. Switzerland: Springer International Publishing, 2016. Chap. 8, pp. 167–186. DOI: 10.1007/978-3-319-41246-7.

[8] M. Benedetto, S. Berrone, A. Borio, S. Pieraccini, and S. Scialò. "A Hybrid Mortar Virtual Element Method For Discrete Fracture Network Simulations". In: *J. Comput. Phys.* 306 (2016), pp. 148–166. DOI: 10.1016/j.jcp.2015.11.034.

[9] M. Benedetto, S. Berrone, S. Pieraccini, and S. Scialò. "The virtual element method for discrete fracture network simulations". In: *Comput. Methods Appl. Mech. Engrg.* 280.0 (2014), pp. 135–156. ISSN: 0045-7825. DOI: 10.1016/j.cma.2014.07.016.

[10] M. Benedetto, S. Berrone, and S. Scialò. "A Globally Conforming Method For Solving Flow in Discrete Fracture Networks Using the Virtual Element Method". In: *Finite Elem. Anal. Des.* 109 (2016), pp. 23–36. DOI: 10.1016/j.finel.2015.10.003.

[11] C. Bernardi, Y. Maday, and A. T. Patera. "A new nonconforming approach to domain decomposition: the mortar element method". In: *Nonlinear partial differential equations and their applications. Collège de France Seminar, Vol. XI (Paris, 1989–1991)*. Vol. 299. Pitman Res. Notes Math. Ser. Longman Sci. Tech., Harlow, 1994, pp. 13–51.

[12] C. Bernardi, Y. Maday, and F. Rapetti. "Basics and some applications of the mortar element method". In: *GAMM-Mitt.* 28.2 (2005), pp. 97–123.

[13] S. Berrone, A. Borio, and S. Scialò. "A posteriori error estimate for a PDE-constrained optimization formulation for the flow in DFNs". In: *SIAM J. Numer. Anal.* 54.1 (2016), pp. 242–261. DOI: 10.1137/15M1014760.

[14] S. Berrone, C. Canuto, S. Pieraccini, and S. Scialò. "Uncertainty quantification in Discrete Fracture Network models: stochastic fracture transmissivity". In: *Comput. Math. Appl.* 70.4 (2015), pp. 603–623. DOI: 10.1016/j.camwa.2015.05.013.

[15] S. Berrone, S. Pieraccini, and S. Scialò. "A PDE-constrained optimization formulation for discrete fracture network flows". In: *SIAM J. Sci. Comput.* 35.2 (2013), B487–B510. ISSN: 1064-8275. DOI: 10.1137/120865884.

[16] S. Berrone, S. Pieraccini, and S. Scialò. "An optimization approach for large scale simulations of discrete fracture network flows". In: *J. Comput. Phys.* 256 (2014), pp. 838–853. ISSN: 0021-9991. DOI: 10.1016/j.jcp.2013.09.028.

[17] S. Berrone, S. Pieraccini, and S. Scialò. "On simulations of discrete fracture network flows with an optimization-based extended finite element method". In: *SIAM J. Sci. Comput.* 35.2 (2013), A908–A935. ISSN: 1064-8275. DOI: 10.1137/120882883.

[18] S. Berrone, S. Pieraccini, and S. Scialò. "Towards effective flow simulations in realistic discrete fracture networks". In: *J. Comput. Phys.* 310 (2016), pp. 181–201. DOI: 10.1016/j.jcp.2016.01.009.

[19] S. Berrone, S. Pieraccini, S. Scialò, and F. Vicini. "A parallel solver for large scale DFN flow simulations". In: *SIAM J. Sci. Comput.* 37.3 (2015), pp. C285–C306. DOI: 10.1137/140984014.

[20] F. Brezzi. "On the existence, uniqueness and approximation of saddle-point problems arising from lagrangian multipliers". In: *Revue française d'automatique, informatique, recherche opérationelle. Analyse numérique* 8.2 (1974), pp. 129–151.

[21] M. C. Cacas, E. Ledoux, G. de Marsily, B. Tillie, A. Barbreau, E. Durand, B. Feuga, and P. Peaudecerf. "Modeling fracture flow with a stochastic discrete fracture network: calibration and validation: 1. The flow model". In: *Water Resour. Res.* 26 (1990), pp. 479–489. DOI: 10.1029/WR026i003p00479.

[22] G. Cammarata, C. Fidelibus, M. Cravero, and G. Barla. "The Hydro-Mechanically Coupled Response of Rock Fractures". English. In: *Rock Mechanics and Rock Engineering* 40.1 (2007), pp. 41–61. ISSN: 0723-2632. DOI: 10.1007/s00603-006-0081-z.

[23] M. Cravero and C. Fidelibus. "A code for scaled flow simulations on generated fracture networks". In: *Comput. Geosci.* 25.2 (1999), pp. 191–195.

[24] W. S. Dershowitz and C. Fidelibus. "Derivation of equivalent pipe networks analogues for three-dimensional discrete fracture networks by the boundary element method". In: *Water Resource Res.* 35 (1999), pp. 2685–2691. DOI: 10.1029/1999WR900118.

[25] J.-R. de Dreuzy, G. Pichot, B. Poirriez, and J. Erhel. "Synthetic benchmark for modeling flow in 3D fractured media". In: *Computers & Geosciences* 50.0 (2013), pp. 59–71.

[26] J. Erhel, J.-R. de Dreuzy, and B. Poirriez. "Flow Simulation in Three-Dimensional Discrete Fracture Networks". In: *SIAM J. Sci. Comput.* 31.4 (2009), pp. 2688–2705. ISSN: 1064-8275. DOI: 10.1137/080729244.

[27] C. Fidelibus. "The 2D hydro-mechanically coupled response of a rock mass with fractures via a mixed BEM-FEM technique". In: *International Journal for Numerical and Analytical Methods in Geomechanics* 31.11 (2007), pp. 1329–1348.

[28] C. Fidelibus, G. Cammarata, and M. Cravero. *Hydraulic characterization of fractured rocks. In: Abbie M, Bedford JS (eds) Rock mechanics: new research.* Nova Science Publishers Inc., New York, 2009.

[29] L. Formaggia, P. Antonietti, P. Panfili, A. Scotti, L. Turconi, M. Verani, and A. Cominelli. "Optimal techniques to simulate flow in fractured reservoir". In: *ECMOR XIV-14th European conference on the mathematics of oil recovery.* 2014.

[30] L. Formaggia, A. Fumagalli, A. Scotti, and P. Ruffo. "A reduced model for Darcy's problem in networks of fractures". In: *ESAIM: Mathematical Modelling and Numerical Analysis* 48 (04 July 2014), pp. 1089–1116. ISSN: 1290-3841. DOI: 0.1051/m2an/2013132.

[31] A. Fumagalli and A. Scotti. "A numerical method for two-phase flow in fractured porous media with non-matching grids". In: *Advances in Water Resources* 62 (2013), pp. 454–464. ISSN: 0309-1708. DOI: 10.1016/j.advwatres.2013.04.001.

[32] Z. Huang, X. Yan, and J. Yao. "A Two-Phase Flow Simulation of Discrete-Fractured Media using Mimetic Finite Difference Method". In: *Communications in Computational Physics* 16.3 (2014).

[33] J. D. Hyman, C. W. Gable, S. L. Painter, and N. Makedonska. "Conforming Delaunay Triangulation of Stochastically Generated Three Dimensional Discrete Fracture Networks: A Feature Rejection Algorithm for Meshing Strategy". In: *SIAM Journal on Scientific Computing* 36.4 (2014), A1871–A1894.

[34] J. Hyman, C. Gable, S. Painter, and N. Makedonska. "Conforming Delaunay Triangulation of Stochastically Generated Three Dimensional Discrete Fracture Networks: A Feature Rejection Algorithm for Meshing Strategy". In: *SIAM Journal on Scientific Computing* 36 (4 2014), A1871–A1894. DOI: 10.1137/130942541.

[35] J. Jaffré and J. E. Roberts. “Modeling flow in porous media with fractures; Discrete fracture models with matrix-fracture exchange”. In: *Numerical Analysis and Applications* 5.2 (2012), pp. 162–167.

[36] M. Karimi-Fard and L. J. Durlofsky. “Unstructured Adaptive Mesh Refinement for Flow in Heterogeneous Porous Media”. In: *ECMOR XIV-14th European conference on the mathematics of oil recovery*. 2014.

[37] A. Klawonn. “FETI Domain Decomposition Methods for Second Order Elliptic Partial Differential Equations”. In: *GAMM – Mitteilungen* 29.2 (2006), pp. 319–341. ISSN: 1522-2608. DOI: 10.1002/gamm.201490036.

[38] V. Lenti and C. Fidelibus. “A *BEM* solution of steady-state flow problems in discrete fracture networks with minimization of core storage”. In: *Computers & Geosciences* 29.9 (2003), pp. 1183–1190. ISSN: 0098-3004. DOI: 10.1016/S0098-3004(03)00140-7.

[39] H. Mustapha and R. Dimitrakopoulos. “High-order stochastic simulation of complex spatially distributed natural phenomena”. In: *Mathematical Geosciences* 42.5 (2010), pp. 457–485.

[40] H. Mustapha and K. Mustapha. “A New Approach to Simulating Flow in Discrete Fracture Networks with an Optimized Mesh”. In: *SIAM J. Sci. Comput.* 29.4 (2007), pp. 1439–1459. ISSN: 1064-8275. DOI: 10.1137/060653482.

[41] J. Nocedal and S. J. Wright. *Numerical Optimization*. Berlin: Springer, 1999.

[42] B. Nœtinger. “A quasi steady state method for solving transient Darcy flow in complex 3D fractured networks accounting for matrix to fracture flow”. In: *J. Comput. Phys.* 283 (2015), pp. 205–223. ISSN: 0021-9991. DOI: 10.1016/j.jcp.2014.11.038.

[43] B. Nœtinger and N. Jarrige. “A quasi steady state method for solving transient Darcy flow in complex 3D fractured networks”. In: *J. Comput. Phys.* 231.1 (2012), pp. 23–38. ISSN: 0021-9991. DOI: 10.1016/j.jcp.2011.08.015.

[44] G. Pichot, J. Erhel, and J. de Dreuzy. “A generalized mixed hybrid mortar method for solving flow in stochastic discrete fracture networks”. In: *SIAM Journal on scientific computing* 34 (2012), B86–B105. DOI: 10.1137/100804383.

[45] G. Pichot, J. Erhel, and J. de Dreuzy. “A mixed hybrid Mortar method for solving flow in discrete fracture networks”. In: *Applicable Analysis* 89 (2010), pp. 1629–643. DOI: 10.1080/00036811.2010.495333.

[46] G. Pichot, B. Poirriez, J. Erhel, and J.-R. de Dreuzy. “A Mortar BDD method for solving flow in stochastic discrete fracture networks”. In: *Domain Decomposition Methods in Science and Engineering XXI*. Lecture Notes in Computational Science and Engineering. Springer, 2014, pp. 99–112.

[47] P. Raviart and J. Thomas. “Primal hybrid finite element methods for 2nd order elliptic equations”. In: *Mathematics of computation* 31.138 (1977), pp. 391–413.

[48] M. Vohralík, J. Maryška, and O. Severýn. “Mixed and nonconforming finite element methods on a system of polygons”. In: *Applied Numerical Mathematics* 51 (2007), pp. 176–193.

[49] B. I. Wohlmuth. “A mortar finite element method using dual spaces for the Lagrange multiplier”. In: *SIAM journal on numerical analysis* 38.3 (2000), pp. 989–1012.

[50] B. I. Wohlmuth. *Discretization Methods And Iterative Solvers Based On Domain Decomposition*. Berlin: Springer, 2001.